

**A neuro-mechanical model for the  
switching of stepping direction  
and transitions between walking  
gaits in the stick insect**

**Inaugural-Dissertation**

zur

Erlangung des Doktorgrades

der Mathematisch-Naturwissenschaftlichen Fakultät

der Universität zu Köln

vorgelegt von

Sascha Alexander Knops

aus Stolberg (Rhld.)

Köln, 2013

Berichtersteller:

Dr. Silvia Gruhn

Prof. Dr. Ansgar Büschges

Tag der mündlichen Prüfung: 9. April 2013

„Der Herr aber liess einen Ostwind ins Land wehen  
jenen ganzen Tag und die ganze Nacht;  
und als es Morgen ward,  
hatte der Ostwind die Heuschrecken gebracht.“

*Exodus 10,13*

# Kurzzusammenfassung

In dieser Arbeit wird ein mathematisches Modell zur Fortbewegung der Stabheuschrecke entwickelt, das physiologische Gegebenheiten berücksichtigt und eine Reihe von biologisch relevanten Eigenschaften nachahmen kann.

Das Modell basiert auf der Erkenntnis, dass sensorische Rückkopplung einen starken Einfluss auf die Koordination der Gliedmaßen hat. Zentrale Mustergeneratoren (CPGs) steuern den Rhythmus der Bewegung und werden durch sensorische Einflüsse zwischen den Segmenten geregelt. Die Aktivität der CPGs wird über Motoneuronen auf die Muskeln übertragen.

Ausgehend von bereits bestehenden Neuronmodellen und neuronalen Netzwerkmodellen wird ein neuro-mechanisches Modell entwickelt, welches sowohl die Kopplung von Gliedmaßen innerhalb eines Beines als auch die Kopplung von verschiedenen Beinen umfasst.

Zunächst werden die mechanischen Modelle für die Bewegung der drei Gelenke, die im wesentlichen zu Fortbewegung beitragen, hergeleitet. Im Anschluss werden diese mechanischen Modelle mit einem neuronalen vereinigt und stellen somit ein neuro-mechanisches System für ein Einzelgelenk dar. Durch sensorische Kopplung dreier Gelenke und mit Hilfe der Einführung eines Schaltmechanismus werden Vorwärts-, Seitwärts- und Rückwärtsschritte eines Mittelbeines ausgeführt. Mit der Verknüpfung von zwei laufenden Mittelbeinen an einen Körper mit starren Vorder- und Hinterbeinen werden Kur-

venlaufsequenzen erzeugt. Nach der Erweiterung des Modells auf die Vorder- und Hinterbeine werden unter der Erzeugung verschiedener Gangarten geeignete intersegmentale sensorische Verbindungen getestet.

Es zeigt sich, dass die Änderung der Laufrichtung durch die Änderung eines einzelnen zentralen Kommandos eingeleitet werden kann und dass während des Kurvenlaufens eine stärkere Krümmung durch ein rückwärtslaufendes Mittelbein erzeugt werden kann. Es stellt sich heraus, dass die Gangarten Tetrapod und Tripod sich durch schwache inhibitorische Verbindungen erzeugen lassen.

# Abstract

In this study, a mathematical model for the locomotion of the stick insect is developed. This model takes physiological conditions into account and it is capable of mimicking biological relevant features.

The model is predicated on the crucial role, that sensory feedback plays in the coordination of limbs during walking. *Central Pattern Generators* (CPGs), which produce the rhythm of locomotion, are affected by sensory influences between the segments. The activities of the CPGs are transferred by the motoneurons to the muscles.

Starting with existing neuron models and neuronal network models, a neuro-mechanical model is developed that includes the coupling of segments inside of a leg as well as the coupling of multiple legs.

Firstly, mechanical models concerning the motion of the three isolated main joints are derived. These mechanical models are fused with the neuronal one. Thus, they represent neuro-mechanical models for the single joints that are coupled via sensory feedback. By means of the introduction of a switching mechanism the model is able to produce forward, backward and sideward stepping of a middle leg. Through the junction of two stepping middle legs to the body of the modeled stick insect, curve walking sequences with different curvatures can be produced. By extending the model to the front and the hind leg, the structure of intersegmental connection between the legs during

the tripod and tetrapod gait can be generated.

The change of stepping direction can be brought about by changing one single central command. If the middle leg is stepping backwards, the curvature during turning is smaller than in the case of sideward stepping. Weakly inhibitory intersegmental connections show the most accommodating leg coordination during both the tetrapod and the tripod gait.

# Contents

<b>1</b>	<b>Introduction</b>	<b>1</b>
<b>2</b>	<b>Methods</b>	<b>6</b>
2.1	Interneuron model . . . . .	7
2.2	Motoneuron model . . . . .	9
2.3	Muscle model . . . . .	11
2.3.1	Coordinate system in the stick insect . . . . .	13
2.3.2	Equation of motion for angle in the FTi-joint . . . . .	18
2.3.3	Equation of motion for angle in the CTr-joint . . . . .	23
2.3.4	Equation of motion for angle in the ThC-joint . . . . .	24
2.3.5	Determination of the spring constants . . . . .	26
2.4	Coupling leg segments . . . . .	28
2.5	Synthesis of neuronal and mechanical models . . . . .	40
2.5.1	A single joint . . . . .	40
2.5.2	Neuro-muscular coupling . . . . .	42
2.5.3	A single leg . . . . .	42
2.5.4	Multiple legs . . . . .	47
2.6	Implementation of the model . . . . .	52
<b>3</b>	<b>Results</b>	<b>55</b>



<i>CONTENTS</i>	ix
3.1 The single joint system . . . . .	56
3.1.1 The mechanical motion . . . . .	56
3.1.2 The neuro-mechanical system . . . . .	59
3.2 Interjoint coupling in a single leg . . . . .	62
3.2.1 Middle leg . . . . .	67
3.2.2 Switching mechanism . . . . .	69
3.2.3 Neuronal basis of curve walking . . . . .	74
3.2.4 Applying the model to ipsilateral legs . . . . .	79
3.3 Intersegmental coupling - Multiple legs . . . . .	84
<b>4 Discussion</b>	<b>96</b>
4.1 Summary of the model structure and its properties . . . . .	96
4.2 Discussion of the results . . . . .	99
4.3 Comparison to existing models . . . . .	103
4.4 Biological significance of the model and outlook . . . . .	106
<b>A Summary of the model parameters</b>	<b>109</b>
A.1 Neuron models . . . . .	109
A.2 Mechanical models . . . . .	117
<b>B Simulation with the coupled femur and tibia</b>	<b>125</b>

# Chapter 1

## Introduction

Locomotion of arthropods and various vertebrates is based on the coordinated movement of leg joints. This movement can be subdivided into two phases: one in which the leg has ground contact and another in which it is lifted off the ground. The former is called stance phase and the latter is named swing phase. During forward walking the stance phase begins with the touch-down of the tarsus at its anterior extreme position (AEP). Accordingly, the body is propelled while the leg moves relatively to the thorax to the posterior extreme position (PEP). Subsequently, the lift-off of the tarsus commences the swing phase. The leg is moved to its AEP and a new stepping cycle begins. The neuronal and mechanical control of several components is crucial for the coordination of leg joints and different legs between each other. The muscular and neuronal mechanisms, involved in arthropod locomotion, have been thoroughly studied in the stick insect (*Carausius morosus*) (Bässler and Büschges, 1998; Büschges et al., 2008, 2011; Dürr et al., 2004; Orlovsky et al., 1999; Ritzmann and Büschges, 2007). In many insects walking patterns are generated decentralized. Central neuronal networks generate basic motor activity that is influenced by sensory feedback.

That means, sensory feedback plays an essential role in the shaping of motor output and in the control of stance and swing phase. The sensory signals are: movement and position signals from the leg joints on the one hand and force and load signals from the leg segments on the other hand (Borgmann et al. 2011; Daun-Gruhn et al. 2011; Zill et al. 2004; Zill et al. 2009; Zill et al. 2011; for a review see Büschges and Gruhn 2008). Leg joints are driven by their individual pattern generating networks (CPGs). These CPGs activate pools of motoneurons that innervate muscles in the respective joints (Akay et al., 2004; Büschges, 1995, 1998, 2005).

The intersegmental coordination of legs has been investigated on the behavioral level (Cruse, 1990; Graham, 1972; von Buddenbrock, 1921; Wendler, 1965, 1978) as well as on the neuro-muscular level by recording EMG activity, intracellular and extracellular electrical activity of motoneurons (MNs) (Büschges, 1995; Büschges et al., 2004; Ritzmann and Büschges, 2007; Büschges et al., 2008; Borgmann et al., 2009; Rosenbaum et al., 2010).

Leg coordination during stepping is subdivided into different walking gaits. While insects walk at high velocities, they adopt a symmetric tripod gait. Three legs are lifted off and three legs have ground contact at the same time (Delcomyn, 1971). At low velocities or under load conditions they adopt an asymmetric tetrapod gait. Two legs are lifted off while four legs have ground contact (Graham, 1972). The coordination of legs in gait generation has been studied carefully in behavioral experiments (Cruse, 1990; Delcomyn, 1989; Dürr et al., 2004; Grabowska et al., 2012). Furthermore, the investigation of video records with regards to free walking stick insects revealed that irregular gaits were mostly due to multiple stepping in the front legs. These findings lead to the assumption that the front legs carry out a searching function and that they are not coupled to the middle legs. However, middle

and hind leg coordination by themselves show regular gaits comparable to quadrupedal walk and wave gaits. These characteristics are retained in front leg amputees.

Details of neuronal and mechanical properties of a forward stepping single leg are well-investigated (Büschges, 2005; Büschges et al., 2008; Dürr et al., 2004; Orlovsky et al., 1999). These findings made it possible to build controllers of the single joint and single leg of the stick insect (Ekeberg et al., 2004) as well as the cat hind leg (Ekeberg and Pearson, 2005; Pearson et al., 2006). Such details for backward and sideward stepping and the neuronal basis for gait generation have remained largely unknown.

One way to gain insight into underlying mechanisms is to create appropriate mathematical models. There are different types of models existing that focus on different aspects of locomotion in animals. There are models concentrating on bio-mechanical properties in locomotion (Holmes et al., 2006), models that center on the role of chains of centrally coupled oscillators in locomotion (Ijspeert et al., 2007), models focusing on behavioral studies (Cruse, 1990) and models that give attention to the role of sensory signals in the coordination of legs during locomotion based on neuro-physiological studies (Ekeberg and Pearson, 2005; Ekeberg et al., 2004).

The first two kinds of models investigate the generation of rhythmic activity by neuronal properties and the synchronization of the network by interneurons. These investigations are aiming at the explanation of the affection of synchronization at different oscillator couplings and different intrinsic frequencies rather than the explanation of rhythmogenesis. The third kind of model concerns discontinuous bistable systems and spares the use of CPGs. Such reflex chains have two stable steady states for the same set of parameters. The switch between these two states is controlled by an input param-

eter. The fourth kind of model takes neuro-physiological experiments into account. Certainly, it does not make use of CPGs. Therefore, the generation of periodic motor output is not possible in the latter two models.

An alternative approach is taken by a model by Daun-Gruhn (2011): According to that CPGs are connected by biologically-inspired synapses modulated by sensory input. This model is extended by taking experimental findings on intersegmental influences (Borgmann et al., 2007, 2009; Ludwar et al., 2005) into account. It aims at elucidating basic neuronal processes during transitions of gaits. These processes are an outcome of sensory influences. Changes are only required in the central drives to the CPGs (Daun-Gruhn and Toth, 2011). In Toth et al. (2012) a model for a single middle leg with two joints is constructed. It includes a neuro-mechanical model that explains the conversion of rhythmic electrical CPG activity into mechanical leg movement. Originally, this neuro-mechanical model only includes the coupled system of the Thorax-Coxa-joint (ThC-joint) and the Coxa-Trochanter-joint (CTr-joint). At the ThC-joint the *protractor coxae* and the *retractor coxae* muscle pair moves the coxa forward and backward. At the CTr-joint the *levator trochanteris* and the *depressor trochanteris* muscle pair moves the femur up and down. Nevertheless, the Femur-Tibia-joint (FTi-joint) about which the tibia is flexed or extended by the *flexor tibiae* and the *extensor tibiae* muscle pair is not included. The model is capable of producing forward and backward stepping and switching between them by changing a single neuronal signal.

This study treats of the further development with regard to the neuro-mechanical model by Toth et al. (2012), which is mentioned above. It also comprises the embedding of an intersegmental coupled network of three ipsilateral legs similar to the model in Daun-Gruhn and Toth (2011). The

novelties in this work are as follows: i) the coupling of the FTi-joint to the existing two joint model (Knops et al., 2012), ii) the capability of sideward stepping through the attachment of the FTi-joint (Knops et al., 2012), iii) the explanation of basic neuronal mechanisms of curve walking through the application of sideward stepping and backward stepping (Knops et al., 2012), iv) the construction of an ipsilateral three-leg model including properties of the neuro-mechanical model, v) the generation of gaits and vi) the transition between gaits.

In this study, chapter 2 presents the methods and techniques used in the construction, implementation and simulation of the aforementioned models. The description of the basic properties of these models and the simulation results achieved with them are presented in chapter 3. In connection with this the results are summed up and discussed in chapter 4. Appendix A presents a concise summary of the model parameters and their numerical values used in the models. Appendix B shows the simulation results obtained with the mechanically coupled femur and tibia.

# Chapter 2

## Methods

This chapter concerns the development of a neuro-mechanical model for the locomotion in the stick insect and it provides a recollection of necessary mathematical tools that are already established. In sections 2.1 and 2.2 the original interneuron and motoneuron models are summarized (cf. Daun-Gruhn (2011); Daun-Gruhn et al. (2011)). The derivation of the mechanical equations of motion for all three main leg joints is presented in section 2.3. After fixing the coordinate system in section 2.3.1 the equation of motion in the FTi-joint is derived in section 2.3.2 (see also Knops et al. (2012)). Pertaining to the other two joints (CTr-joint and ThC-joint), the derivation of the equation of mechanical motion is summarized on the basis of Toth et al. (2012) in sections 2.3.3 and 2.3.4. Section 2.3.5 the dynamical parameters in all three main joints are determined by a procedure that was first published in Toth et al. (2012). How the equation of motion concerning a coupled system of the CTr-joint with the FTi-joint can be deduced is shown in section 2.4. The synthesis of mechanical and neuronal models and a successive buildup of a three-legged locomotor system is performed in section 2.5. Section 2.5.1 refers to the single joint system (Toth et al., 2012) and section 2.5.3 relates

to the coupled three-joint system (Knops et al., 2012). The intersegmental neuronal connection between three ipsilateral legs on a neuro-mechanical basis is presented in section 2.5.4. This chapter concludes with technical comments about the implementation of the model in section 2.6.

## 2.1 Interneuron model

There are two features observed in CPGs: endogenously bursting neurons and mutually inhibitory connections (Calabrese, 1995; Satterlie, 1985; Selverston and Moulins, 1985). Rhythmic activity is produced on the level of basal excitatory activity and on the level of patterning by inhibitory coupling (Grillner et al., 2005). For that purpose, Daun-Gruhn (2011) modeled a CPG as two Hodgkin-Huxley-type neurons mutually coupled by inhibitory synapses (Hodgkin and Huxley, 1952). Due to its mutual inhibition, neurons are organized into two antagonistic groups (Izhikevich, 2007). The neurons carry a slowly-inactivating sodium current and they are tuned such that they are tonically active without coupling. Actually, this current is present in most neuron types and it is shown in Daun et al. (2009) that the sensitivity of the oscillation period to variations of the excitatory input as well as the degree to which the phase can be separately controlled, strongly depend on intrinsic cellular mechanisms that are involved in rhythmogenesis and phase transitions. The usage of a slowly-inactivating sodium current leads to the widest range of oscillation periods and the greatest degree of independence of phase duration control at asymmetric inputs (Daun et al., 2009). Despite of that there is not much known about the compositions of the currents in the stick insect (Westmark et al., 2009), slowly-inactivating persistent currents play an important role in neuronal networks of other animals (Katz and Hooper,



2007; van Drongelen et al., 2006; Zhong et al., 2007).

The electrical activity of the non-spiking interneurons (CPG neurons and other interneurons) is described by the following equation system:

$$\begin{aligned}
C_m \frac{dV}{dt} &= -(I_{NaP} + I_L + I_{syn} + I_{app}) \\
I_{NaP} &= g_{NaP} m_\infty(V) h(V - E_{Na}) \\
I_L &= g_L (V - E_L) \\
I_{syn} &= g_{syn} s_\infty(V_{syn})(V - E_{syn}) \\
I_{app} &= g_{app} (V - E_{app}) \\
\frac{dh}{dt} &= (h_\infty(V) - h) / \tau_h(V)
\end{aligned}$$

with  $V = V(t)$  being the membrane potential,  $g_i$  being the maximal conductances of the membrane currents,  $E_i$  being the reversal potential,  $C_m$  being the membrane capacitance.  $h = h(t)$  denotes the inactivation variable of the slowly-inactivating sodium current  $I_{NaP}$ . The function  $m_\infty(V)$  is the steady-state value at  $V$  of the activation variable  $m$  of  $I_{NaP}$ , the function  $h_\infty(V)$  is the steady-state value at  $V$  of the inactivation variable  $h$  of  $I_{NaP}$  and the function  $s_\infty(V_{syn})$  is the actual value of the synaptic activation induced by another cell with membrane potential  $V_{syn}$ . The latter three functions are enunciated in the following formula:

$$z_\infty(V) = \frac{1}{1 + \exp \gamma_z (V - V_z)} \quad (2.1)$$

with  $z = m, h, s$ . The sensory input to the interneurons is represented by the applied current  $I_{app}$  and the strength can be tuned by varying  $g_{app}$ . This is relevant with reference to the adjustment of the oscillatory period and the phase relation of CPG neurons. The parameters for all interneurons and synapses used here are listed in tables A.2 - A.3 of Appendix A.

## 2.2 Motoneuron model

The motoneurons are modeled by a Hodgkin-Huxley type neuron model (Hodgkin and Huxley, 1952) as well. In contrast to the interneuron model, these neurons produce proper action potentials and exhibit adaptive behavior, i.e. decreasing firing frequency during sustained stimuli. These properties can be achieved by the use of four intrinsic ionic membrane currents: the fast inactivating sodium current  $I_{Na}$ , the delayed rectifier potassium current  $I_K$ , an outward (potassium) current  $I_q$  responsible for the adaptation of firing, and the leakage current  $I_L$  (Daun-Gruhn et al., 2011). A synaptic current  $I_{syn}$  and an applied current  $I_{app}$  introduced in section 2.1 are included, too. The currents  $I_{Na}$  and  $I_K$  are adapted from Traub et al. (1991). The motoneuron model used in this study is taken from Toth and Gruhn (2011), and the basic equations are

$$C_m \frac{dV}{dt} = -(I_{Na} + I_K + I_q + I_L + I_{syn} + I_{app}) \quad (2.2)$$

with

$$I_{Na} = g_{Na} m_{Na}^2 h_{Na} (V - E_{Na}) \quad (2.3)$$

$$I_K = g_K m_K (V - E_K) \quad (2.4)$$

$$I_q = g_q m_q (V - E_q) \quad (2.5)$$

$$I_L = g_L (V - E_L) \quad (2.6)$$

$$I_{syn} = g_{syn} s_{\infty}(V_{syn}) (V - E_{syn}) \quad (2.7)$$

$$I_{app} = g_{app} (V - E_{app}) \quad (2.8)$$

$g_i$  being the maximal conductances of the membrane currents,  $E_i$  being the reversal potential and  $i = Na, K, q, syn, app$ . The inactivation variable  $h_i$  and the activation variable  $m_i$ , respectively, are described by

$$\frac{dy}{dt} = \alpha_y(V)(1 - y) - \beta_y(V)y \quad (2.9)$$

where  $y = h_{Na}, m_{Na}, m_K$ . The coefficients  $\alpha(V)$  and  $\beta(V)$  are non-linear functions of the membrane potential  $V$ , depending on the membrane current.

For the activation variable  $m_{Na}$  in the sodium current  $I_{Na}$ , there is

$$\alpha_{m_{Na}} = \frac{a_{m1}(a_{m2} - V)}{\exp(a_{m3}(a_{m2} - V)) - 1} \quad (2.10)$$

$$\beta_{m_{Na}} = \frac{b_{m1}(b_{m2} - V)}{\exp(b_{m3}(b_{m2} - V)) - 1} \quad (2.11)$$

For the inactivation variable  $h_{Na}$  in the sodium current  $I_{Na}$ , there is

$$\alpha_{h_{Na}} = a_{h1} \exp(a_{h3}(a_{h2} - V)) \quad (2.12)$$

$$\beta_{h_{Na}} = \frac{b_{h1}}{\exp(b_{h3}(b_{h2} - V)) + 1} \quad (2.13)$$

The numerical values of the parameters can be found in table A.5 in the Appendix A.

For the activation variable  $m_K$  in the potassium current  $I_K$ , there is

$$\alpha_{m_K} = \frac{a_{m1}(a_{m2} - V)}{\exp(b_{h3}(b_{h2} - V)) - 1} \quad (2.14)$$

$$\beta_{m_K} = b_{m1} \exp(b_{m3}(b_{m2} - V)) \quad (2.15)$$

The numerical values of the parameters can be found in table A.6 in the Appendix A. Note, that the potassium current is not inactivating and thus the inactivation variable  $h$  does not appear in its equation.

The adaptation current  $I_q$  leads to a decrease of firing frequency in the motoneuron at sufficiently long stimuli. For the activation variable  $m_q$  one has

$$\frac{m_q}{dt} = r_q(m_{q\infty}(V) - m_q) \quad (2.16)$$

$$m_{q\infty} = \frac{1}{1 + \exp(s_q(V - V_{hq}))} \quad (2.17)$$

$$r_q = \text{const} \quad (2.18)$$

where  $m_{q\infty}$  is the steady-state value of  $m_q$  at  $V$ . The numerical values of the parameters can be found in table A.7 in Appendix A.

The parameters concerning the leakage current  $I_L$  are listed in table A.8 in Appendix A.

## 2.3 Muscle model

In this section, it is shown how the equations of motion, relating to mechanical movement, can be deduced. This is carried out explicitly for the FTi joint as it appears in Knops et al. (2012). It is a proceeding work concerning the extension of an existing neuro-mechanical model for the two proximal joints sited in the ThC and CTr (cf. Toth et al. (2012)). The equations for the latter two joints are repeated briefly. A detailed description can be found in Toth et al. (2012). The femur-tibia joint (FTi-joint) is driven by flexor-extensor muscle pair (see figure 2.1). In the following, the expressions FE system and FTi-joint are treated as synonyms. The same applies to the LD system (CTr-joint) and the PR system (ThC-joint).

The mechanical motion of a single joint in the stick insect is brought about by the activity of antagonistic muscles. In a single leg, there are three such muscle pairs (each located at a respective joint) that in essence produce the locomotion of the insect. At the Thorax-Coxa-joint (ThC-joint) the *protractor coxae* and the *retractor coxae* (henceforth protractor-retractor) muscle pair moves the coxa forward and backward, at the Coxa-Trochanter-joint (CTr-joint) the *levator trochanteris* and the *depressor trochanteris* (henceforth levator-depressor) muscle pair moves the femur up and down, and at the Femur-Tibia-joint (FTi-joint) the tibia is flexed or extended by the *flexor tibiae* and the *extensor tibiae* (henceforth flexor-extensor) muscle pair. The model for all the muscle pairs constructed here are based on the same principles, which are a simplification of the Hill model (Hill, 1953). The simpli-

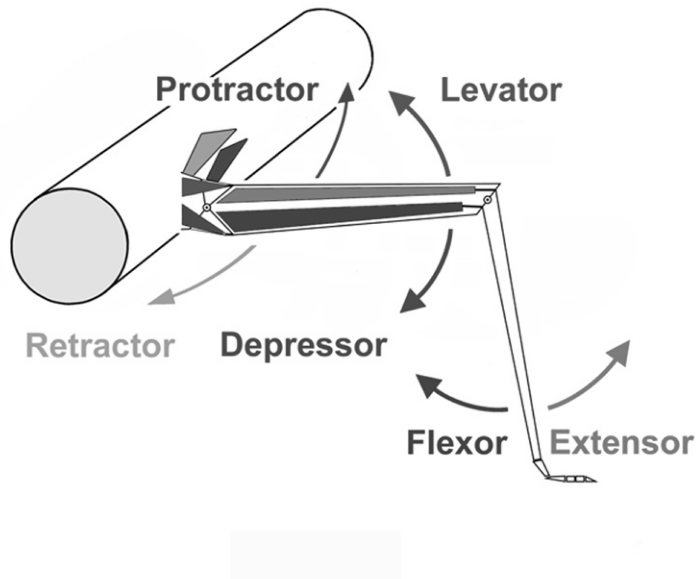


Figure 2.1: Schematic illustration of the leg joints and the basic movement directions. Adapted with permission from M. Gruhn.

fication is done by the consolidation of all active and passive elastic muscle properties (cf. figure 2.2 A) into a single spring with variable elasticity module, i.e. spring constant (cf. figure 2.2 B). Guschlbauer (2009) found out that the muscles obey a non-linear elasticity law

$$F = k(l - l_{min})^2 \quad (2.19)$$

for the muscle force  $F$  with the variable spring constant  $k$ , actual length  $l$  and minimal length  $l_{min}$  of the muscle.

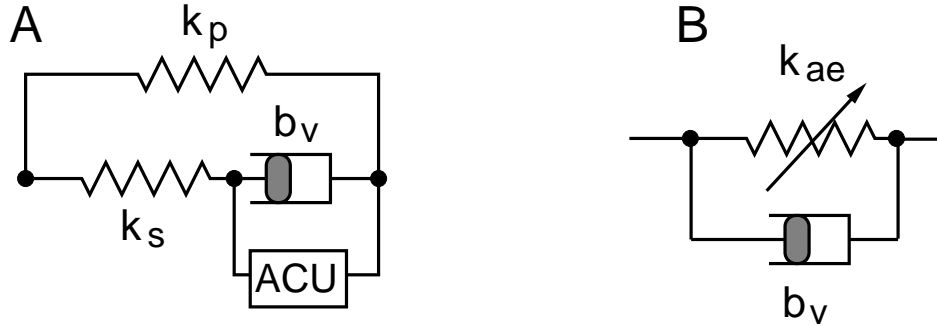
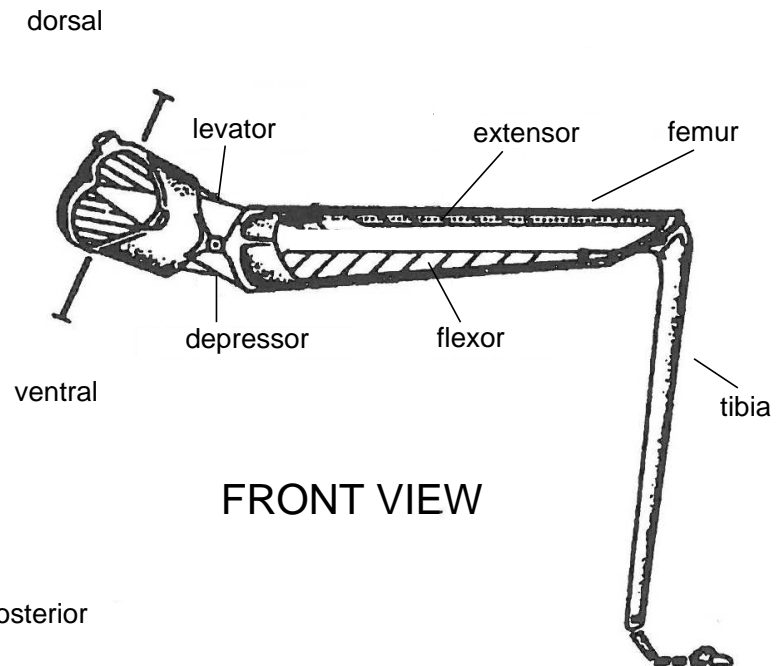


Figure 2.2: A: Hill's muscle model and B: simplified muscle model used. In A,  $k_p$ : modulus of the passive parallel elasticity,  $k_s$ : modulus of the passive serial elasticity,  $b_v$ : viscosity coefficient characterizing the viscosity of the muscle, ACU: active contraction unit responsible for the development of (isotonic or isometric) contraction force. The model illustrated in map B is obtained by omitting the passive serial elasticity, and by merging ACU with the passive parallel elasticity. Thus in B,  $k_{ae}$ : variable modulus of the active, nonlinear elasticity,  $b_v$  as in A. Picture taken from Toth et al. (2012) with permission.

### 2.3.1 Coordinate system in the stick insect

The motion of a joint is characterized by the change of the respective joint angle. These angles are (from proximal to distal):  $\alpha$  in the ThC-joint,  $\beta$  in the CTr-joint and  $\gamma$  in the FTi-joint. A front and plan view of the stick insect's leg is shown in figure 2.3. The coxa-trochanter and the femur are merged to a *simplified* femur, since it has a negligible length and mass.

A



B

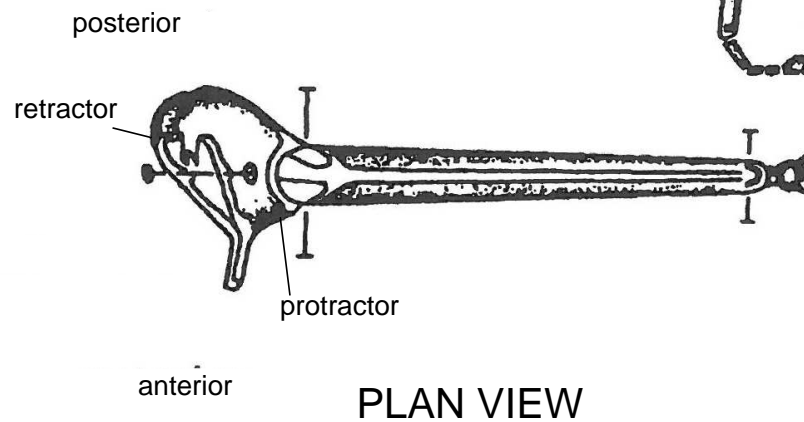


Figure 2.3: Front view (A) and plan view (B) of the stick insect's middle leg. The femur and the tibia are moved by the protractor-retractor coxae, levator-depressor trochanteris, and extensor-flexor tibiae Bässler (1983).

The angular movement of the angle  $\alpha$  is generated by the protractor-retractor muscle pair. The range of the angular motion is determined by the anterior extreme position (AEP) and posterior extreme position (PEP). The zero position of  $\alpha$  is when the femur is bent forward and parallel with the thorax (see figure 2.4). Consequently, the rearmost position eventuates when the femur is parallel with the thorax corresponds to the angle  $\alpha = 180^\circ$ . These extreme positions are unlikely to occur in natural conditions during locomotion of the stick insect. Hence they do not appear in the simulations. The levator-depressor muscle pair moves the femur up and down (angle  $\beta$ ) between the extremal angles determined by the ground contact during the stance phase and the highest elevated position of the femur during the swing phase. The angle  $\beta = 0^\circ$  is attained if the femur (or more precisely trochanter-femur) will align with the coxa segment. One should keep in mind that the coxa is declined downwards from the y-axis by an angle  $\psi$  (figure 2.5 A). The motion of the angle  $\gamma$  is mainly determined by the flexor-extensor muscle pair. Thereby the tibia can be moved towards or away from the body. At the angle  $\gamma = 0^\circ$  the leg is fully stretched. At  $\gamma = 180^\circ$  the tibia is parallel to the femur, a non-physiological position (figure 2.5 B).



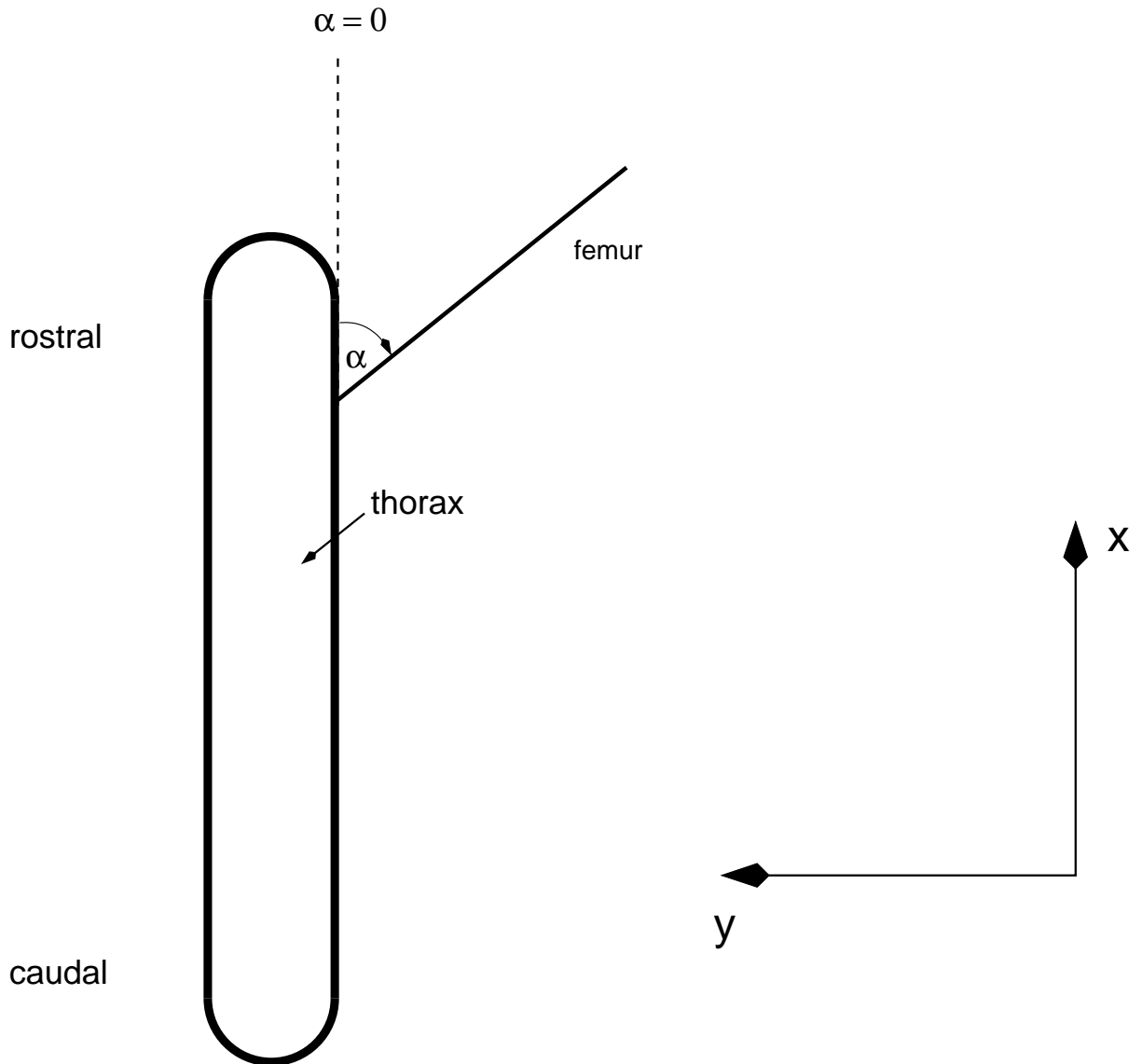


Figure 2.4: Top view on the thorax of the stick insect and the walking plane in the coordinate system used for the simulation. The rostral part is situated in the positive direction of the x-axis and the caudal part in the negative direction. The angle  $\alpha$  increases with a caudal movement of the femur.

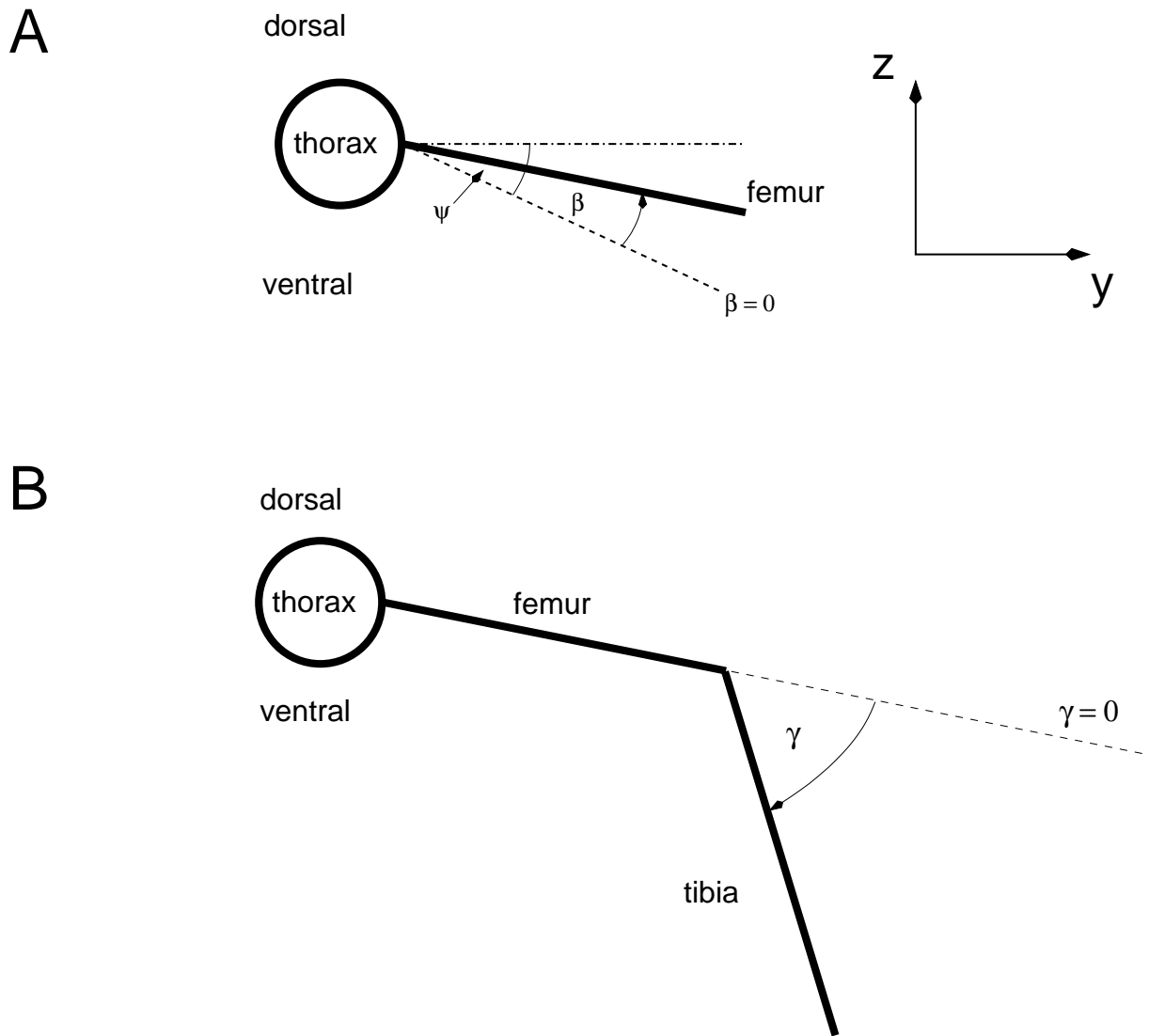


Figure 2.5: Front view on the thorax of the stick insect in the coordinate system used for the simulation. A:  $\beta$  increases with dorsal movement of the femur. The zero-point of  $\beta$  is given by the declination of the  $y$ -axis by the angle  $\psi$ . B:  $\gamma$  measures the flexion of the tibia relative to the femur. The zero-position is achieved for an outstretched tibia and the angle increases with the flexion of the tibia.

### 2.3.2 Equation of motion for angle in the FTi-joint

In this section, the equation of the angular movement  $\gamma$  in the FTi-joint will be derived when the other two angles ( $\alpha$  and  $\beta$ ) are kept constant. The derivation follows the one in Knops et al. (2012). Figure 2.6 A shows the geometrical arrangement of the extensor-flexor (FE) muscle system. The tendon of the extensor  $T_E$  is fixed to the tibia at point A. The tendon of the flexor  $T_F$  at is fixed at point B. The rotation axis of the tibia is at O. It is perpendicular to the plane of the figure. It is known (Guschlbauer et al., 2007; Guschlbauer, 2009) that  $\overline{AO} = d$  and  $\overline{BO} = 2d$ . The tendons are moved by contraction of the muscle fibers, one of their ends fixed to the tendon, the other one to the cuticle (oblique lines between  $C_E$  and  $T_E$ , and  $C_F$  and  $T_F$ , respectively). The zero position of the angle  $\gamma$  is when the femur and the tibia are collinear, i.e. at outstretched leg. In figure 2.6 B a single muscle fiber is schematically displayed. The distance between tendon and cuticle is  $\overline{EG} = h$ . The fiber is fixed to the tendon at point C, and to the cuticle at point G. In this position, it has length  $l_0$ , and its angle with the tendon is  $\phi_0$ . If the muscle contracts (with a force  $F_m$ ), point C of the muscle fiber at the tendon will be shifted to point D, due to the force  $F_p$  parallel to the tendon. The angle between tendon and fiber at D is  $\phi$ . The angle  $\gamma$  between femur and tibia is thus determined by the movement of the tendon. Experiments by Guschlbauer (cf. Knops et al. (2012)) show that variation of  $h$  at different angles  $\gamma$  in both the flexor and the extensor is negligible (cf. figure 2.7). The distance  $h$  between the tendon and the cuticle is therefore considered to be constant during contraction. The mean value of this distance is  $h_E = 0.34$  mm for the extensor, and  $h_F = 0.42$  mm for the flexor. The equation of mechanical motion of the tibia reads

$$I_T \ddot{\gamma} = F_{pF} \cdot 2d \sin \gamma - F_{pE} \cdot d \sin \gamma + M_v \quad (2.20)$$

with the moment of inertia  $I_T$ , the parallel forces  $F_{pF}$  and  $F_{pE}$  in the flexor and the extensor muscles, and the distances  $2d$  and  $d$  from the rotation point of the FTi-joint.  $M_v$  is the torque due to viscosity that is produced by two force components acting on the lever:

$$\begin{aligned}
M_v &= 2dF_{vF} + dF_{vE} \\
&= -2db_{v,FE}v_F - db_{v,FE}v_E \\
&= -4d^2b_{v,FE}\dot{\gamma} - d^2b_{v,FE}\dot{\gamma} \\
&= -5d^2b_{v,FE}\dot{\gamma}
\end{aligned} \tag{2.21}$$

since the viscosity force is proportional to, and counteracts the velocity. The viscosity constant  $b_{v,FE}$  is set to be the same for both muscles. The equation of motion for the angle in the FTi-joint finally reads

$$\ddot{\gamma} = \frac{d}{I_T} [(2F_{pF} - F_{pE}) \sin \gamma - 5b_{v,FE}d\dot{\gamma}] \tag{2.22}$$

The forces  $F_{pF} = F_{pF}(l_F)$  and  $F_{pE} = F_{pE}(l_E)$  are the projections of the corresponding muscle forces on the direction of movement of the tendon:

$$F_{pF} = F_{mF} \cos \phi_F \tag{2.23}$$

$$F_{pE} = F_{mE} \cos \phi_E \tag{2.24}$$

where  $\phi_F = \phi_F(l_F)$  and  $\phi_E = \phi_E(l_E)$  are angles between the fibers and tendons in the respective muscles and depend on the fiber length. According to findings by Guschlbauer et al. (2007); Guschlbauer (2009) (cf. equation (2.19)), the muscle forces are quadratic functions of the muscle length:

$$F_{mF} = k_F(l_F - l_{Fmin})^2 \tag{2.25}$$

$$F_{mE} = k_E(l_E - l_{Emin})^2 \tag{2.26}$$

$l_{Fmin}$  and  $l_{Emin}$  are the minimal lengths of the fibers, i.e. the lengths when the fibers are unstrained. Since the muscle fibers are arranged in parallel, the

spring constants  $k_F$  and  $k_E$  of the entire muscles are the sum of individual fiber spring constants. The fiber length is calculated by using the cosine theorem

$$l_F(\gamma) = \sqrt{l_{F0}^2 + s_F^2(\gamma) - 2l_{F0}s_F(\gamma)\cos\phi_{F0}} \quad \text{and} \quad (2.27)$$

$$l_E(\gamma) = \sqrt{l_{E0}^2 + s_E^2(\gamma) - 2l_{E0}s_E(\gamma)\cos\phi_{E0}} \quad (2.28)$$

with  $\cos\phi_{F0} = \sqrt{1 - (h_F/l_{F0})^2}$  and  $\cos\phi_{E0} = \sqrt{1 - (h_E/l_{E0})^2}$  and the shifts  $s_F(\gamma) = -2d\sin\gamma$  and  $s_E(\gamma) = d\sin\gamma$ .  $l_{F0}$  and  $l_{E0}$  are fiber lengths,  $\phi_{F0}$  and  $\phi_{E0}$  are the corresponding angles at  $\gamma = \gamma_0 = 90^\circ$ .

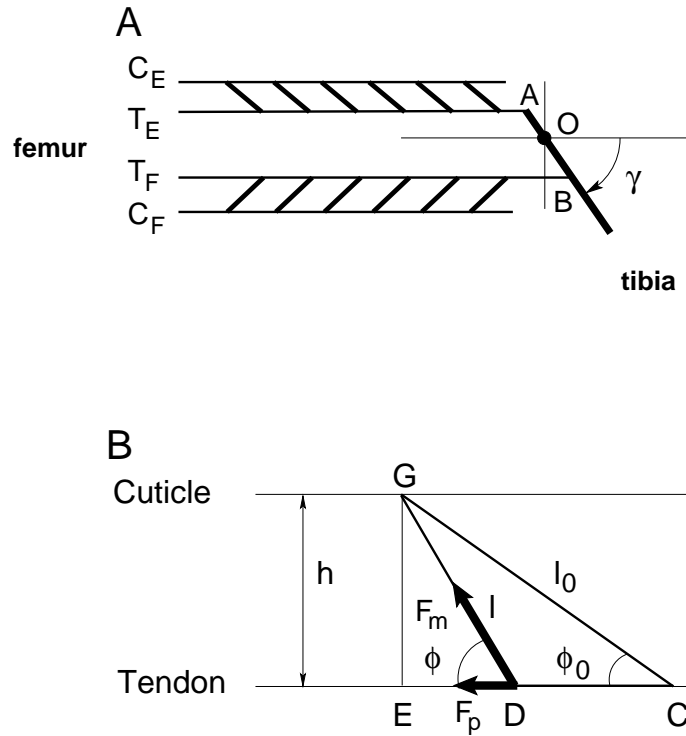


Figure 2.6: A: Geometric arrangement of the flexor and extensor muscles. The extensor tendon  $T_E$  is fixed to the tibia at point A, and the flexor tendon  $T_F$  at point B. The extensor muscle fibers (thick oblique lines), arranged in parallel, mechanically connect  $T_E$  with the cuticle of the extensor  $C_E$ . Similarly, the flexor fibers do so between  $T_F$  and the flexor cuticle  $C_F$ . The tibia rotates, with angle  $\gamma$ , about the axis at point O. This axis is perpendicular to the plane of the figure. B: Geometrical arrangement of a single muscle fiber between tendon and cuticle, and muscle forces. The fiber is fixed to the cuticle at point G.  $l_0$ : length of the muscle fiber when its other end is at position C (reference length);  $l$ : its length at point D (generic length);  $h$ : distance between tendon and cuticle;  $\phi_0$  and  $\phi$ : angles corresponding to the positions at C and D, respectively.  $F_m$ : muscle force in the fiber at point D (length  $l$ );  $F_p$ : parallel component of  $F_m$  moving the tendon. This figure appears as it is in Knops et al. (2012).

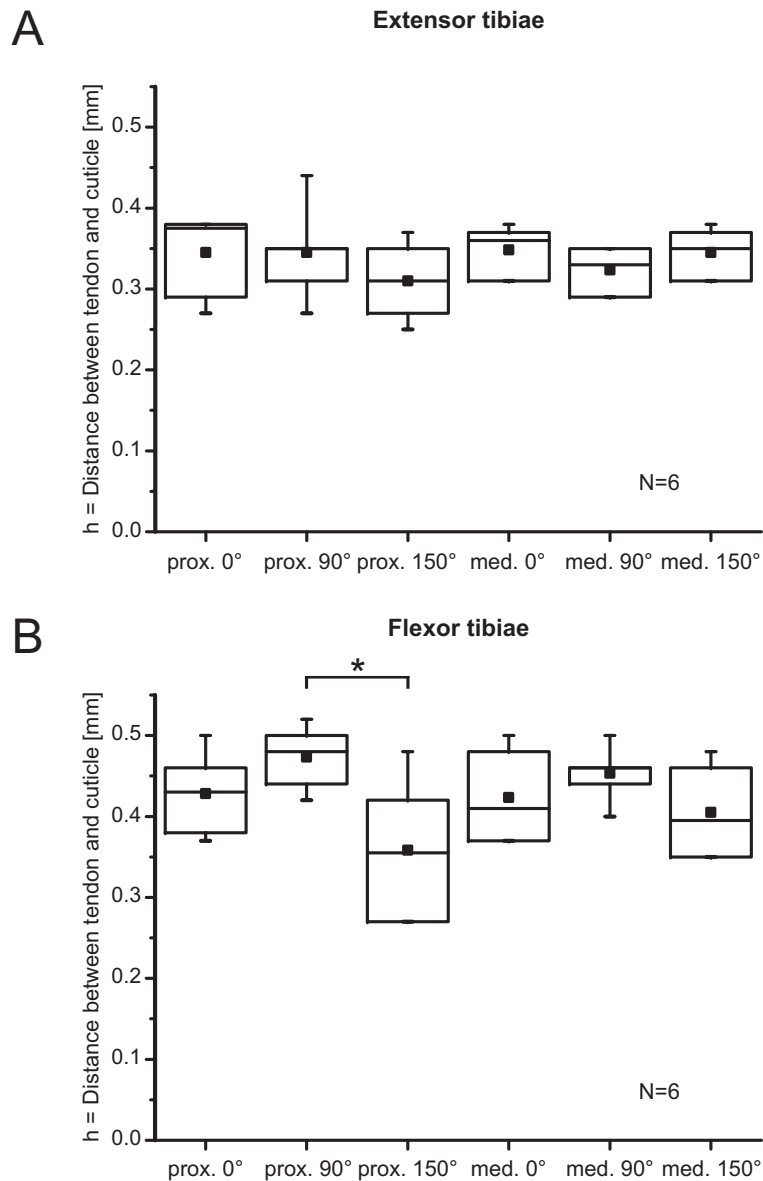


Figure 2.7: Boxplots of the distance  $h$  between tendon and cuticle edge versus the angle at the FTi-joint for the medial and the proximal regions of the muscles for three different flexion angles ( $0^\circ$ ,  $90^\circ$  and  $150^\circ$ ). A: extensor tibiae muscle, B: flexor tibiae muscle. In each box: data are obtained from the same 6 animals, Upper edge: 75 percentile; bottom edge: 25 percentile; line: median; small black square: mean value. Data from C. Guschlbauer, published in Knops et al. (2012).

### 2.3.3 Equation of motion for angle in the CTr-joint

In this section, a brief description of the equations of mechanical motion at the CTr-joint is given (cf. Toth et al. (2012)). The angle  $\alpha$  is kept constant and the tibia is omitted. Figures 2.8 (i) and (ii) show the geometrical arrangement of the levator-depressor (LD) system in the CTr-joint. The basic idea is that both muscles have the same length  $d$ , if the coxa-trochanter section is fully stretched. If the femur is moved up and down it will rotate about an axis at  $B$ , perpendicular to the plane of the figure. One of the muscles is elongated along the perimeter with the radius  $r$  and the center at  $B$ . The other muscle is shortened by the same amount. The actual lengths of the levator and depressor muscles are function of the rotation angle  $\beta$  and read

$$l_L = d - r\beta \quad (2.29)$$

$$l_D = d + r\beta \quad (2.30)$$

The equation of motion is

$$I_{FT}\ddot{\beta} = r(F_L - F_D - F_{v,LD}) \quad (2.31)$$

where  $I_{FT}$  is again the inertial momentum of the femur,  $\ddot{\beta}$  is the angular acceleration (second time derivative of the angle  $\beta$ ) and  $F_L$  and  $F_D$  are the levator and depressor elastic muscle forces. Anew, according to equation (2.19) the muscle forces obey

$$F_L = k_L(l_L - l_{Lmin})^2 \quad (2.32)$$

$$F_D = k_D(l_D - l_{Dmin})^2 \quad (2.33)$$

with the viscosity force  $F_{v,LD} = b_{v,LD}v = b_{v,LD}r\dot{\beta}$  and the viscosity coefficient  $b_{v,LD}$  for the LD system. The final form of the equation of mechanical motion



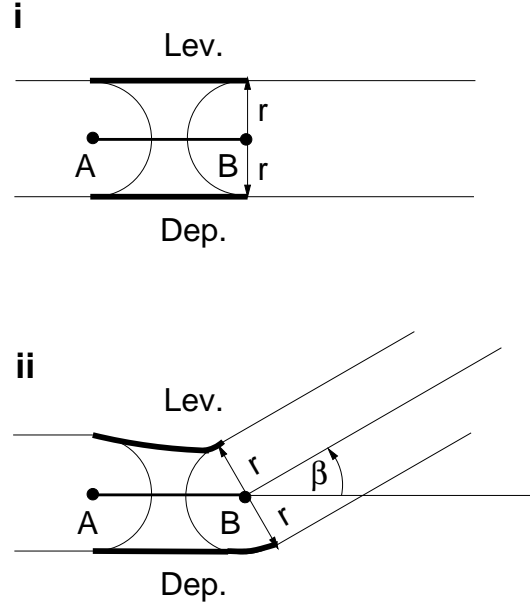


Figure 2.8: Two geometric situations of the levator-depressor joint are shown. In i) the system is in fully stretched state (a non-physiological situation) when both muscles are assumed to have the same length: the distance between the points  $A$  and  $B$ ,  $d = \overline{AB}$ . The femur is on the right hand side. It hinges about the axis through the point  $B$ , orthogonal to the plane of the figure. In ii), the femur is tilted upward by an angle  $\beta$ . The shortening of the levator and the elongating of the depressor muscle (Toth et al., 2012).

in the LD system then reads

$$\ddot{\beta} = c_1(F_L - F_D) - c_2\dot{\beta} \quad (2.34)$$

with  $c_1 = r/I_{FT}$  and  $c_2 = b_{v,LD}r^2/I_{FT}$ .

### 2.3.4 Equation of motion for angle in the ThC-joint

In this section, a brief description of the equations of mechanical motion in the ThC-joint is delivered (see Toth et al. (2012)). Figure 2.9 shows the geometrical arrangement of the protractor-retractor system (PR) in the ThC-joint. The rotation axis of the ThC-joint (thick black point) is perpendicular

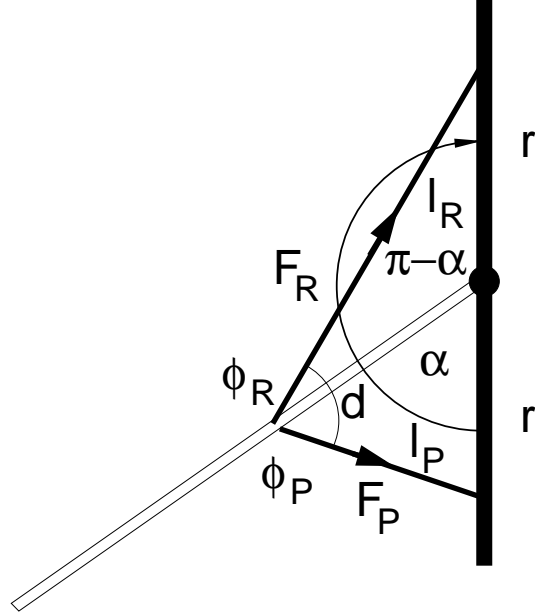


Figure 2.9: Top view of the simplified geometrical arrangement. The posterior-anterior direction is the one from up to down — the same as in figure 2.3 B. The thick black line represents the thorax, while the unfilled rod the femur. The angle  $\alpha$  characterizing the position of the femur is counted from anterior to posterior (as indicated).  $F_R$  and  $F_P$  are the forces in the retractor and protractor muscle, respectively. The corresponding muscle lengths are  $l_R$  and  $l_P$  (Toth et al., 2012).

to the plane of the figure and is the junction of the thorax (thick black line) and the femur (empty rod). The forces  $F_P$  for the protractor and  $F_R$  for the retractor are represented by the thick arrows. The muscles have the lengths  $l_P$  and  $l_R$ , respectively and attain the angles  $\phi_P$  and  $\phi_R$ , respectively between the muscle fibers and the femur. In this simplified model the muscles join the femur at the same distance  $d$  from the rotation point, and they join the thorax at the distance  $r$ . The equation of motion reads

$$I_{FT}\ddot{\alpha} = F_R d \sin \phi_R - F_P d \sin \phi_P - F_{v,PR} d \quad (2.35)$$

with the moment of inertia  $I_{FT}$  of the femur, the angular acceleration  $\ddot{\alpha}$ , the muscle forces

$$F_P = k_P(l_P - l_{Pmin})^2 \quad (2.36)$$

$$F_R = k_R(l_R - l_{Rmin})^2 \quad (2.37)$$

obeying equation 2.19 and  $F_{v,PR} = b_{v,PR}v = b_{v,PR}\dot{\alpha}d$  the viscosity force that is assumed to be linearly proportional to the actual velocity  $v = \dot{\alpha}d$ . Herein  $\dot{\alpha}$  is the angular velocity and  $b_{v,PR}$  is the viscosity coefficient for the PR system. The sine theorem for triangles yields

$$I_{FT}\ddot{\alpha} = rd \sin \alpha \left( \frac{F_R}{l_R} - \frac{F_P}{l_P} \right) - b_{v,PR}d^2\dot{\alpha} \quad (2.38)$$

and the cosine theorem the actual muscle lengths  $l_P$  and  $l_R$  become functions of  $\alpha$ :

$$l_R^2 = r^2 + d^2 + 2rd \cos \alpha \quad (2.39)$$

$$l_P^2 = r^2 + d^2 - 2rd \cos \alpha \quad (2.40)$$

Finally, the equation of motion for the angle  $\alpha$  reads

$$\ddot{\alpha} = c_3 \sin \alpha \left( \frac{F_R}{l_R} - \frac{F_P}{l_P} \right) - c_4\dot{\alpha} \quad (2.41)$$

with the constants  $c_3 = rd/I_{FT}$  and  $c_4 = b_{v,PR}d^2/I_{FT}$ .

### 2.3.5 Determination of the spring constants

This section deals with the determination of spring constants first published in Toth et al. (2012). The movement of the limbs is associated with the change of respective joint angles driven by antagonistic muscles. In a periodic and cyclic motion each joint angle moves in a certain range. The direction of the angular motion is determined by the time courses of the muscle forces.

Therefore, a change in direction is due to a switch in the contraction forces. This is gained by a change in spring constants (cf. equation (2.19)). The switch time is controlled by the CPG and it takes place at stationary points of the movement, i.e. where the angular velocity and the angular acceleration vanish (Toth et al., 2012). The dynamics of the muscles have to be set such that the joint angle reaches its extremal value by the time of the switch in the CPG. The dynamics are determined by the spring constants and viscosity. For the angle in the FTi-joint at time  $T_{sw}$ , one has

$$\gamma(T_{sw}) = \gamma_e, \quad \dot{\gamma}(T_{sw}) = 0, \quad \text{and} \quad \ddot{\gamma}(T_{sw}) = 0 \quad (2.42)$$

These conditions used in equations (2.22), (2.25) and (2.26) lead to the following ratio of the spring constants:

$$a_{FE} = \frac{k_F}{k_E} = \frac{1}{2} \frac{(l_E - l_{Emin})^2 \cos \phi_E}{(l_F - l_{Fmin})^2 \cos \phi_F} \quad (2.43)$$

The lengths  $l_F$ ,  $l_E$  and angles  $\phi_F$ ,  $\phi_E$  are functions of the angle  $\gamma$ . As there are two extreme angles  $\gamma_e$  (maximum flexion and maximum extension), it leads to two different values for  $a_{FE}$ : one for the flexion and another for the extension, where the angle at which the switch takes place has to be substituted into equation (2.43).

Analogously, the same procedure can be done for the angle  $\beta$  (by using equations (2.34), (2.32) and (2.33)):

$$a_{LD} = \frac{k_D}{k_L} = \left( \frac{d - r\beta_e - l_{Lmin}}{d + r\beta_e - l_{Dmin}} \right)^2 \quad (2.44)$$

with the extremal angle  $\beta_e$  in the CTr-joint and for the angle  $\alpha$  (by using equations (2.41), (2.36) and (2.37))

$$a_{PR} = \frac{k_R}{k_P} = \frac{l_R(\alpha_e) (l_P(\alpha_e) - l_{Pmin})^2}{l_P(\alpha_e) (l_R(\alpha_e) - l_{Rmin})^2} \quad (2.45)$$

with the extremal angle  $\alpha_e$  in the ThC-joint. The determination of the numerical values of the spring constants and the viscosity coefficient has to be accomplished by computer simulations (see section 3.1). In these simulations, only the equation of the mechanical (angular) motion is used. Consequently, the switch times are predetermined.

## 2.4 Coupling leg segments

So far, the equations of mechanical motions (angular movements) for the three isolated joints (muscle systems) are derived. However, due to mechanical coupling of the leg segments the motion of one joint can influence the motion of the others. For example, if the tibia moves, changing the angle in the FTi-joint, a force will be effective on the femur, too. This influence is most obvious for the CTr-joint since the local angles are in the same plane, i.e. their rotation axes are parallel. In general, the movement of the femur mechanically interacts with the movement of the tibia and vice versa. Hence it is not enough to look at the isolated joints.

The torques at the femur experience an increased moment of inertia to be overcome, and this counts for the tibia as well. It is by, no means, trivial to derive the equations of mechanical motion (the angular movements  $\beta$  and  $\gamma$ ) for this coupled system. Using the principles laid down by Lagrange (Lagrange, 1997) however, enables us to make a systematic derivation of those equations. The system presented here is in essence a double pendulum. The derivation requires the calculation of the kinetic and (mechanical) potential energy of the system from which the Lagrangian  $\mathcal{L} = T - U$  is obtained. In this case, the Lagrangian is a function of the angles  $\beta$  and  $\gamma$ . Having obtained the equations of mechanical motion in terms of the conservative system, i.e.

for the one with no dissipative forces such as viscosity, one can add these forces (the torques generated by them) to its equations. The derivation to follow is lengthy but straightforward.

As one can see in Appendix B, the influence of the motion is in both joints negligible. Experiments by Hooper et al. (2009) also show, that the torques due to passive mechanical coupling can be neglected in small animals such as the stick insect. Based on the reduction of computational time the mechanics that take effects within the joints will be treated separately.

### Kinetic Energy

Assuming the trochanter-femur as a thin stick of length  $L_F$  and mass  $M_F$ , the kinetic energy of the femur reads

$$T_F = \frac{1}{2} I_F \dot{\beta}^2 \quad (2.46)$$

with the angular velocity  $\dot{\beta}$  and the momentum of inertia  $I_F = \frac{1}{3} M_F L_F^2$  of the femur when it rotates about an axis at the origin of the coordinate system and perpendicular the plane of the figure.

The kinetic energy for a movement of a point mass  $dm_i$  of the tibia at  $(y_i, z_i)$  in the  $y - z$ -plane is given by

$$T_{T,i} = \frac{1}{2} dm (y_i^2 + z_i^2) \quad (2.47)$$

Figure 2.10 shows the trochanter-femur (in parallel with the vector  $\vec{v}_F$ ) and the tibia (in parallel with the vector  $\vec{v}$ ). Be  $\vec{v} = l \cdot \vec{e}_v$  with the unit vector  $\vec{e}_v$ ,  $l \in [0, L_T]$  and the length of the tibia  $L_T$ . The magnitude of  $\vec{v}_F$  is the constant femur length  $L_F$ . The vector  $\vec{r} = \vec{v}_F + \vec{v}$  now describes any point on the tibia. Assuming  $\beta$  to be the positively oriented angle between the  $y$ -axis and  $\vec{v}_F$  and  $\gamma$  to be the negatively oriented angle between the vector

$\vec{v}_F$  and the vector  $\vec{v}$ , the coordinates of the vector  $\vec{r}$  are as follows:

$$y_r = L_F \cos \beta + l \cos(\beta - \gamma) \quad (2.48)$$

$$z_r = L_F \sin \beta + l \sin(\beta - \gamma) \quad (2.49)$$

The time derivative is:

$$\dot{y}_r = -L_F \dot{\beta} \sin \beta - l(\dot{\beta} - \dot{\gamma}) \sin(\beta - \gamma) \quad (2.50)$$

$$\dot{z}_r = L_F \dot{\beta} \cos \beta + l(\dot{\beta} - \dot{\gamma}) \cos(\beta - \gamma) \quad (2.51)$$

The squares of the time derivatives are:

$$\dot{y}_r^2 = L_F^2 \dot{\beta}^2 \sin^2 \beta + 2L_F l \dot{\beta}(\dot{\beta} - \dot{\gamma}) \sin \beta \sin(\beta - \gamma) + l^2 (\dot{\beta} - \dot{\gamma})^2 \sin^2(\beta - \gamma) \quad (2.52)$$

$$\dot{z}_r^2 = L_F^2 \dot{\beta}^2 \cos^2 \beta + 2L_F l \dot{\beta}(\dot{\beta} - \dot{\gamma}) \cos \beta \cos(\beta - \gamma) + l^2 (\dot{\beta} - \dot{\gamma})^2 \cos^2(\beta - \gamma) \quad (2.53)$$

Adding up the squares of the time derivatives yields

$$\dot{y}_r^2 + \dot{z}_r^2 = L_F^2 \dot{\beta}^2 + l^2 (\dot{\beta} - \dot{\gamma})^2 + 2L_F l \dot{\beta}(\dot{\beta} - \dot{\gamma}) \cos \gamma \quad (2.54)$$

The kinetic energy of the  $i$ -th point in the tibia segment that is reached by the vector  $\vec{r}$  is

$$T_{T,i} = \frac{1}{2} dm_i (\dot{y}_{r,i}^2 + \dot{z}_{r,i}^2) \quad (2.55)$$

and the total kinetic energy is then

$$T_T = \frac{1}{2} \int_i dm_i (\dot{y}_{r,i}^2 + \dot{z}_{r,i}^2). \quad (2.56)$$

Assuming a 1-dimensional mass distribution  $M_T = \rho L_T$  respectively  $dm_i = \rho dl$  with the constant mass density  $\rho$  and using (2.54) the kinetic energy of the tibia can be written as

$$T_T = \frac{\rho}{2} \int_0^{L_T} dl (L_F^2 \dot{\beta}^2 + l^2 (\dot{\beta} - \dot{\gamma})^2 + 2L_F l \dot{\beta}(\dot{\beta} - \dot{\gamma}) \cos \gamma) \quad (2.57)$$

This is the integration over the tibia from the FTi joint  $l = 0$  to the tarsus  $l = L_T$ . Evaluating the integral leads to:

$$\begin{aligned}
T_T &= \frac{\rho}{2} \left( L_F^2 \dot{\beta}^2 l + \frac{1}{3} l^3 (\dot{\beta} - \dot{\gamma})^2 + L_F l^2 \dot{\beta} (\dot{\beta} - \dot{\gamma}) \cos \gamma \right) \Big|_0^{L_T} \\
&= \frac{\rho}{2} (L_F^2 \dot{\beta}^2 L_T + \frac{1}{3} L_T^3 (\dot{\beta} - \dot{\gamma})^2 + L_F L_T^2 \dot{\beta} (\dot{\beta} - \dot{\gamma}) \cos \gamma) \\
&= \frac{1}{2} (M_T L_F^2 \dot{\beta}^2 + \frac{1}{3} M_T L_T^2 (\dot{\beta} - \dot{\gamma})^2 + M_T L_F L_T^2 \dot{\beta} (\dot{\beta} - \dot{\gamma}) \cos \gamma)
\end{aligned}$$

Now, adding the kinetic rotation energy  $T_F = \frac{1}{6} M_F L_F^2 \dot{\beta}^2 = \frac{1}{2} I_F \dot{\beta}^2$  yields the total kinetic energy  $T_{total} = T$  of the CTr-FTi system:

$$\begin{aligned}
T &= T_F + T_T \\
&= \frac{1}{2} I_F \dot{\beta}^2 + \frac{1}{2} I_T (\dot{\beta} - \dot{\gamma})^2 + \frac{1}{2} M_T L_F^2 \dot{\beta}^2 \\
&\quad + \frac{1}{2} M_T L_F L_T \dot{\beta} (\dot{\beta} - \dot{\gamma}) \cos \gamma
\end{aligned} \tag{2.58}$$

Setting  $\beta = \phi$  and  $\beta - \gamma = \theta$  leads to an expression where both angles are positively oriented and both have the same axis for the zero point:

$$T = \frac{1}{2} I_F \dot{\phi}^2 + \frac{1}{2} I_T \dot{\theta}^2 + \frac{1}{2} M_T L_F^2 \dot{\phi}^2 + \frac{1}{2} M_T L_F L_T \dot{\phi} \dot{\theta} \cos(\phi - \theta) \tag{2.59}$$

A comparison with a double pendulum of two point masses  $m_1, m_2$  fixed at cords of lengths  $l_1, l_2$  (cf. fig 2.11 and for a paradigm Nolting (2010)) shows a similarity in the structure of the appearance of kinematic variables  $\phi$  and  $\theta$  and their time derivatives:

$$T_{dp} = \frac{m_1}{2} l_1^2 \dot{\phi}^2 + \frac{m_2}{2} l_2 \dot{\theta}^2 + \frac{m_2}{2} l_1^2 \dot{\phi}^2 + m_2 l_1 l_2 \dot{\phi} \dot{\theta} \cos(\phi - \theta) \tag{2.60}$$

However, the CTr-FTi system can not be regarded as a system of limbs whose masses are concentrated in one point e.g. the center of mass. Using  $m_1 = M_F$ ,  $m_2 = M_T$ ,  $l_1 = L_F$ ,  $l_2 = L_T$ ,  $I_F^* = \frac{1}{3} M_F L_F^2$ ,  $I_T^* = \frac{1}{3} M_T L_T^2$  in (2.60) and equating coefficients with (2.59) shows a discrepancy for example



in the quadratic terms by a factor 3.

The total kinetic energy in equation (2.59) consists of four terms. The first one describes the femur, that rotates around one of its ends in the origin. The second term describes the same effect with regard to the tibia. Thereby the third term, which is due to *Steiner's theorem*, can be explained: The rotation point of a mass  $M_T$  is shifted by  $L_F$  from the origin and rotates with  $\dot{\beta}$ . The fourth term establishes the fact that the tibia can be folded out or in. This is proportional to the cosine of the angle  $\gamma$ . This term raises the total kinetic energy for an unfolded tibia ( $\gamma = 0$ ) and reduces it for a folded tibia ( $\gamma = 180^\circ$ ).

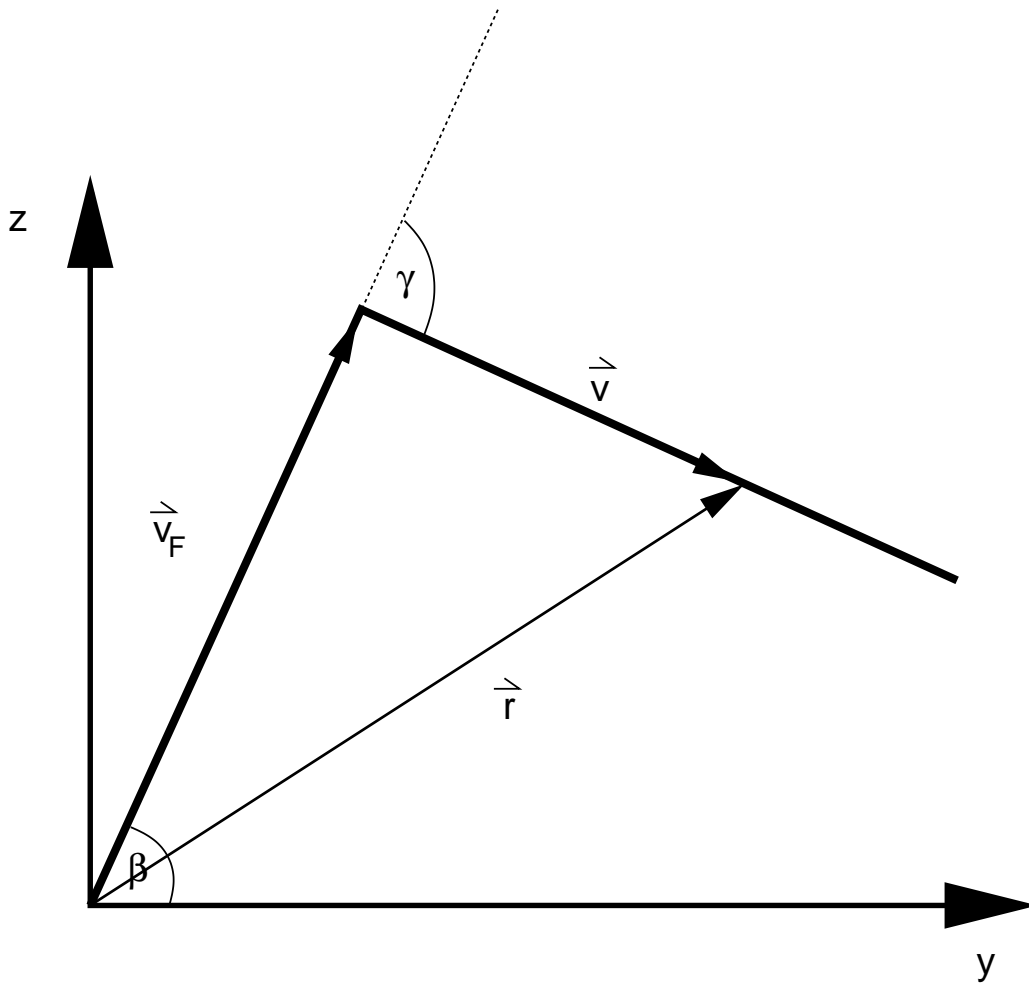


Figure 2.10: Sketch of the two limb system for the integration of kinetic energy necessary for the development of the equations of motion. The femur emanates from the origin of the coordinate system, and it forms the angle  $\beta$  with the  $y$ -axis. The femur moves with velocity  $\vec{v}_F$ . The tibia is flexed from the femur by the angle  $\gamma$  and each point on the tibia in distance  $\vec{r}$  are moved by the velocity  $\vec{v}$ .

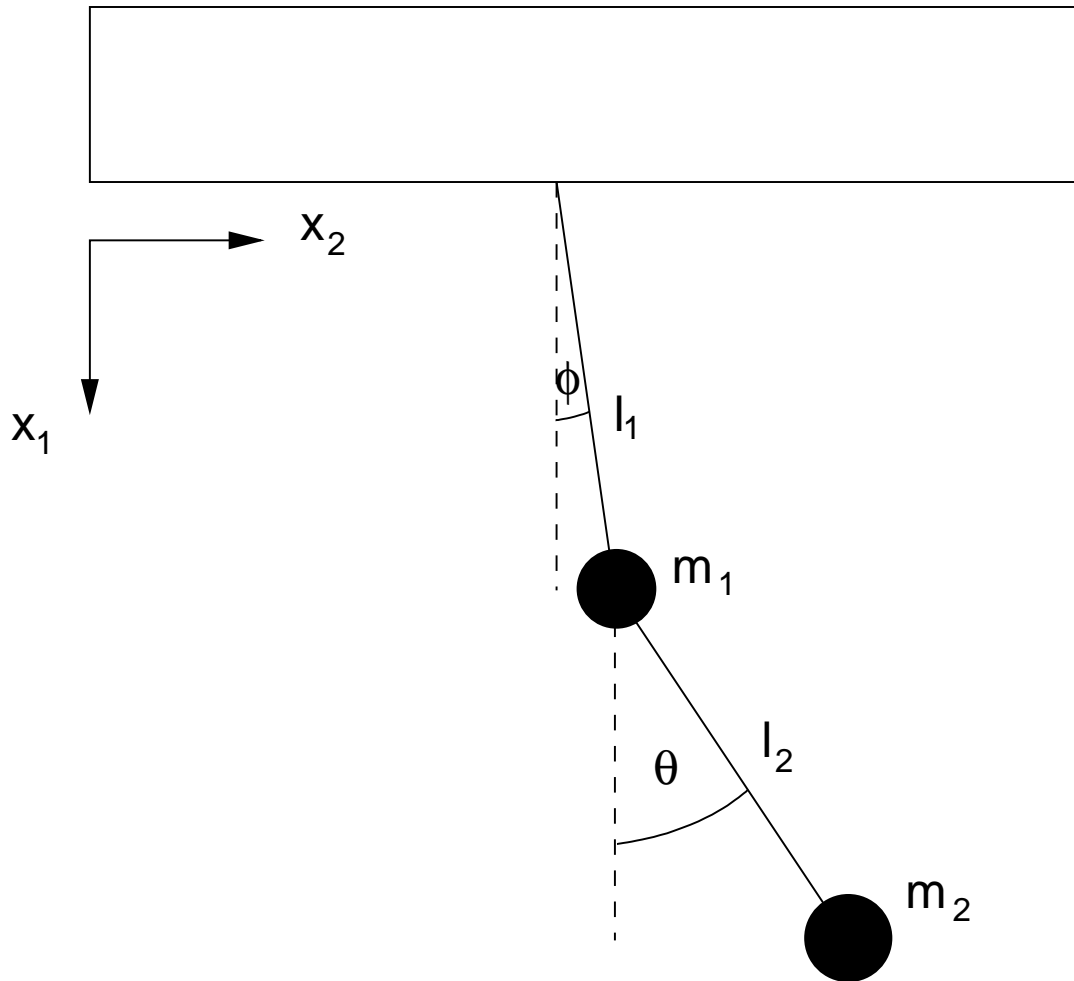


Figure 2.11: Sketch of a double pendulum. A point mass  $m_1$  is attached to a mounting by a cord with length  $l_1$ . The deviation from the equilibrium position is  $\phi$ . A second point mass  $m_2$  is attached to mass  $m_1$  by a cord with length  $l_2$ . The deviation from the equilibrium position is  $\theta$ .

## Potential Energy

The potential energy  $U$  of the CTr-FTi-system is given by

$$\begin{aligned} U &= U_L(l_L(\beta)) + U_D(l_D(\beta)) + U_E(l_E(\gamma)) + U_F(l_F(\gamma)) \\ &= U(l_L(\beta), l_D(\beta), l_E(\gamma), l_F(\gamma)) \end{aligned}$$

The negative partial derivative of the (mechanical) potential energy with respect to the muscle length is equal to the respective muscle force:

$$-\frac{\partial U_L}{\partial l_L} = F_L \quad (2.61)$$

$$-\frac{\partial U_D}{\partial l_D} = F_D \quad (2.62)$$

$$-\frac{\partial U_E}{\partial l_E} = F_E \quad (2.63)$$

$$-\frac{\partial U_F}{\partial l_F} = F_F \quad (2.64)$$

Using  $\beta$  and  $\gamma$  as generalized coordinates the derivatives of the potentials yield the torques, i.e. the generalized forces:

$$\begin{aligned} -\frac{\partial U_L}{\partial \beta} &= -\frac{\partial U_L}{\partial l_L} \frac{\partial l_L}{\partial \beta} = F_L \frac{\partial l_L}{\partial \beta} = M_L \\ -\frac{\partial U_D}{\partial \beta} &= -\frac{\partial U_D}{\partial l_D} \frac{\partial l_D}{\partial \beta} = F_D \frac{\partial l_D}{\partial \beta} = M_D \\ -\frac{\partial U_E}{\partial \gamma} &= -\frac{\partial U_E}{\partial l_E} \frac{\partial l_E}{\partial \gamma} = F_E \frac{\partial l_E}{\partial \gamma} = M_E \\ -\frac{\partial U_F}{\partial \gamma} &= -\frac{\partial U_F}{\partial l_F} \frac{\partial l_F}{\partial \gamma} = F_F \frac{\partial l_F}{\partial \gamma} = M_F \end{aligned}$$

The fiber forces are given by quadratic force length relation (Guschlbauer, 2009)

$$F_L(\gamma) = k_L(l_L(\beta) - l_{L,min})^2 \quad (2.65)$$

$$F_D(\gamma) = k_D(l_D(\beta) - l_{D,min})^2 \quad (2.66)$$

$$F_E(\gamma) = k_E(l_E(\gamma) - l_{E,min})^2 \quad (2.67)$$

$$F_F(\gamma) = k_F(l_F(\gamma) - l_{F,min})^2 \quad (2.68)$$

with the stretch-dependent lengths  $l_L$ ,  $l_D$ ,  $l_E$ ,  $l_F$ , the constant minimal lengths  $l_{L,min}$ ,  $l_{D,min}$ ,  $l_{E,min}$ ,  $l_{F,min}$  and variable spring constants  $k_L$ ,  $k_D$ ,  $k_E$ ,  $k_F$  (see section 2.3).

## Equations of Motion

The equations of motion will be deduced from the Lagrangian.

$$\mathcal{L} = T - U = T(\gamma, \dot{\beta}, \dot{\gamma}) - U(\beta, \gamma)$$

The derivatives are:

$$\frac{\partial \mathcal{L}}{\partial \beta} = -\frac{\partial U}{\partial \beta} = F_L \frac{\partial l_L}{\partial \beta} + F_D \frac{\partial l_D}{\partial \beta} \quad (2.69)$$

$$\begin{aligned} \frac{\partial \mathcal{L}}{\partial \gamma} &= \frac{\partial T}{\partial \gamma} - \frac{\partial U}{\partial \gamma} \\ &= \frac{\partial T}{\partial \gamma} + F_E \frac{\partial l_E}{\partial \gamma} + F_F \frac{\partial l_F}{\partial \gamma} \\ &= -\underbrace{\left(\frac{1}{2} M_T L_F L_T \sin \gamma\right)}_C \dot{\beta} (\dot{\beta} - \dot{\gamma}) + F_E \frac{\partial l_E}{\partial \gamma} + F_F \frac{\partial l_F}{\partial \gamma} \end{aligned} \quad (2.70)$$

$$\begin{aligned} \frac{\partial \mathcal{L}}{\partial \dot{\beta}} &= \frac{\partial T}{\partial \dot{\beta}} \\ &= I_F \dot{\beta} + I_T (\dot{\beta} - \dot{\gamma}) + M_T L_F^2 \dot{\beta} + \frac{1}{2} M_T L_F L_T \cos \gamma (2\dot{\beta} - \dot{\gamma}) \\ &= \underbrace{(I_F + I_T + M_T L_F^2 + M_T L_T L_F \cos \gamma)}_A \dot{\beta} - \underbrace{(I_T + \frac{1}{2} M_T L_T L_F \cos \gamma)}_B \dot{\gamma} \\ \frac{d}{dt} \frac{\partial \mathcal{L}}{\partial \dot{\beta}} &= A \ddot{\beta} - B \ddot{\gamma} - \underbrace{\left(\frac{1}{2} M_T L_F L_T \sin \gamma\right)}_C (2\dot{\beta} - \dot{\gamma}) \dot{\gamma} \end{aligned} \quad (2.71)$$

$$\begin{aligned} \frac{\partial \mathcal{L}}{\partial \dot{\gamma}} &= \frac{\partial T}{\partial \dot{\gamma}} \\ &= I_T (\dot{\beta} - \dot{\gamma}) - \frac{1}{2} M_T L_F L_T \dot{\beta} \cos \gamma \\ &= -\underbrace{(I_T + \frac{1}{2} M_T L_T L_F \cos \gamma)}_B \dot{\beta} + I_T \dot{\gamma} \\ \frac{d}{dt} \frac{\partial \mathcal{L}}{\partial \dot{\gamma}} &= -B \ddot{\beta} + I_T \ddot{\gamma} + \underbrace{\left(\frac{1}{2} M_T L_F L_T \sin \gamma\right)}_C \dot{\beta} \dot{\gamma} \end{aligned} \quad (2.72)$$

Substituting these results into the corresponding Euler-Lagrange equations, there are

$$A\ddot{\beta} - B\ddot{\gamma} - C(2\dot{\beta} - \dot{\gamma})\dot{\gamma} - \underbrace{F_L \frac{\partial l_L}{\partial \beta} - F_D \frac{\partial l_D}{\partial \beta}}_{F_1} = 0. \quad (2.73)$$

$$-B\ddot{\beta} + I_T\ddot{\gamma} + C\dot{\beta}^2 - \underbrace{F_E \frac{\partial l_E}{\partial \gamma} - F_F \frac{\partial l_F}{\partial \gamma}}_{F_2} = 0 \quad (2.74)$$

Multiplication of (2.74) with  $B$  and adding this to (2.73) multiplied with  $I_T$  yields

$$\ddot{\beta} = -\frac{BC}{D(\gamma)}\dot{\beta}^2 + \frac{CI_T}{D(\gamma)}(2\dot{\beta} - \dot{\gamma})\dot{\gamma} - \frac{I_T}{D(\gamma)}F_1 - \frac{B}{D(\gamma)}F_2 \quad (2.75)$$

with the determinant

$$D(\gamma) = AI_T - B^2$$

Putting equation (2.75) in (2.74) yields:

$$\ddot{\gamma} = \frac{B}{I_T D(\gamma)} \left[ -C \left( B + \frac{D(\gamma)}{B} \right) \dot{\beta}^2 + CI_T (2\dot{\beta} - \dot{\gamma}) \dot{\gamma} - I_T F_1 - \left( B + \frac{D(\gamma)}{B} \right) F_2 \right] \quad (2.76)$$

Finally, using the dissipation function

$$G = -\frac{c_2 b_{v,LD} r}{2} \dot{\beta}^2 - \frac{5d^2 b_{v,FE}}{2I_T} \dot{\gamma}^2 \quad (2.77)$$

with the constants  $c_2$ ,  $b_{v,LD}$ ,  $b_{v,FE}$ ,  $r$ ,  $d$  and  $I_T$  used for the uncoupled systems and adding the terms

$$\frac{\partial G}{\partial \dot{\beta}} = -c_0 b_{v,LD} r \dot{\beta} \quad (2.78)$$

$$\frac{\partial G}{\partial \dot{\gamma}} = -\frac{5d^2 b_{v,FE}}{I_T} \dot{\gamma} \quad (2.79)$$

leads to the following equations of motion

$$\begin{aligned}\ddot{\beta} &= -\frac{BC}{D(\gamma)}\dot{\beta}^2 + \frac{CI_T}{D(\gamma)}(2\dot{\beta} - \dot{\gamma})\dot{\gamma} - \frac{I_T}{D(\gamma)}F_1 - \frac{B}{D(\gamma)}F_2 - c_0b_{v,LD}r\dot{\beta} \\ \ddot{\gamma} &= \frac{B}{I_T D(\gamma)} \left[ -C\left(B + \frac{D(\gamma)}{B}\right)\dot{\beta}^2 + CI_T(2\dot{\beta} - \dot{\gamma})\dot{\gamma} - I_T F_1 - \left(B + \frac{D(\gamma)}{B}\right)F_2 \right] \\ &\quad - \frac{5d^2b_{v,FE}}{I_T}\dot{\gamma}\end{aligned}$$

As it is shown in Appendix B, the mechanical coupling between the femur and tibia can be neglected.

## Effective momentum of inertia

Even though the effect of the mechanical coupling between femur and tibia is small enough to be neglected (cf. Appendix B), the moment of inertia of the tibia will still affect the mechanical motion of the femur. To take this into account, a correction is made here by computing the so-called effective moment of inertia of the femur-tibia mechanical system (see Knops et al. (2012)). First, the momentum is

$$\tilde{I}_{FT}(\gamma) = I_F + I_T + M_T L_F^2 + M_T L_T L_F \cos \gamma \quad (2.80)$$

with  $I_F = \frac{1}{3}M_F L_F^2$  and  $I_T = \frac{1}{3}M_T L_T^2$  the momentums of inertia of the femur and the tibia, with their masses  $M_F$  and  $M_T$  and lengths  $L_F$  and  $L_T$ . Then, the effective momentum of inertia is calculated by averaging over the range of  $\gamma$ .

$$I_{FT} = \frac{1}{\gamma_{max} - \gamma_{min}} \int_{\gamma_{min}}^{\gamma_{max}} \tilde{I}_{FT}(\gamma) d\gamma \quad (2.81)$$

$$I_{FT} = I_F + I_T + M_T L_F^2 + M_T L_T L_F \frac{\sin \gamma_{max} - \sin \gamma_{min}}{\gamma_{max} - \gamma_{min}} \quad (2.82)$$

where  $\gamma_{max}$  and  $\gamma_{min}$  are the extremal values of the FTi-joint angle, whose numerical values are listed in tables A.14, A.18 and A.21. This procedure is



a first approach and a rough approximation, but it yields acceptable results. The values of  $I_{FT}$  are used whenever the tibia is not amputated.

## 2.5 Synthesis of neuronal and mechanical models

In this section, the principles of the neuro-muscular coupling as described in Toth and Gruhn (2011), Daun-Gruhn et al. (2011), Toth et al. (2012) and Knops et al. (2012) are briefly recapitulated. Subsequently, it is shown how sensory signals induced by mechanical motion of the joints have been included in the single-leg, and the multi-leg model.

### 2.5.1 A single joint

Figure 2.12 shows a single joint network consisting of interneurons, motoneurons and muscles controlled by the latter. The interneurons C1 and C2 form the CPG that rhythmically drives the motoneurons MN1 and MN2 via the inhibitory interneurons IN1 and IN2. This is achieved by rhythmic inhibition from the CPG and tonic depolarization of the MN by the conductance  $g_{MN}$  (cf. experimental results by Büschges (1998, 2005); Gabriel (2005); Westmark et al. (2009)). The CPG neurons receive central excitatory drive  $g_{app1}$  and  $g_{app2}$  and peripheral input through the pathway constituted via the interneurons IN3 and IN4. It represents sensory input from the campaniform sensilla (CS) and conveys the excitation to C2 via IN4 and the inhibition to C1 via IN3, which itself is excited by IN4. Experimental findings and accompanying simulation results regarding the LD system underlie the construction of this pathway. The same basic structure mentioned above is used

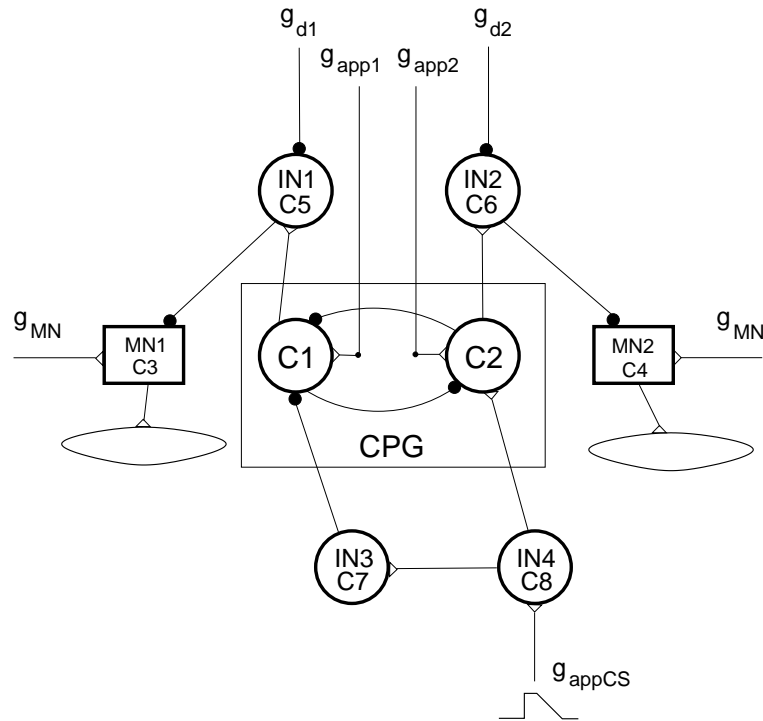


Figure 2.12: Neuro-mechanical network of a single joint. CPG: central pattern generator; MN: motoneuron; IN: interneuron; INCS: sensory interneuron receiving stimuli from the CS; empty triangles: excitatory synapses; filled circles: inhibitory synapses;  $g_{app1}$ ,  $g_{app2}$  are the conductances of the central driving currents to the CPG neurons,  $g_{d1}$ ,  $g_{d2}$  are those of the driving currents to the interneurons IN1, IN2, respectively, which inhibit the corresponding MNs but receive excitation from the CPG. The conductance  $g_{appCS}$  determines the intensity of the excitation from the stimuli to the campaniform sensilla (CS). The ramp symbol stands for the CS stimulation (Toth and Gruhn, 2011).

for all joints in all legs, but numerical values of the parameters may differ (cf. Appendix A).

### 2.5.2 Neuro-muscular coupling

The neuro-muscular coupling is taken as an excerpt from Toth et al. (2012). The time course of the variable spring constant  $k$  in the muscle model is described by:

$$k(t) = k_{\infty} - [k_{\infty} - k(t_0)] \exp(-(a_0 + b)(t - t_0)) \quad (2.83)$$

during an action potential, where  $a_0$  is much larger than  $b$ , and

$$k(t) = k(t_1) \exp(-b(t - t_1)) \quad (2.84)$$

otherwise.  $k_{\infty}$  denotes the stationary value of  $k(t)$ .

### 2.5.3 A single leg

This section treats of three leg joints, that are coupled together considering feedback signals from sense organs (see Knops et al. (2012)). Figure 2.13 shows the neuro-muscular network of a single leg in the stick insect. It is a network that is composed of three joints introduced in section 2.5.1. These are from top to bottom the PR system, the LD system and the FE system. The structure of each network is fundamentally the same. They just differ from each other with respect to peripheral input from the CS to the LD system. This perception ascribes to experiments by Borgmann et al. (2011) where the stimulation of the CS in a partially amputated femur of the middle leg can terminate the permanent silent state of the depressor MN that goes along with the activation of the levator MN. Therefore, it is assumed that in an intact middle leg the LD system receives a sufficiently high excitation

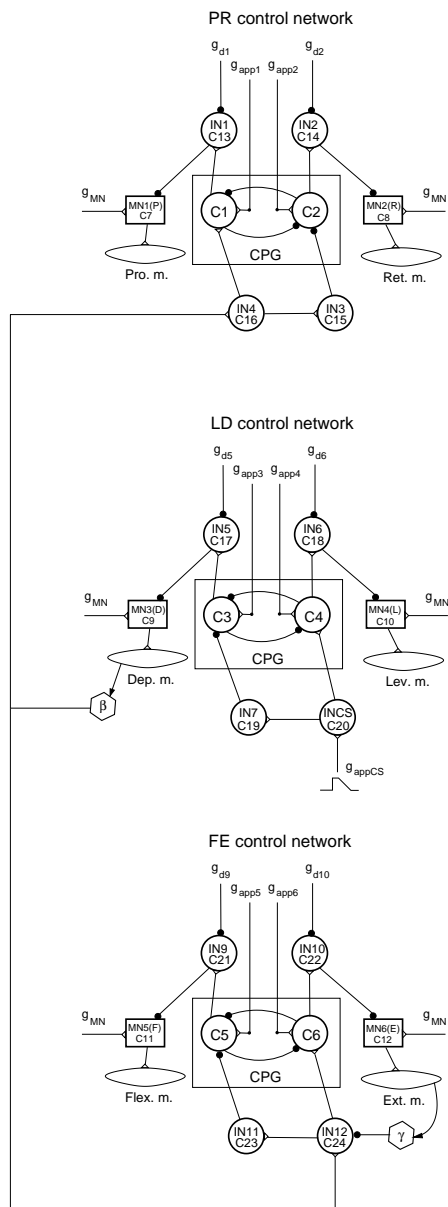


Figure 2.13: Coupled neuro-mechanical system consisting of three single joints (see figure 2.12). Pro m., Ret m., Dep m., Lev m., Flex m., Ext m.: the muscles innervated by the corresponding MNs.  $\beta$ -hexagon in the LD system: combined sensory signal originating in the LD system and conveyed to the PR and FE system;  $\gamma$ -hexagon in the FE system: inhibitory signal from the femoral chordotonal organ counteracting the excitatory signal from the LD system.

from the CS that puts the CPG into its active state (Daun-Gruhn et al., 2011). The peripheral input excites the depressor CPG neuron C4 via IN8 and inhibits the levator CPG neuron C3 per IN7. The levator and depressor muscles are innervated by their respective motoneurons MN3 and MN4. The threshold value of the angle  $\beta$  represents peripheral excitatory signals such as ground contact and load and position signals. That means, if the threshold angle in the LD is exceeded the PR system and the FE system will receive an excitatory input signal. These sensor signals can be merged in the case when environmental influences are not changed during walking. For example, if the slope changes during walking load and position signals have to be treated separately.

In the PR system the IN4 excites the CPG neuron of the retractor C1 and IN3 inhibits the CPG neuron of the protractor C2. The protractor and retractor muscles are activated by the respective motoneurons MN1 and MN2. In the FE system the flexor CPG neuron C6 is excited by IN12 whereas the extensor CPG neuron C5 is inhibited by IN11. The flexor and extensor muscles are innervated by their respective motoneurons MN5 and MN6. Both the PR and the FE system function as reflex chains in this case. They are not active in the absence of the (excitatory) peripheral input and can be brought to movement under the impact of sensory signals. Hence, the coupling is arranged such that the switch from protraction to retraction and from extension to flexion are elicited at the begin of the stance phase, i.e. when the angle  $\beta$  attains a critical value. The interneuron IN12 receives an inhibitory intrajoint input signal from the femoral chordotonal organ (fCO) represented by the angle  $\gamma$ .

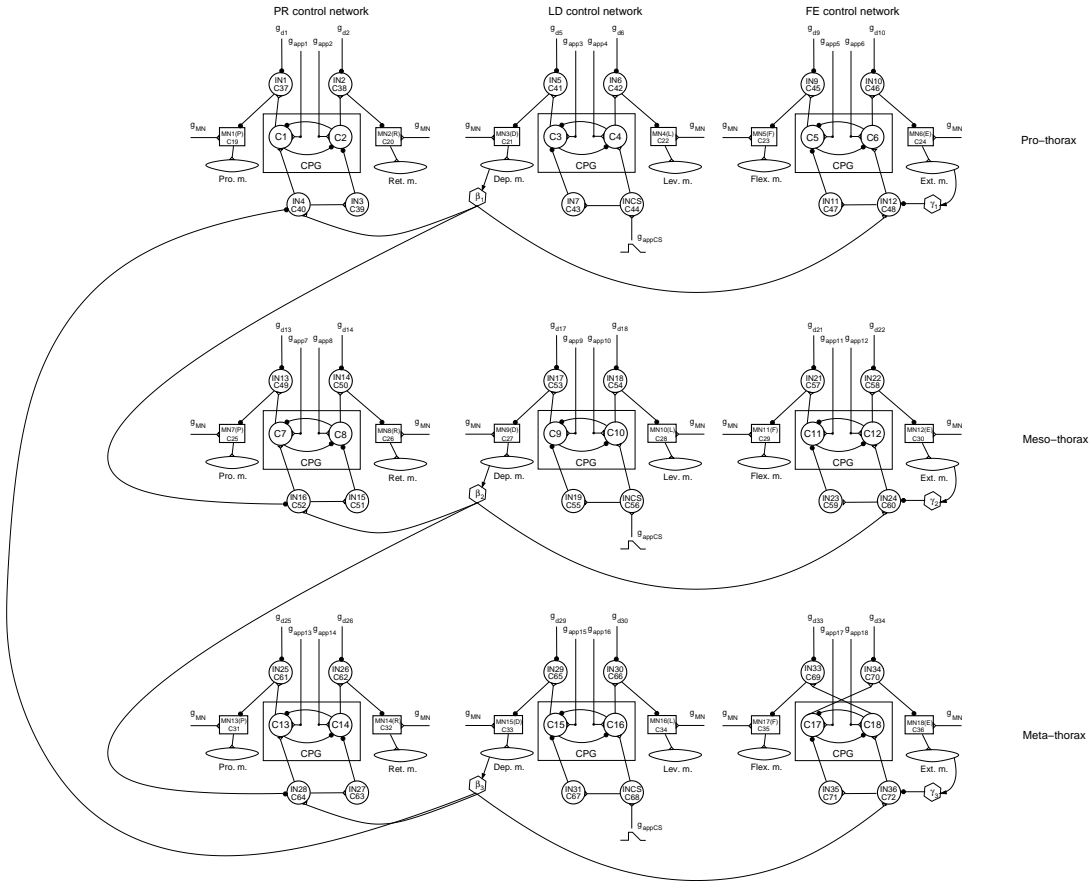


Figure 2.14: Composition of the model for three ipsilateral legs (see figure 2.13) complete with intersegmental coupling by inhibitory synapses emanating from the hexagons with the  $\beta_i$  and entering into the peripheries of the PR systems. The FE system of the meta-thorax differs from the other two FE systems by crossed connections from the CPG to the MNs.

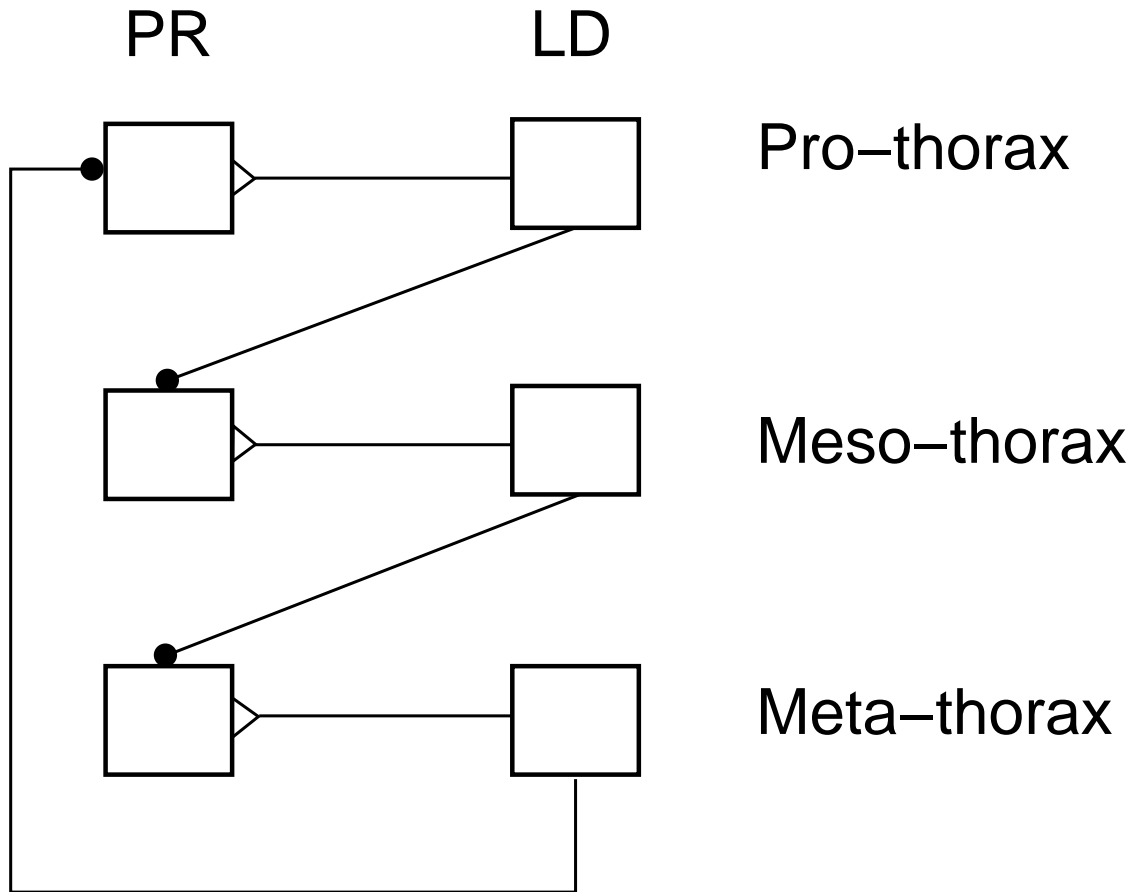


Figure 2.15: Simplified sketch of the network in figure 2.14. Boxes: neuro-mechanical systems for the PR systems (left row) and the LD systems (right row); empty triangles: excitatory synapses; filled circles: inhibitory synapses. Upper boxes: front leg, middle boxes: middle leg, bottom boxes: hind leg.

### 2.5.4 Multiple legs

Figure 2.14 shows the neuro-muscular network for three coupled legs in the stick insect. It consists of three single legs that are intersegmentally coupled via sensory signals represented by the angles  $\beta_1$ ,  $\beta_2$  and  $\beta_3$  (corresponding to the angle  $\beta$  defined above). The cyclic inhibitory influence from the respective LD systems is directed to the next caudal PR system, in other words, the middle leg receives input from the front leg, the hind leg receives input from the middle leg whereas the front leg receives input from the hind leg. The intersegmental influence connection ends at the same peripheral neuron as the intrasegmental influence connection. For example, the connection from  $\beta_1$  in the front leg and the connection from  $\beta_2$  in the middle leg both end at the IN16 of the PR system in the middle leg. A simplified sketch of the intersegmental connection of three legs is shown in figure 2.15. The FE system is not shown here because there is no contribution from it to the intersegmental connection.

The different types of gaits (tripod or tetrapod) are generated by specifying proper starting times of the intrinsically oscillating LD systems. In the case of an ideal tetrapod only one ipsilateral leg can be in swing phase. That means, if one considers equal properties (such as the ratio of swing and stance phase or cyclic period) for each of the ipsilateral legs, the starting times of the legs will have to differ by one third of the cyclic period (see figure 2.17). This approximation relies on experimental observations by Graham (1972). Due to a metachronal wave traveling from rear to front the middle leg is lifted about the begin of the stance phase in the hind leg, the front leg is lifted about the begin of the stance phase in the middle leg and the hind leg is lifted about the begin of the stance phase in the front leg and so on. In the case of an ideal tripod alternating two legs or one leg is in swing. More precisely, on the



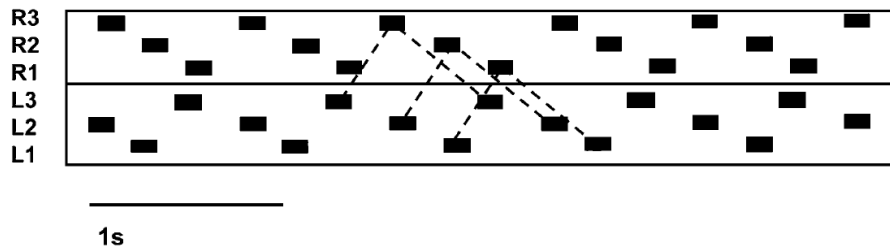


Figure 2.16: Foot fall pattern during a tetrapod gait in the stick insect considering front legs (1), middle legs (2), hind legs (3) on the left (L) and the right (R) side. Black boxes mark the swing phase of the respective leg (Graham, 1972).

ipsilateral side both the front leg and hind leg are in the swing phase where the middle leg is in the stance phase, or vice versa. These are two states that require a phase lag of one half (see figure 2.19). This again relies on experimental observations (Delcomyn, 1971). Furthermore, the tripod gait is used during fast walking in insects. Consequently, the central drive to the LD systems is tuned so that the cyclic period shortens. Figures 2.16 and 2.18 show examples for ideal walking patterns with the two gaits.

A switch between two gaits is achieved by the central inhibition of the levator CPG neuron in the respective leg, i.e. by forcing the depressor CPG neuron to be active and then resetting the CPG at proper times, with the result that the phase lag between the legs attains suitable values.

Once a simulation with the ipsilateral network (figure 2.14) is done, two identical walking patterns, one for the left side and one for the right side, can be put together side by side with a shift corresponding to the phase lag. This is an artificial contralateral coupling that saves the expansion of increasing the network. The main point is to gain insight into the impact that a gait switch has on the walking patterns in the stick insect.

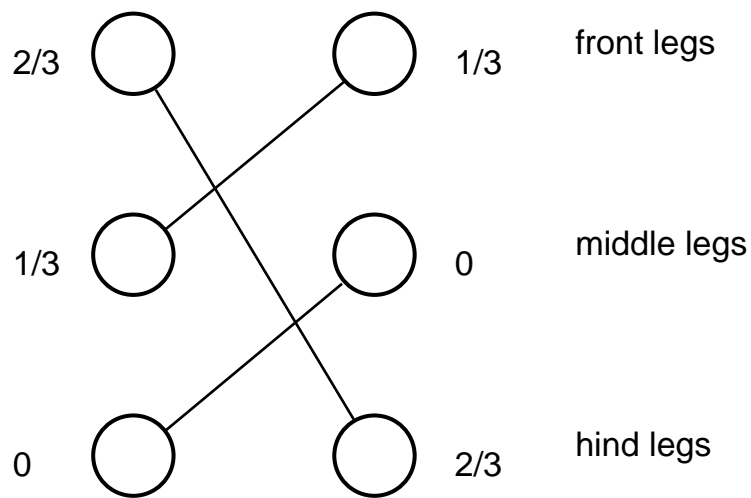


Figure 2.17: Phase lags in the tetrapod gait of the stick insect. No specification is made about left or right due to mirroring. Legs (circles) that step synchronously are connected with a line. In this example, the time reference is set to zero for the left hind leg (L3) and thus the right middle leg (R2). It is indicated by the numbers 0 alongside the circles. The cycles of left middle (L2) and the right front leg (R1) are delayed by a third of the period (numbers  $1/3$  alongside the circles) and the left front leg (L1) and the right hind leg (R3) are delayed by two third of the period (numbers  $2/3$  alongside the circles).

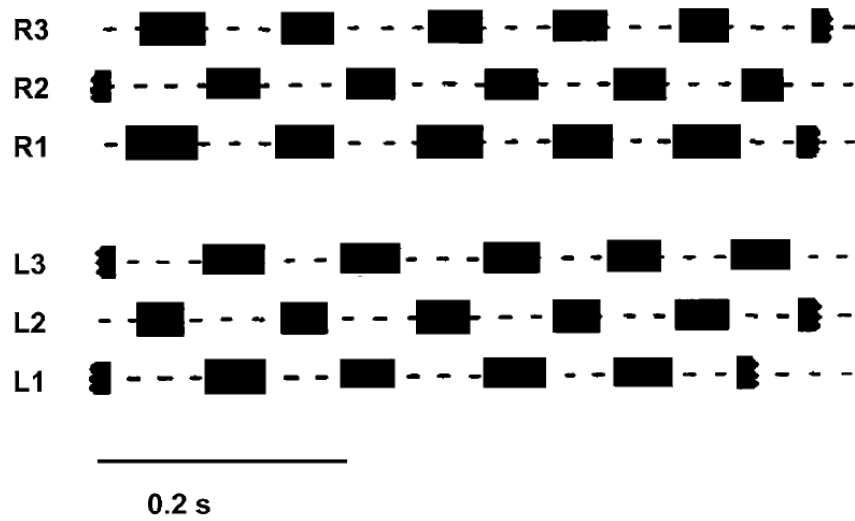


Figure 2.18: Foot fall pattern during a tripod gait in the stick insect considering front legs (1), middle legs (2), hind legs (3) on the left (L) and the right (R) side. Black boxes mark the swing phase of the respective leg (Delcomyn, 1971).

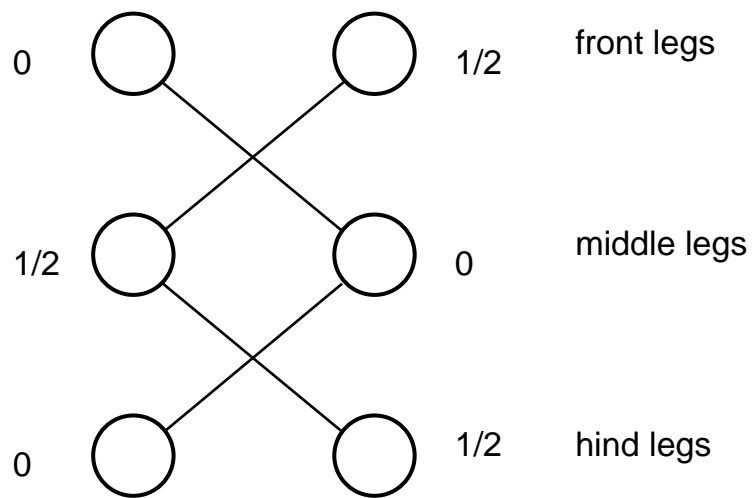


Figure 2.19: Phase lags in the tripod gait of the stick insect. No specification is made about left or right due to mirroring. Legs (circles) that step synchronously are connected with a line. The time reference in this example is set to zero for the left hind leg (L3) and thus the right middle leg (R2) and the left front leg (L1). This is indicated by the numbers 0 alongside the circles. The cycles of the right hind leg (R3), left middle (L2) and the right front leg (R1) are delayed by one half of the period with respect to the reference (numbers 1/2 alongside the circles).

## 2.6 Implementation of the model

Each simulation presented in this study is done in one of the following three ways:

- i) Simulations for the adjustment of dynamical parameters are done with the Octave software package (Eaton, 2008).
- ii) The numerical simulations of the neuro-mechanical network are done by using the CVODE software package (Cohen and Hindmarsh, 1996) for numerical integration that is based on the programming language C. The single joint system consists of 8 neurons and is described by 26 differential equations. A 9 s long sequence takes a computation time of 2 s. The single leg system (24 neurons) is described by 78 equations and takes 15 s to solve a 9 s long sequence. A three leg system (72 neurons) consists of 234 equations and takes about 180 s to solve a 9 s long sequence.
- iii) Graphical simulations for the visualization of insect walking (supplementary material on Gruhn Lab Webpage (2012) (see references)) are done with the physics simulator ODE Smith (2006). Despite the features of that simulator (calculation of torques, forces, consideration of friction with the ground), this study does not make use of it (see discussion in section 4). The pre-calculated output of the neuro-mechanical system (angular motion) is applied to the joints of the stick insects' body in the ODE environment, such that the 3-dimensional interaction of all joints and segments in relation to each other can easily be observed. This procedure is a special feature in this study that supports the conventional depiction of the time course of physical quantities. The simulation with ODE is to be considered as a qualitative one and not a quantitative one. Moreover, the simulator allows the investigation of the propulsion and locomotion of the insect body.

There are different setups for graphical simulation with ODE:

1. The stick insect (one-leg preparation) is fixed to a **horizontal slider**: It can only move forth and back. It can neither move to the left nor to the right nor up or down. This setup is mostly employed for the observation of the propulsion during forward and backward stepping. The tarsus has friction with the ground.
2. The stick insect (one-leg preparation) is fixed to a **vertical slider**: It can only move up and down. It can neither move forward or backward nor left or right. The tarsus has no friction with the ground. The setup is mostly employed for the observation of angular motion in close proximity in a constant view. Apart from the slight bouncing of the body this resembles a slippery surface experiment.
3. A variation of the latter setup is applied for the six-legged animal during the tripod gait, tetrapod gait and their transitions. Hereunto, the body is attached to a **hinge joint combined with a vertical slider**. Thereby, the bobbing movement of the anterior and posterior parts of the body can be additionally be ensured. For example, the abdomen can be declined to the ground.
4. A **restrictively free walking insect** consisting of two stepping middle legs which have friction with the ground and each two hind and front legs kept at fixed joint angles: The fixed legs have no friction with the ground and stabilize the body. There is no contralateral coupling between the two stepping legs. The input originates from two one-leg simulations (not necessarily the same) properly shifted in time.
5. A **free walking insect** consisting of six stepping legs which have friction with the ground: The left and right ipsilateral sides are simulated

separately. There is no contralateral coupling between the two sides. The input originates from the two simulations properly shifted in time.

# Chapter 3

## Results

In this section, an intersegmental network for the locomotion of the stick insect is going to be used for the simulation of insect walking. It is a network that consists of three legs with three joints each. The mechanics of the joints established for the middle legs can simply be applied to the front and the hind legs. Nevertheless, a few dynamical parameters have to be tuned in the other ipsilateral legs due to different leg sized and masses. The neuronal system of all joints is assumed to be identical with a few exceptions that are mentioned where relevant. Afterwards the three joints are coupled intrasegmentally via sensory feedback. The resulting one-leg system can easily be applied to other legs considering intersegmental coupling.

The study begins with the neuro-mechanical properties of the FE system in the well-investigated middle leg (Knops et al., 2012). After the survey of the FE system, the PR and LD system are added; in order to investigate the locomotion of the intact middle leg (Toth et al., 2012). The application to the front and hind leg, then, allows an examination of locomotion on the ipsilateral side of the stick insect.

Section 3.1 concerns the determination of mechanical parameters in the FE



system in the middle leg (Knops et al., 2012). The properties of angular motion, angular velocity of the FTi-joint as well as the muscle forces and lengths are considered. The applied method can be transferred to the PR and LD system of the middle leg (Toth et al., 2012) as well as all the joints of the other legs (see Appendix A). Furthermore, the neuro-mechanical performance of the isolated FE system (Knops et al., 2012) is studied. Section 3.2 treats of the simulation of locomotion in a single leg that consists of a coupled system of three joints (Knops et al., 2012). It begins with a detailed study of forward stepping and switching mechanisms to backward and side-ward stepping in the middle leg in sections 3.2.1 and 3.2.2 (Toth et al., 2012; Knops et al., 2012). This leads to the view on different strategies for curve walking in section 3.2.3 (Knops et al., 2012). The extension of the coupling scheme to the front and the hind leg on the basis of the results of the isolated joints is done in section 3.2.4. Finally, section 3.3 deals with the nature of intersegmental coupling in different gaits and switching mechanisms between gaits.

## 3.1 The single joint system

### 3.1.1 The mechanical motion

Using equation (2.43) with extremal angles  $\gamma_{min} = 45^\circ$  and  $\gamma_{max} = 110^\circ$  (see table A.14) yields a ratio  $a_{FE} = 0.013$  for the extension and a ratio  $a_{FE} = 0.580$  for the flexion. This is a quotient of the spring constants of the antagonistic muscle pair, hence their absolute value is unknown. Setting the spring constant for the extensor muscle during flexion to a certain value, for instance,  $k_E = 510 \frac{\text{mN}}{\text{mm}^2}$ , this yields a value of  $k_F = 296 \frac{\text{mN}}{\text{mm}^2}$  during flexion. With a viscosity constant  $b_{v,FE} = 12.5 \frac{\text{g}}{\text{s}}$  for both muscles. The time course

of the angular movement at the FTi-joint is shown in figure 3.1 A. The pe-

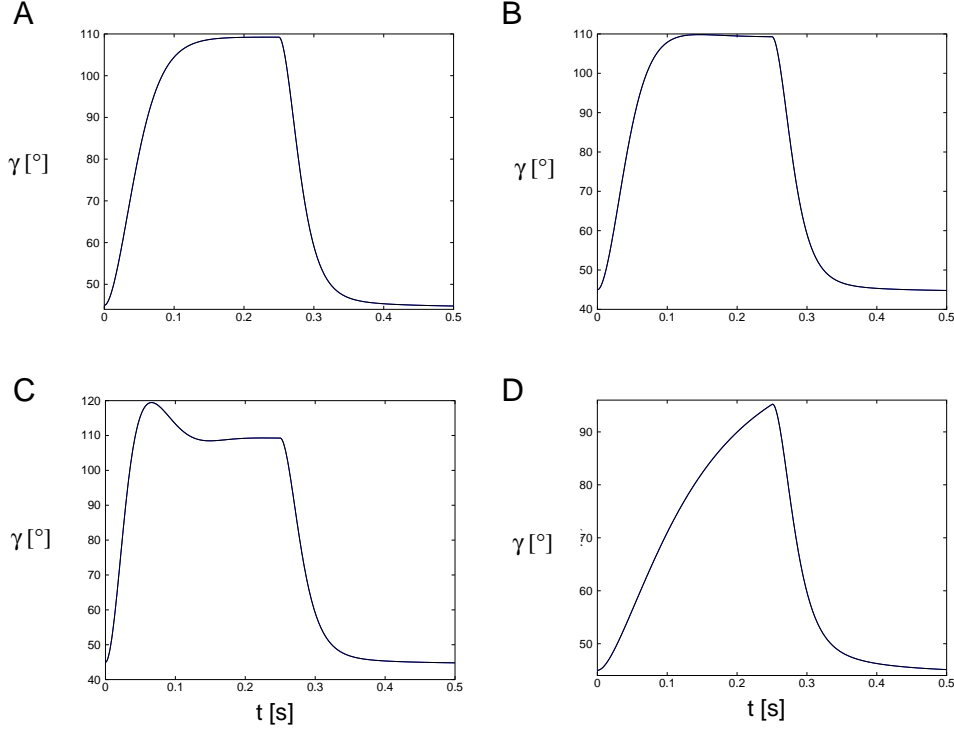


Figure 3.1: Motion of the joint angle  $\gamma$  in the FTi-joint under the variation of the spring constant exemplarily for the flexion. A:  $k_E = 510 \frac{\text{mN}}{\text{mm}^2}$  and  $k_F = 296 \frac{\text{mN}}{\text{mm}^2}$ , B:  $k_E = 700 \frac{\text{mN}}{\text{mm}^2}$  and  $k_F = 406 \frac{\text{mN}}{\text{mm}^2}$ , C:  $k_E = 1100 \frac{\text{mN}}{\text{mm}^2}$  and  $k_F = 638 \frac{\text{mN}}{\text{mm}^2}$ , D:  $k_E = 250 \frac{\text{mN}}{\text{mm}^2}$  and  $k_F = 145 \frac{\text{mN}}{\text{mm}^2}$ .

riod is set to  $T_P = 500$  ms and a phase relation of 1:1 between flexion and extension is assumed (Graham, 1972; Büschges, 2005). The angular motion begins with flexion and switches at an accurate time point  $t = 250$  ms to extension. Then, at  $t = 500$  ms, the switch to flexion would happen again. The numerical values of the spring constant during extension are listed in table A.14. Now, holding the viscosity  $b_{v,FE}$  at a fixed value and setting  $k_E$  and therefore  $k_F = a_{FE}k_E$  to higher values, the angular motion becomes quicker, that means, the curve is steeper during flexion (figure 3.1 B and C).

With increasing spring constants this can result in an overshoot beyond the maximal angle  $\gamma_{max} = 110^\circ$ . Conversely, setting  $k_E$  and  $k_F = a_{FE}k_E$  to smaller values has the effect of a slower movement (cf. Fig 3.1 D). It can result in such a slow motion that the maximal angle  $\gamma_{max} = 110^\circ$  is not attained during flexion. The same applies to the dynamical parameters during extension. With the variation of the viscosity constant while holding the spring constants fixed, the motion can be made slower by increasing  $b_{v,FE}$  or faster by decreasing  $b_{v,FE}$ .

The chosen values for dynamical parameters are listed in table A.14.

The numerical values of the dynamical parameters of the PR system and the LD system are determined in a similar way. The cyclic period is the same as in the previous case. However, the phase relation for retraction and protraction is 1:3 whereas the phase relation for levation and depression is 3:5 (Büschges, 2005). Thus, the phase durations are  $T_{ret} = 125$  ms for retraction,  $T_{pro} = 375$  ms for protraction,  $T_{lev} = 188$  ms for levation and  $T_{dep} = 312$  ms for depression. Considering the extremal angles in the PR system (see table A.17), the dynamical parameters are adjusted with the same requirements. With regard to the LD system, there is a need for a faster lift-off and a faster touch-down of the leg. So the spring constants  $k_L$  and  $k_D$  are tendentially greater or the viscosity constant  $b_{v,LD}$  is tendentially smaller. The numerical values of the dynamical parameters – as well as the used segment sizes and masses – are listed in tables A.13 - A.16.

Finally, assuming that the front and hind leg have equal geometries and taking the specific values of the extremal joint angles into account, the numerical values of the dynamical parameters can be determined by using the corresponding segment sizes and masses. The values are listed in tables A.18 - A.23.

### 3.1.2 The neuro-mechanical system

The time points for phase switching in the muscles are determined by the CPG. If the parameters  $\epsilon$  and  $C_m$  of the CPGs are tuned appropriately, the cyclic period will be adjusted to  $T_P = 510$  ms. The phase relations between antagonistic CPG neurons are adjusted by tuning the central input values  $g_{app,i}$  that are listed in table A.2. Figure 3.2 shows the time course of CPG neurons, motoneurons and angular motion in the FTi-joint of the middle leg.

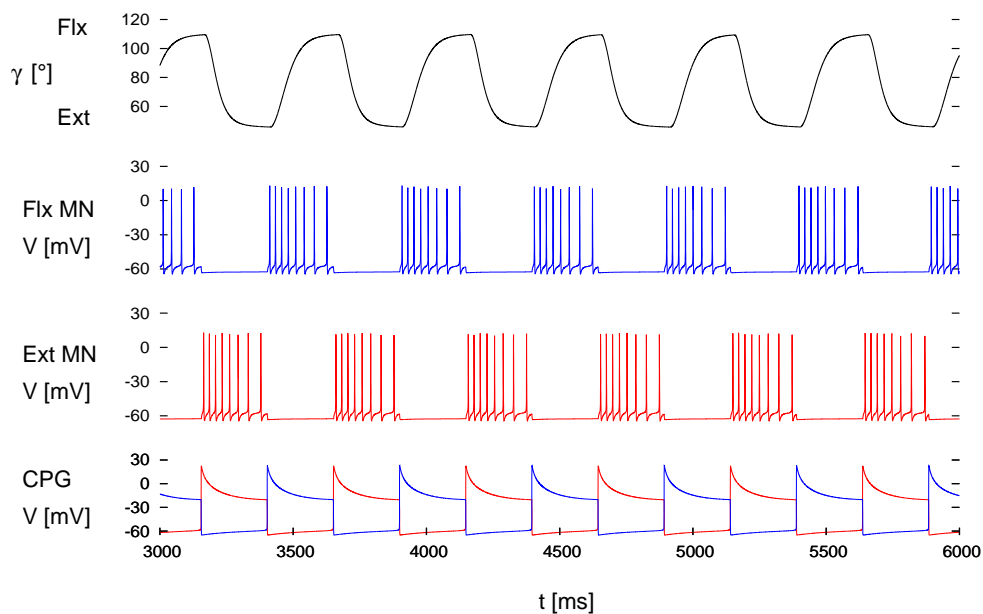


Figure 3.2: Simulation results obtained with the model of a single, isolated FTi-joint. Time course of the angle  $\gamma$  describing the mechanical movement of the tibia (top panel); corresponding flexor motoneuron activity (blue, second panel); extensor motoneuron activity (red, third panel); and CPG activity (bottom panel).

The bottom panel anon shows the CPG activity while the two middle panels show the motoneuron activities. The activity of the extensor CPG

neuron (red, bottom panel) inhibits the activity of the flexor motoneuron (blue, second panel) via the inhibitory interneuron IN1 (cf. figure 2.12). Similarly, the extensor motoneuron (red, third panel) is inhibited by IN2.

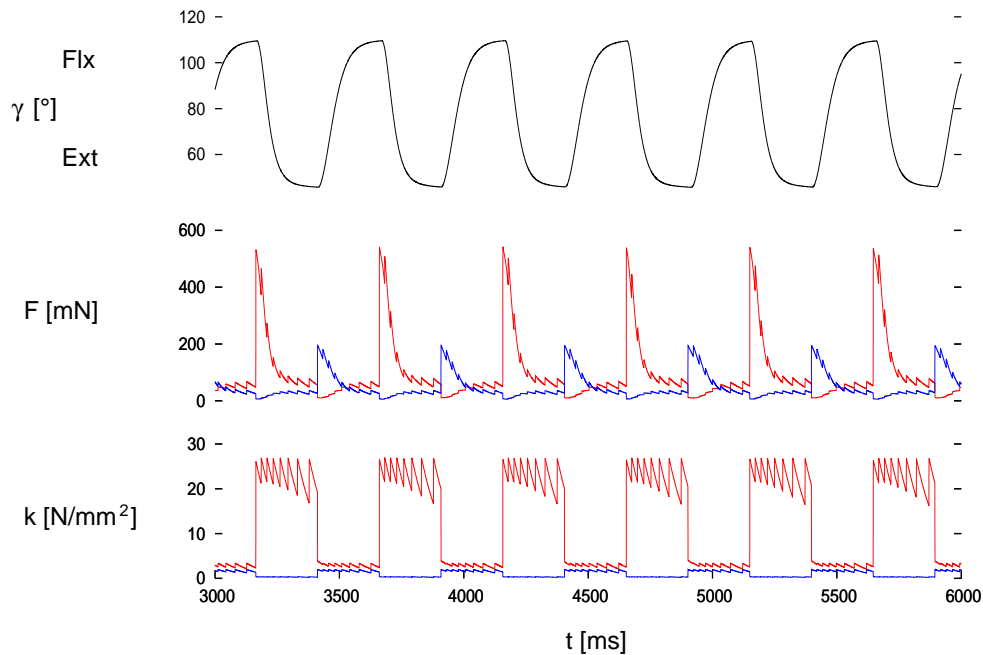


Figure 3.3: Mechanical movement in the neuro-mechanical system consisting of the flexor-extensor muscles and the neuronal network (CPG, MNs and INs) that controls the muscle activity. Time courses of the mechanical variables: angle ( $\gamma$ ) (top panel), forces in the extensor (red) and flexor (blue) muscle (middle panel), and the corresponding elasticity moduli ( $k_E$  and  $k_F$ ) (bottom panel) driven by the action potentials of the extensor and flexor MNs.

The time course of the angular motion is shown with the corresponding muscle forces and spring constants in figure 3.3. At the time points, when the movement of the tibia switches its direction, the transient forces increase. This results from the change of spring constants that is initiated by the switch of motoneuron activity. When the leg begins its extension the extensor muscle force is much greater than the force of the flexor muscle and the forces

in the two muscles converge, but they do not meet due to unequal lever arms. During flexion the forces exchange roles. Indeed, the measured values of muscle forces are in the same order of magnitude (Guschlbauer, 2009). Forces of the extensor muscle in the middle leg amounts about 100 - 200 mN and the flexor muscle in the same leg about 300 - 600 mN.

The mechanical equivalents for the LD and the PR system are analogously implemented the same way. Using the mechanical and geometrical properties of front and hind legs, the neuro-mechanical system can be applied to the front and the hind legs but with possibly different numerical values of the parameters.

Furthermore, experimental data of sideward walking (gathered by M. Gruhn and published in Knops et al. (2012)) revealed that the phase relation of extensor and flexor activity differs from 1:1 in this case (see figure 3.4 A and B). These data show a longer flexion phase and a shorter extension phase, which also results in a higher angular velocity during extension. Now, tuning the central inputs to smaller values (from  $g_{app,ext} = 0.209$  nS and  $g_{app,flx} = 0.100$  nS to  $g_{app,ext} = 0.190$  nS and  $g_{app,flx} = 0.120$  nS, respectively) leads to a phase relation in the simulation that is comparable to the experimental data (cf. figure 3.4 C and D). An alternative data set of leg sizes and masses is used. Thence, the dynamical parameters of the mechanical systems in the middle leg that are determined in the calculation differ somewhat from those used in Toth et al. (2012) and Knops et al. (2012).

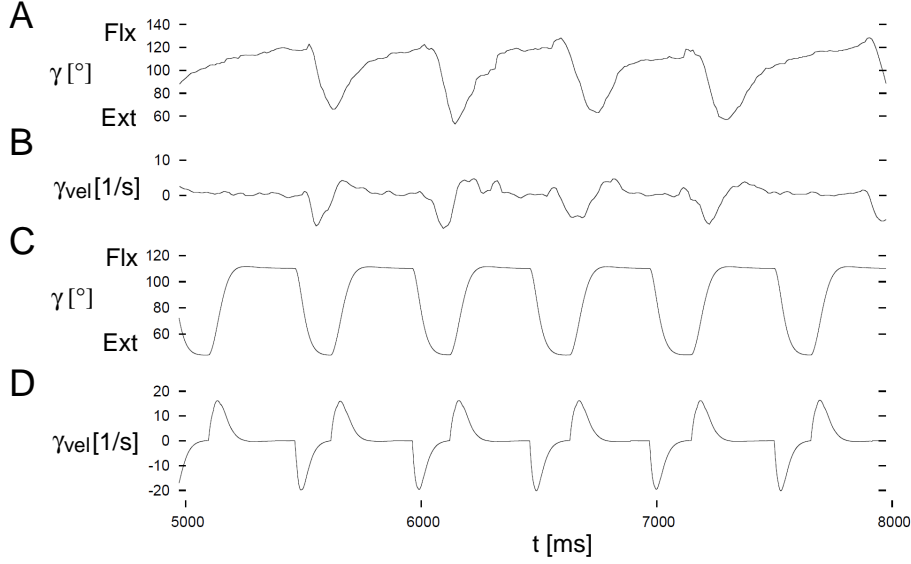


Figure 3.4: A: angle and B: angular velocity of the tibia movement in the experiment; C and D: the corresponding variables in the simulations.

## 3.2 Interjoint coupling in a single leg

In the following section, the three joints have been introduced before are coupled via sensory feedback. All networks feature the same structure. The disparity now consists in a change in the input to the peripheral interneurons. After a short transient time at the beginning, the LD system is permanently stimulated by the CS, i.e. the conductance of the INCS in figure 2.13 is increased to a sufficient high value (from  $g_{app,CS} = 0.29$  nS to  $g_{app,CS} = 2.00$  nS), which makes it intrinsically oscillating. In the absence of sensory feedback the interneuron IN4 in the PR system and the interneuron IN12 in the FE system receive small excitatory inputs ( $g_{app,IN4} = g_{app,IN12} = 0.60$  nS). The sensory feedback signal comes from the LD system. In the model, this signal is a composition of afferent information such as ground contact, position and load signals lumped together into a single parameter

represented by the joint angle  $\beta$  in the LD system. When the joint angle deceeds a critical value  $\beta_{thr} = 38^\circ$  the conductances to the interneurons of the PR system is increased to a value ( $g_{app,IN4} = 3.90$  nS) that is sufficiently high for eliciting the reflex in the CPG unit. This causes the retraction movement of the femur through indirect excitation of the retractor CPG neuron (cf. two-joint system in Toth et al. (2012)). Similarly, the flexion of the tibia is elicited when the angle in the LD system deceeds a critical value  $\beta_{thr} = 50^\circ$ . Biologically, this value can be justified, because the hair fields of the campaniform sensilla that detect the position of the limb are not necessarily the same for the two subsystems, the PR and the FE. This value shows the most suitable starting time and in particular the ending time for the flexion (cf. figure 3.5). For that purpose, the conductance of the interneurons of the FE system is increased to  $g_{app,IN12} = 3.00$  nS. Furthermore, a stabilizing intrajoint coupling mediated by position signals from the femoral chordotonal organ (fCO) is represented by the angle  $\gamma$ . If the angle in the FTi-joint exceeds the critical value  $\gamma_{thr} = 90^\circ$  (cf. figure 3.6) the conductance in the interneuron IN12 will be reduced to a smaller value ( $g_{app,IN12} = 1.90$  nS) during ground contact (cf. figure 3.7). It turns out that the threshold angle is necessary for the shortening of the flexion phase. Otherwise the flexion lasts until the end of the stance phase (figure 3.6 D). This is not observed in walking insects (Grabowska, unpublished video records). However, there is a conspicuousness with regard to the front and middle leg: The switch from flexion to extension happens in the middle of the stance phase. The activation of an inhibitory interjoint coupling shortens the flexion phase by a suitable amount. The variation of the threshold angle has no appreciable impact and the threshold value is assumed to be near the maximal angle at the FTi-joint. This corresponds to an inhibition near the



end of flexion induced by the fCO. In this case the strength of the inhibition is set to a value sufficient for an appropriate shortening of the flexion.

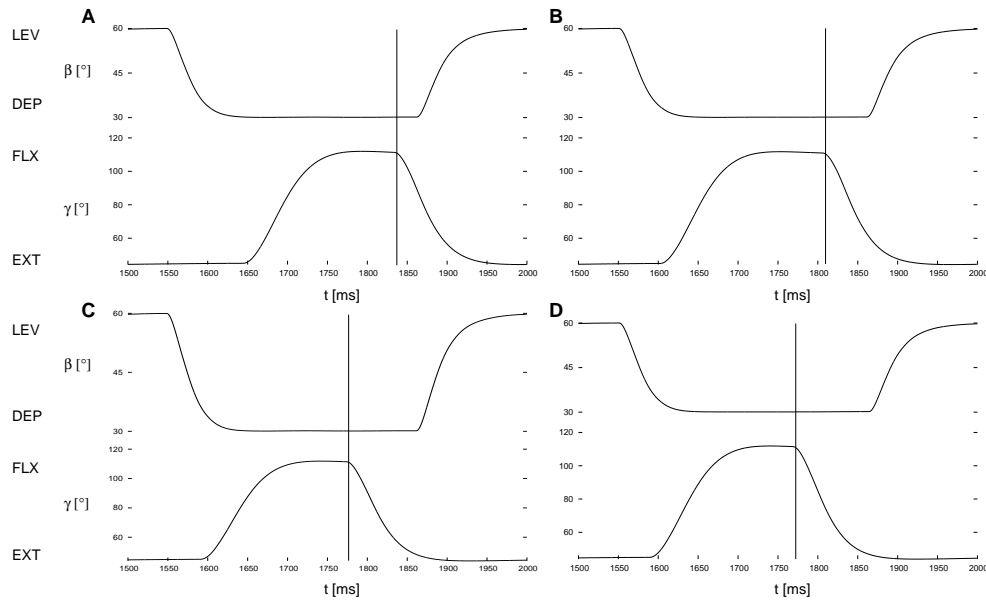


Figure 3.5: Variation of the critical angle  $\beta_{thr}$  at which the flexion of the tibia is elicited. Time course of the angle  $\beta$  in the CTr-joint (upper curve) compared to the time course of the angle  $\gamma$  in the FTi-joint (lower curve). Vertical lines indicate the time point of the switch. A:  $\beta_{thr} = 31^\circ$ , B:  $\beta_{thr} = 38^\circ$ , C:  $\beta_{thr} = 50^\circ$ , D:  $\beta_{thr} = 55^\circ$ .

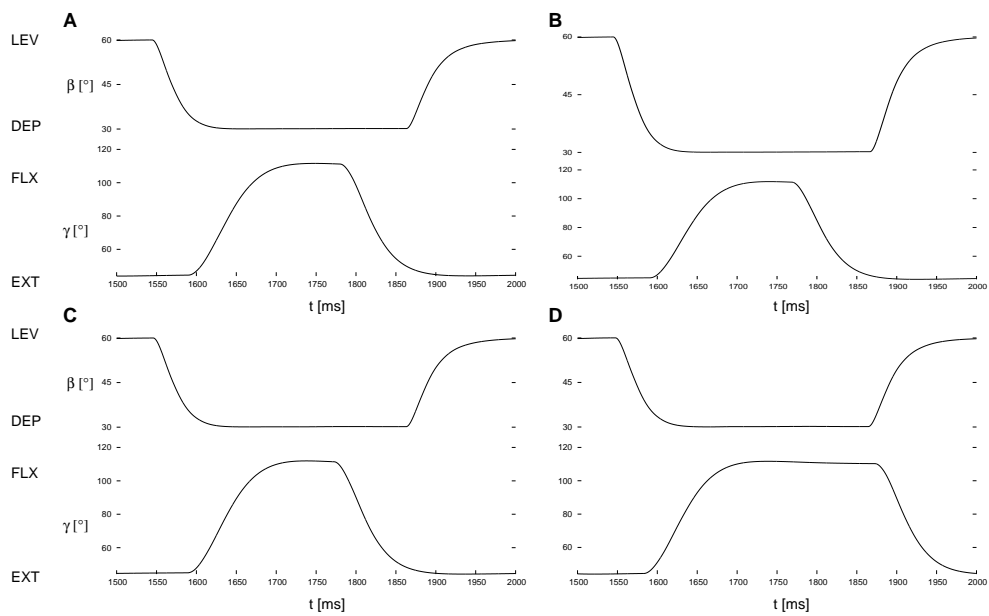


Figure 3.6: Variation of the critical angle  $\gamma_{thr}$  at which the flexion of the tibia stops. Time course of the angle  $\beta$  in the CTr-joint (upper curve) compared to the time course of the angle  $\gamma$  in the FTi-joint (lower curve). A:  $\gamma_{thr} = 60^\circ$ , B:  $\gamma_{thr} = 90^\circ$ , C:  $\gamma_{thr} = 109^\circ$ , D: no intrajoint coupling.

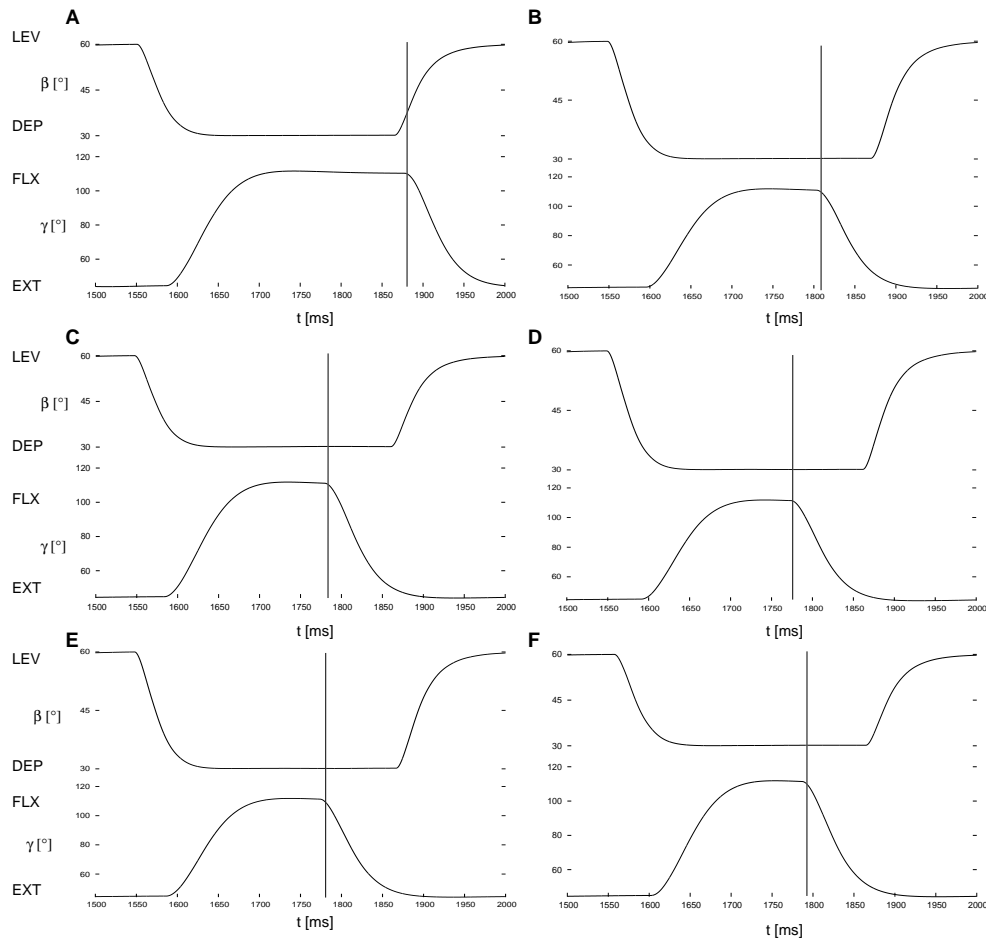


Figure 3.7: Variation of the inhibition strength caused by the intrajoint coupling in the FTi-joint. Time course of the angle  $\beta$  in the CTr-joint (upper curve) compared to the time course of the angle  $\gamma$  in the FTi-joint (lower curve). The conductance in the interneuron IN12 ( $g_{app,IN12} = 3.00$  nS) is set to different values. Vertical lines indicate the time point when the flexion switches to extension. A:  $g_{app,IN12} = 2.90$  nS, B:  $g_{app,IN12} = 2.70$  nS, C:  $g_{app,IN12} = 2.40$  nS, D:  $g_{app,IN12} = 1.90$  nS, E:  $g_{app,IN12} = 1.40$  nS, F:  $g_{app,IN12} = 0.90$  nS.

### 3.2.1 Middle leg

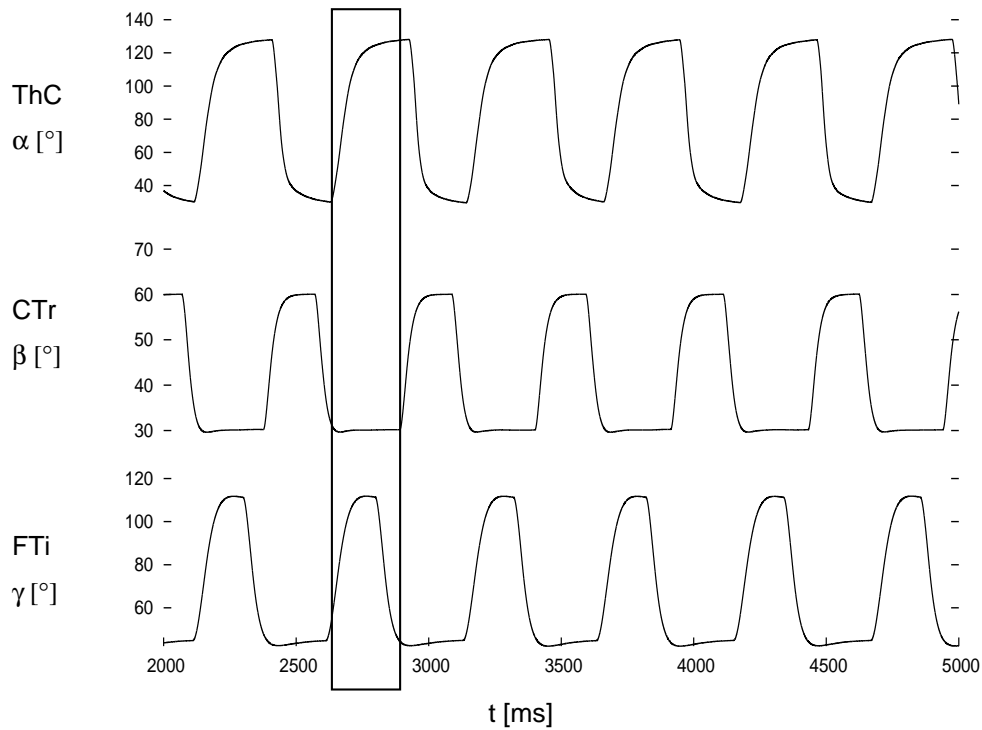


Figure 3.8: Time courses of the three joint angles  $\alpha$  (ThC joint, upper panel),  $\beta$  (CTr joint, middle panel) and  $\gamma$  (FTi joint, bottom panel) in the model of a stick insect's middle leg. The boxed area helps to compare the phases in individual joints and corresponds to the stance phase.

Figure 3.8 shows the time course of the three joint angles during forward walking. One of the stance phases of the middle leg is marked by a box. Shortly before the angle reaches its minimal position, the retraction of the femur and the flexion of the tibia are elicited. The critical value for the coupling of the PR system is chosen, because retraction of the leg has to be started shortly before the tarsus of the leg has ground contact and it has to end shortly after the tarsus has lifted off the ground. The critical value for the coupling of the FE system to the LD system is chosen such that the

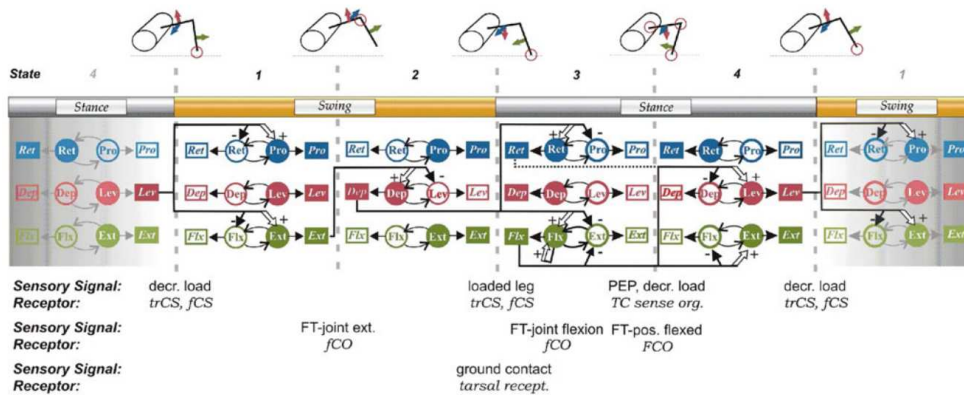


Figure 3.9: Known sensory influences on the timing of motor activity in the stick insects middle leg. CPGs are depicted as circles, motoneurons are depicted as boxes. Connections between neurons are schematically shown as arrows. Depending on their affiliation to the muscles protractor, retractor, levator, depressor, flexor, extensor neurons are labeled Pro, Ret, Lev, Dep, Flx, Ext. Filled symbols denote active neurons, empty symbols denote inactive neurons. Sensory influence can be excitatory (+) or inhibitory (-). The sequence of a stepping cycle is divided into stance and swing phase or four phases, respectively. Sensory signals are load, position and ground contact. Sense organs are the femoral chordotonal organ fCO, the trochanteral and the femoral campaniform sensilla trCS and fCS, respectively (Daun-Gruhn and Büschges, 2011).

flexion of the tibia has to start when the tarsus of the leg is at its AEP. This causes the propulsion of the body in the first part of the stance phase. The timing of the motor control is supported by experimental results that are summarized in a review by Büschges (2005). The load on the leg that is sensed by the trochanteral and femoral campaniform sensilla leads to the onset of retractor and flexor activity. This is depicted as the arrow from the depressor motoneuron (box) that leads to the retractor and flexor CPG neurons (circles) between phases 2 and 3 in figure 3.9.

The flexion is switched to extension via intrajoint coupling through the fCO by the choice of the critical value of  $\gamma$ . Therefore the tibia switches to

extension in the later part of the stance phase and guarantees the propulsion of the body. See also the arrow from the flexor motoneuron to the extensor CPG neuron between phases 3 and 4 in figure 3.9. Experimental data (video records of Grabowska et al. (2012) and EMG records from intact walking stick insects on a slippery surface (Rosenbaum et al., 2010)) support the choice of the switch point at middle point of the stance phase. A video with the visualization of the simulated data is shown in the supplementary material *Suppl01* and *Suppl02* on the Gruhn Lab Webpage (2012). The arrangement with the free walking insect consists of two walking middle legs that are coupled with a phase shift of 50%.

The numerical values of the dynamical parameters are listed in tables A.14, A.15 and A.17. Here, an alternate set of parameters for the ThC-joint is used. The angular range (tread mill experiment by Schumm and Cruse (2006)) is a little wider than the one used in section 3.2.4. The usage of these values is acceptable for an isolated middle leg. If three legs on the ipsilateral side of the stick insect work together, the range of the middle leg will have to be narrowed. Otherwise the middle leg would collide with the front leg or the hind leg.

### 3.2.2 Switching mechanism

A recent study by Toth et al. (2012) a neuro-mechanical model of the coupled PR and LD systems is established that is capable of performing forward and backward stepping and switching between them. In Knops et al. (2012) the model is extended by attaching the FE system to it. Figure 3.10 shows the time course of the three main joint angles in the stick insects middle leg. The sequence begins with forward walking, switches to backward walking at  $t = 6000$  ms and then switches to forward walking at  $t = 9250$  ms. Rosen-

baum et al. (2010) showed that the activity of protractor MN and retractor MN is exchanged during backward stepping and the MNs in the LD and FE systems keep on working unchanged. This property is reproduced in the simulation. The underlying mechanism is proposed in Toth et al. (2012).

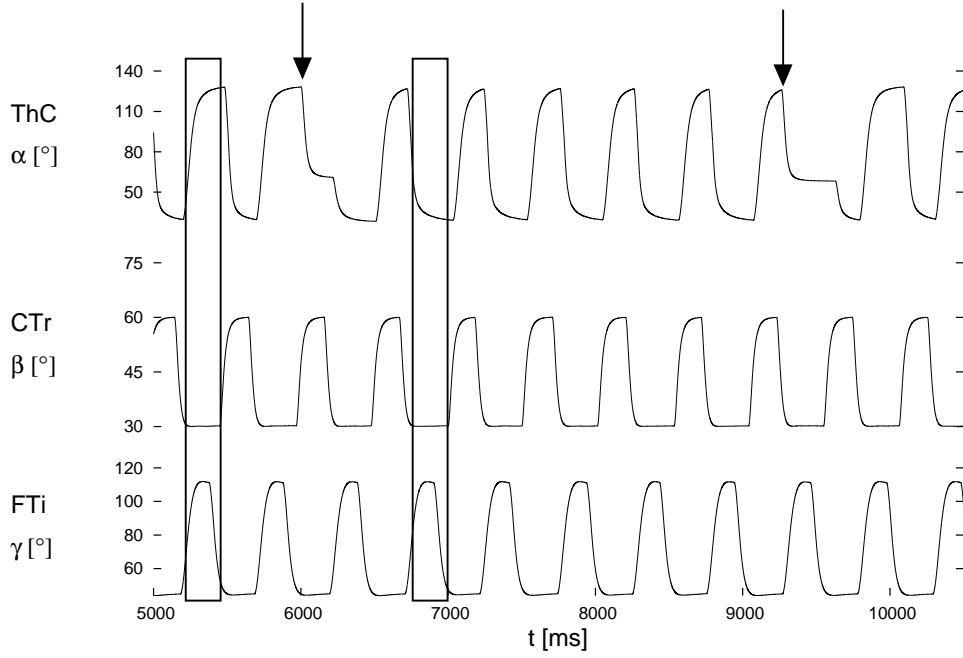


Figure 3.10: Time courses of the three joint angles  $\alpha$  (ThC joint, upper panel),  $\beta$  (CTr joint, middle panel) and  $\gamma$  (FTi joint, bottom panel) in the model of the stick insect's middle leg. Arrow at  $t = 6000$  ms: switch from forward to backward walking; arrow at  $t = 9250$  ms: switch from backward to forward walking. The boxed areas help compare the phases of the movement at the individual joints and correspond to the stance phase.

The simulation is capable of mimicking data from Rosenbaum et al. (2010) while the retractor and protractor muscles exchange their activities during backward walking and the activities in the other muscles remain unchanged. Figure 3.11 shows parallel and cross connections between the CPG and the interneurons IN1 and IN2. The parallel connection is active during forward walking. This is caused by the central excitation of the neuron SF in the

CPG-like neuron pair in the box in figure 3.11 that inhibits the neuron SB. If now a central command excites the neuron SB instead of SF the neuron SF will be inhibited. The parallel connection is now presynaptically inhibited. The cross connection becomes active, because its presynaptic inhibition is dropped. This results in an exchange of the MN activities without changing the CPG activities in the PR system. The LD system and the FE system remain unaffected. A change of CPG activities would have caused a transient time in the order of one cyclic period. That same mechanism can be used

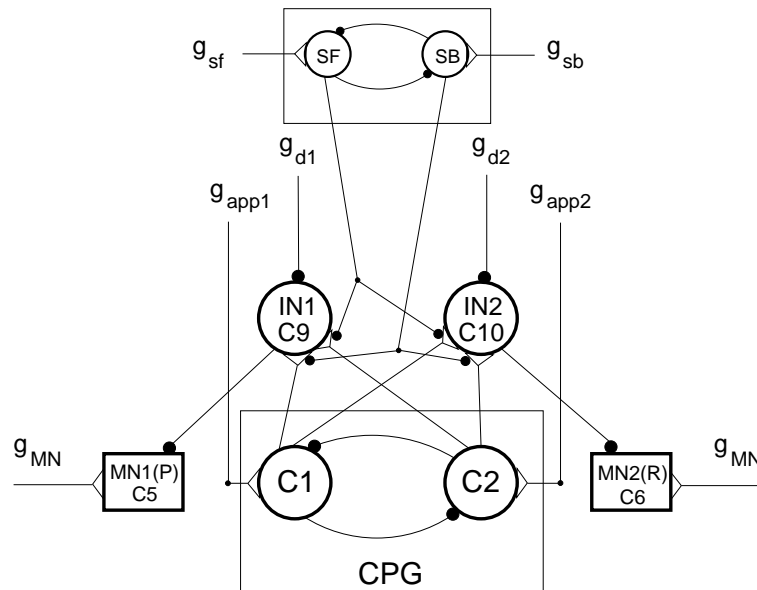


Figure 3.11: Proposed neuronal switching mechanism between forward, sideward and backward stepping. The upper part of the protractor-retractor system is shown (cf. figure 2.13) in addition with a small, CPG-like control network consisting of the mutually inhibitory neurons SF and SB that brings about the switch between the directions of movement. Small filled circles on excitatory synapses are presynaptic inhibitions. Taken from Toth et al. (2012) with permission.

for the generation of sideward stepping. Sideward stepping can be achieved by stiffening the ThC-joint and by keeping it at a stationary joint angle. In



Knops et al. (2012) this is implemented by the simultaneous inhibition of both the neurons SF and SB. All presynaptic inhibitions to the excitatory synapses to interneurons IN1 and IN2 are inactivated and all excitatory connections from the CPG become active. The interneurons IN1 and IN2 are simultaneously active and hence, the motoneurons driving the protractor and retractor muscles are simultaneously inhibited. Depending on the point of time at which the switch is initiated the joint can be fixed at three different stationary angles. There can more stationary angles be achieved, when a differentiation is made between slow and fast muscle fibers. However, this study includes only fast muscle fibers.

If the switch command occurs while the protractor MN is firing, the femur will be fixed at the AEP of the middle leg ( $\alpha = 28^\circ$ ). If the switching command occurs at the beginning of the active retractor phase, the femur will be fixed at  $\alpha = 102^\circ$ . If it occurs at the end of the retractor phase, the femur will be fixed at the PEP of the middle leg ( $\alpha = 128^\circ$ ). In this model, sideward walking is executed by fixing the leg at  $\alpha = 102^\circ$ . Since the extension phase becomes shorter and the flexion phase becomes longer during sideward walking (data gathered by M. Gruhn, see figure 3.4) the central drives  $g_{app5}$  and  $g_{app6}$  to the CPG of the FE system have to be changed as described in section 3.1.2. The motion of the CTr-joint remains unchanged during sideward stepping. Figure 3.12 shows the mechanical motion and neuronal activity at a switch from forward walking to sideward walking. The angle converges to a constant value, when it is fixed at a certain point of time. Both interneurons are active and both motoneurons are inhibited. It can be seen that the switch occurs at the beginning of the retraction phase since a single spike of the retractor motoneuron is discernible in figure 3.12. The CPG neurons are not affected during the process.

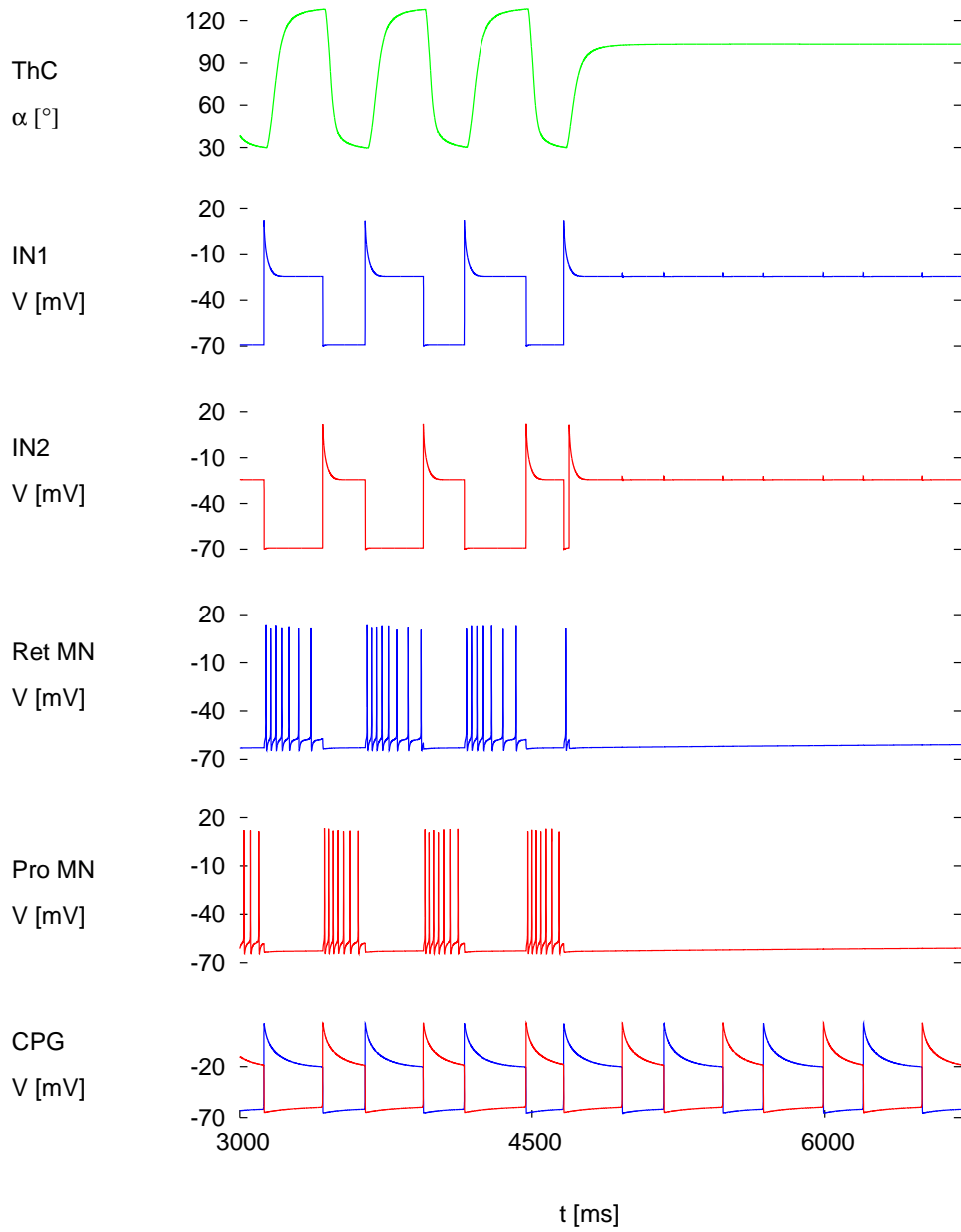


Figure 3.12: Mechanical movement and neuronal activity in the PR system before and after fixing the retraction position of the femur, i.e. the angle  $\alpha$ . The command to keep  $\alpha$  constant arrives at  $t = 4690$  ms. The stationary retraction angle is  $\alpha = 102^\circ$ . Picture taken from Knops et al. (2012).

### 3.2.3 Neuronal basis of curve walking

As it can be learned from experimental findings, there are two main methods that are applied to curve walking in the stick insect (Cruse et al., 2009; Dürr and Ebeling, 2004; Gruhn et al., 2009; Jander, 1982, 1985; Rosano and Webb, 2007). One way to perform curve walking is to shorten the stride length of the inner middle leg (Dürr and Ebeling, 2004; Gruhn et al., 2009; Jander, 1982, 1985). A decrease in the stride length is achieved by reducing the angular range in the PR system; in an extreme case the ThC-joint is fixed and the inner leg is restricted to sideward stepping. The other possibility to shorten the stride length is to change the walking direction of the inner middle leg from forward to backward (Gruhn et al., 2009).

In order to compare these strategies, the both cases are simulated with the model published in Knops et al. (2012). In these simulations, two walking middle legs (simulated with CVODE (Cohen and Hindmarsh, 1996)) are attached to the thorax of the stick insect in the ODE environment (Smith, 2006). One of the legs is constantly walking forward whereas the other leg is just walking forward at the beginning. Subsequently, the walking direction of the other leg switches to one of the methods for curve walking and finally, it switches back to forward walking. To achieve a stabilization of the body, the front and hind legs are also attached with fixed joint angles. The tarsi of the front and hind legs have no friction with the ground. The left and the right middle leg are alternating with a phase shift of half of a period of the stepping period. This phase shift is imposed artificially.

#### **Turning generated by temporary switching to backward stepping**

The simulated stick insect starts walking forward. After a few steps, when the left middle leg switches to backward stepping, it seems to rotate about

a vertical axis through the body. Thus, it changes its walking direction on the spot with a small or negligible radius. After a few additional steps, the left middle leg switches back to forward stepping, and the stick insect continues walking straight in a new direction. Figure 3.13 A shows a sequence of screen shots during the simulation. The full video can be found in the supplementary material *Suppl03* (Gruhn Lab Webpage, 2012). Figure 3.14 shows the complete trajectory of the movement. The first part, which is depicted as a blue line, is forward walking. It is followed by the turning phase with the inner middle leg stepping backward, which is illustrated in form of a red curve. Finally, the black line emanating from the red one is again forward walking.

### **Turning generated by temporary switching to sideward stepping**

Again, the simulated stick insect starts walking forward. After executing the same number of steps as in the previous paragraph, the left middle leg switches to sideward stepping. The right middle leg continues stepping forward, but the left middle leg pulls the body to the inner side of the curve. This curve has a larger radius than the one before. After executing the same number of steps as before, the left middle leg switches back to forward stepping, and the stick insect continues walking straight. Figure 3.13 B displays a sequence of screen shots of the simulation (see also supplementary file *Suppl04* (Gruhn Lab Webpage, 2012)). Comparing the trajectory of this turning movement with that of the preceding one, one can see the clear difference in the turning paths (red versus green curve) resulting in different turning angles. The directions of the straight walking in the final part of the trajectory (black lines) differ from each other quite remarkably. While the angle of turning is much larger in the first case, the walking distance is much

longer in the latter one.

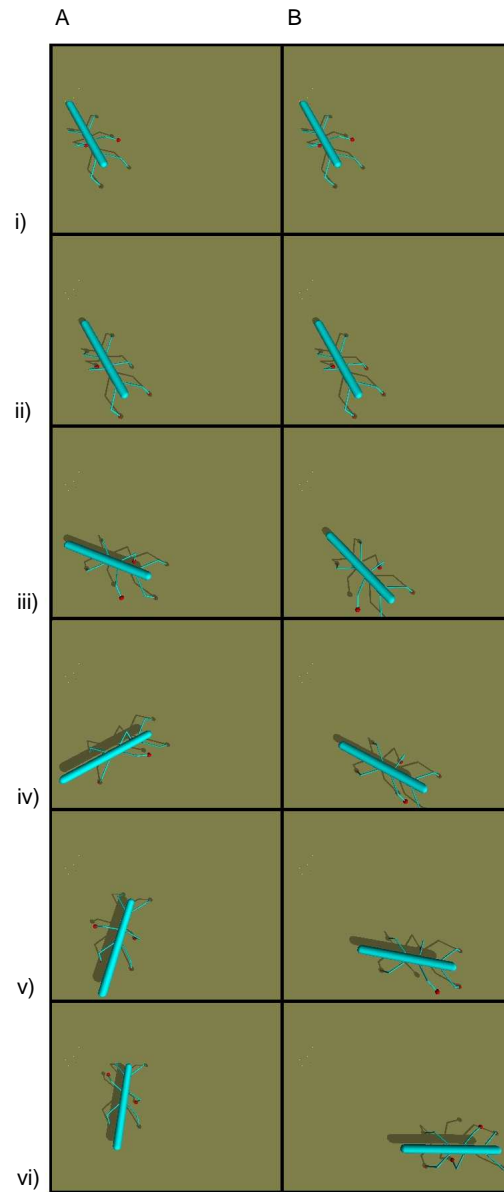


Figure 3.13: Curve walking of the simulated stick insect in two different modes. A: curve walking with backward stepping; B: curve walking with sideward stepping. Only the middle legs are driven actively by angle vectors  $\alpha(t), \beta(t), \gamma(t)$  on either side of the simulated insect. The two signal vectors are set to have a phase difference of half of a stepping period. The other four legs are passive, and kept in fixed positions; they stabilize the trunk during movement. Picture taken from Knops et al. (2012).

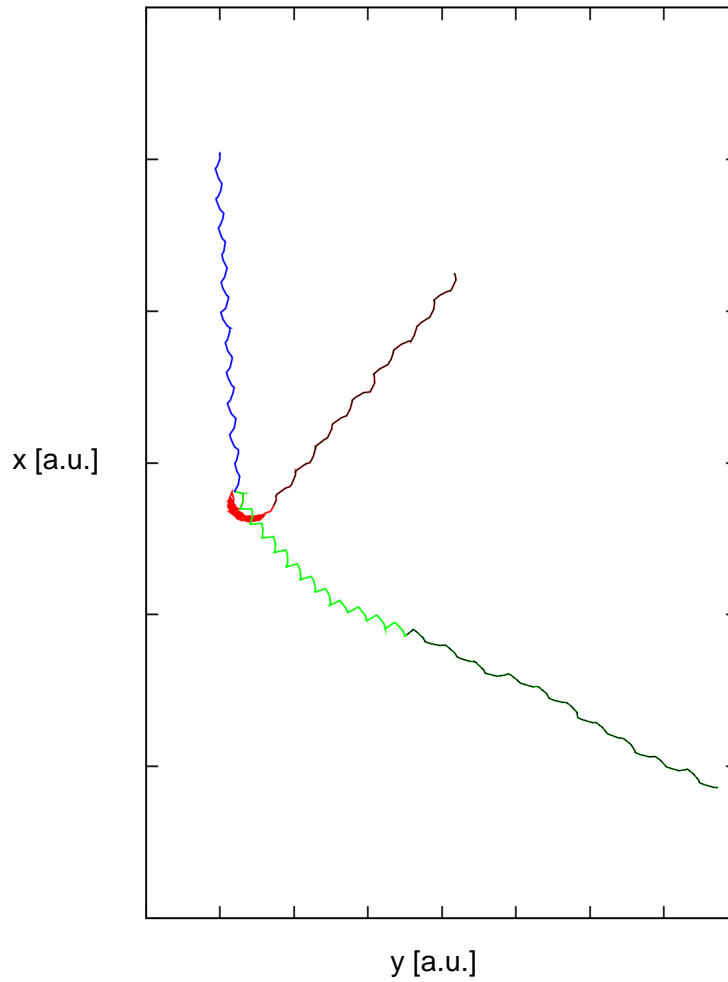


Figure 3.14: Trajectory of the simulated stick insect walking in the plane. The trajectory describes the movement of the center of the body in arbitrary units (a.u.). Blue line: forward walking (identical for both turning modes); red line: backward stepping of the inner middle leg during turning; green line: sideward stepping of the inner middle leg during turning; black lines: forward walking after turning. Picture taken from Knops et al. (2012).

### 3.2.4 Applying the model to ipsilateral legs

To implement the intersegmental coupling of ipsilateral legs, the model of the walking middle leg is adapted to be used for the front and the hind legs. The coupling scheme, neuronal and mechanical properties are nearly the same as for the middle legs. There are only slight differences that will be described in the following. First, numerical values of the lengths and masses of the legs differ in front, middle and hind legs. In the simulation, these differences are taken into account. Due to the changed values of the momentum of inertia, a re-adjustment of the stationary spring constant values, as well as the viscosity coefficient values is carried out for both the front leg and hind leg model. The corresponding numerical values are listed in tables A.13 - A.23. Second, the hind leg has a working range in the ThC-joint that is sited to the rearer part, i.e. the angular range is larger for the hind leg. The front and middle legs feature a flexion at the beginning of the stance phase and an extension of the leg at the end of the stance phase. However, the hind legs must perform an extension of the leg during most of the stance phase. This can be achieved by exchanging the synaptic paths between the CPG neurons and the interneurons IN33 and IN34 (c.f. figure 2.14). Basically, it is the same mechanism that is used for the switch between stepping directions. Third, for the sake of uniformity, the working ranges for the ThC-joint angles are taken from a data set from M. Gruhn (unpublished results).

The neuronal features are shown previously and therefore they will only be discussed if necessary. Figure 3.15 shows the time course of the three main joint angles in the front leg. The angular range in the CTr- and FTi-joints is the same as it is with regards to the middle leg. However, the angular range in the ThC-joint differs from that of the middle leg. Qualitatively, the time course of the angle  $\alpha$  looks the same as it does in the simulation



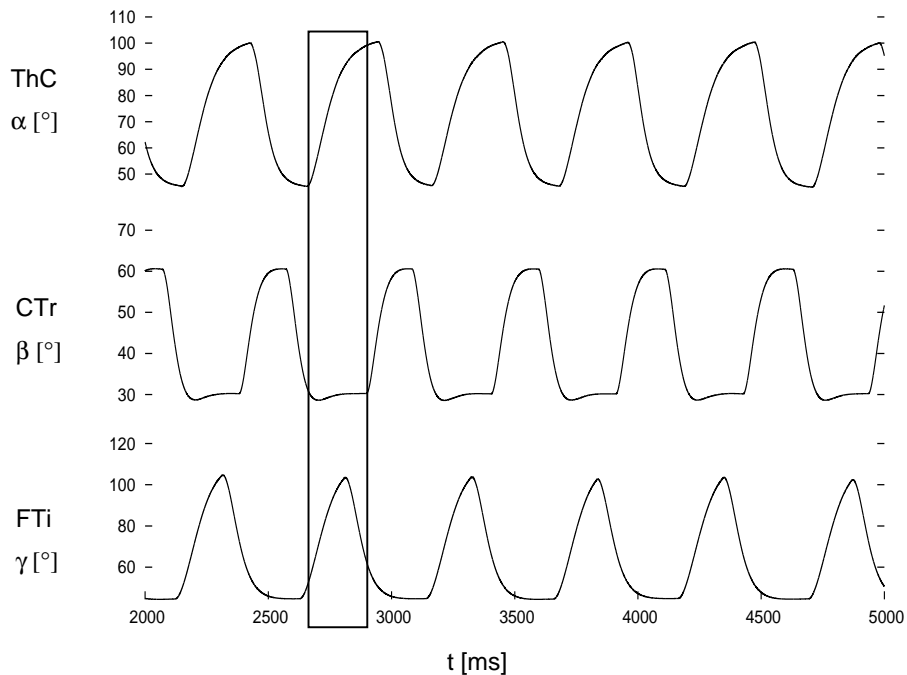


Figure 3.15: Time courses of the three joint angles  $\alpha$  (ThC joint, upper panel),  $\beta$  (CTr joint, middle panel) and  $\gamma$  (FTi joint, bottom panel) in the model of a stick insect's front leg. The box enframes a stance phase.

for the middle leg. This holds for the time course of the angle  $\beta$ . It turns out that the parameters for the spring constant and the viscosity in the FE system are hard to tune, i.e. the range, in which the parameters can be adjusted, is small in comparison to the one of the parameters of the middle leg. Thus, the time course of the angle  $\gamma$  appears not to satisfy the conditions of switching (cf. section 3.1). A more appropriate time course would have been achieved with a smaller viscosity or greater spring constants in the FE system. However, such values cause the mechanical oscillation to break down. The parameters used here are listed in tables A.18 - A.20. A visualization of the walking insect in supplementary material *Suppl05* and *Suppl06* (Gruhn Lab Webpage, 2012) shows a realistic movement of the joint angles. Figure

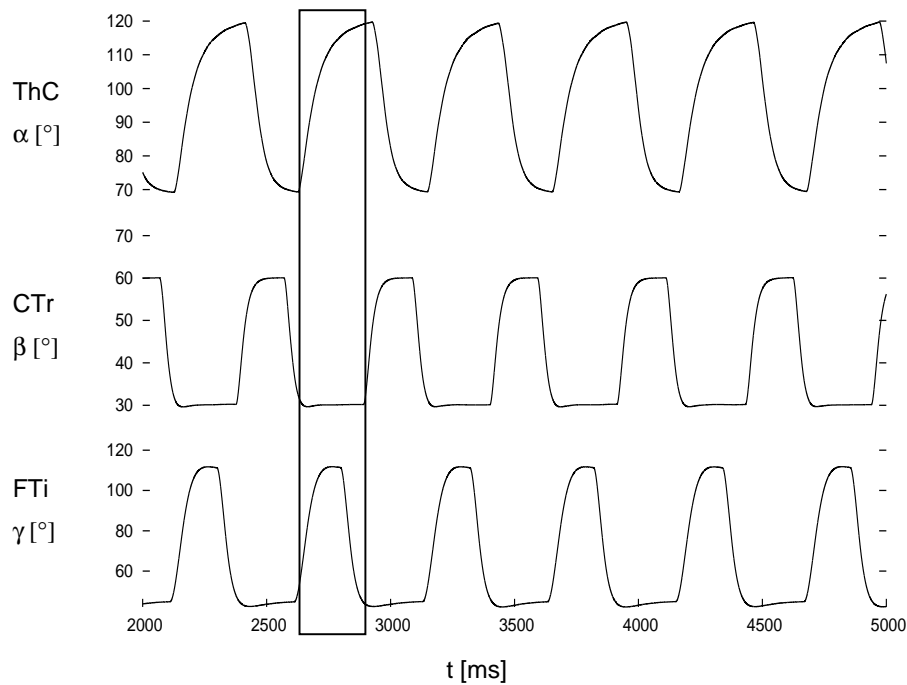


Figure 3.16: Time courses of the three joint angles  $\alpha$  (ThC joint, upper panel),  $\beta$  (CTr joint, middle panel) and  $\gamma$  (FTi joint, bottom panel) in the model of a stick insect’s middle leg. The box enframes a stance phase.

3.16 documents the time course of the three main joint angles in the middle leg. This is qualitatively the same as described above. There are minor changes in the dynamical parameters and in the angle range of the ThC-joint (see table A.14 - A.16). The smaller angle range is compatible with the angle range in the front and hind legs. A higher range would have caused the middle legs to hit the front and hind legs. *Suppl07* and *Suppl08* (Gruhn Lab Webpage, 2012) show the simulated walking stick insect.

The tuning of the parameters in the hind leg shows the same issues as the front leg with respect to the angular motion in the ThC-joint. The angle range in the FTi-joint is also modified. This refers to the dissimilarity of the segment lengths in the front, middle and hind legs. The middle leg is

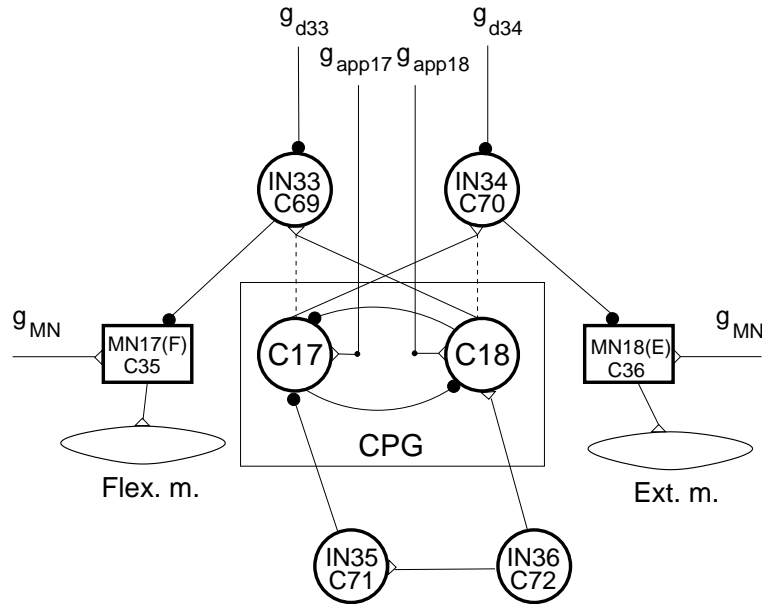


Figure 3.17: Modified single joint network (cf. figures 2.12 and 2.14). The connection from the CPG neurons to the MNs in the meta-thoracic FE system is crossed in contrast to FE systems in the other segments (cf. dashed lines).

shorter than the front leg. Hence, if one considers the insect standing just on the front and middle legs the thorax will be declined caudally. However, the hind leg is longer than the middle leg. For reasons of height compensation, the angle range in the FTi-joint is adjusted such that the thorax is sited nearer to the ground. Another feature of the hind leg is that the femur declines to the rear, i.e. the angle range in the ThC-joint is wider than in the front and middle legs. As a consequence, the tibia has to be extended for achieving the propulsion of the body. Figure 3.17 shows the network of the isolated FTi-joint. It resembles the single joint network (see figure 2.12). The only difference consists in the link from C17 and C18 to IN33 and IN34. This results in an angular movement in the FTi-joint such that the hind leg exerts an extension during ground contact (see figure 3.18). A visualization

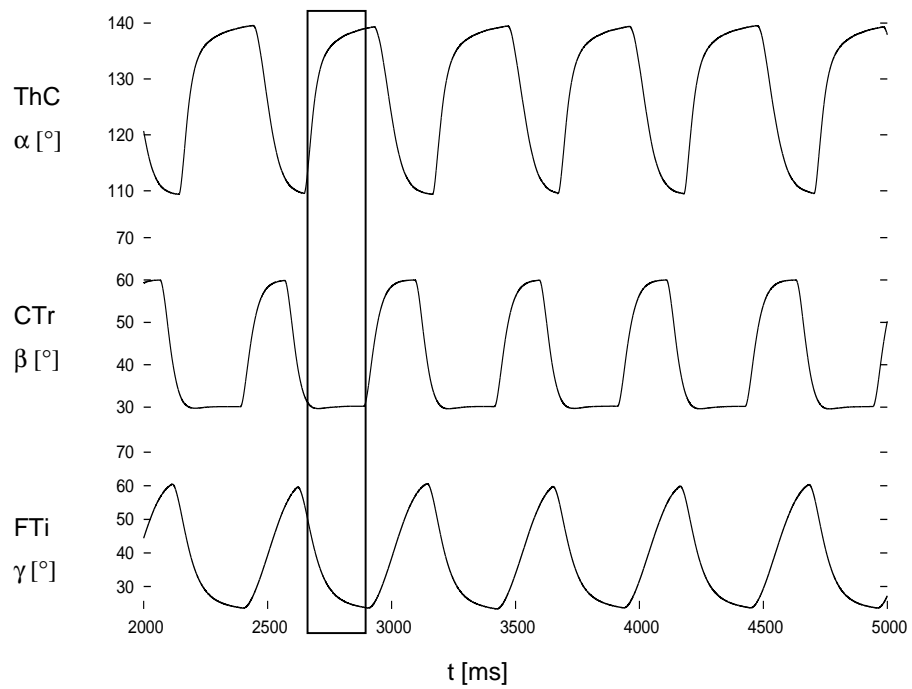


Figure 3.18: Time courses of the three joint angles  $\alpha$  (ThC joint, upper panel),  $\beta$  (CTr joint, middle panel) and  $\gamma$  (FTi joint, bottom panel) in the model of a stick insect's hind leg. The box enframes a stance phase.

is provided in *Suppl09* and *Suppl10* (Gruhn Lab Webpage, 2012).

### 3.3 Intersegmental coupling - Multiple legs

As mentioned in section 2.5.4, the intersegmental synaptic connections are realized by weak inhibitory connections. This influence dampens the excitatory intrasegmental input from the respective LD system. The intrasegmental influence is, for example, triggered by the angle  $\beta_2$  in the middle leg. If it exceeds a certain threshold angle  $\beta_2 = 38^\circ$ , the peripheral interneuron IN16 to the PR system will be raised from  $g_{app,IN16} = 1.6$  nS to  $g_{app,IN16} = 3.3$  nS. The weak intersegmental influence reduces these values by  $\Delta g_{app,IN16} = 0.6$  nS. The threshold value is assumed to have the same value ( $\beta_1 = 38^\circ$ ). If this value is exceeded (interleg ground contact) and the threshold value in the respective leg is exceeded (intraleg ground contact) the conductance to IN16 will be set to  $g_{app,IN16} = 3.3$  nS. In case of interleg ground contact and intraleg lift-off the conductance is set to  $g_{app,IN16} = 1.0$  nS. With this set up of parameters it is possible to bring about the two main gaits in the stick insect: the tetrapod and the tripod gait. The same coupling structure and the same coupling strengths are applied to all the legs. Even though this is just an assumption, it is nevertheless preferable to have a unified and minimal configuration that has not to be changed during gait transitions or changes in the environment, for example.

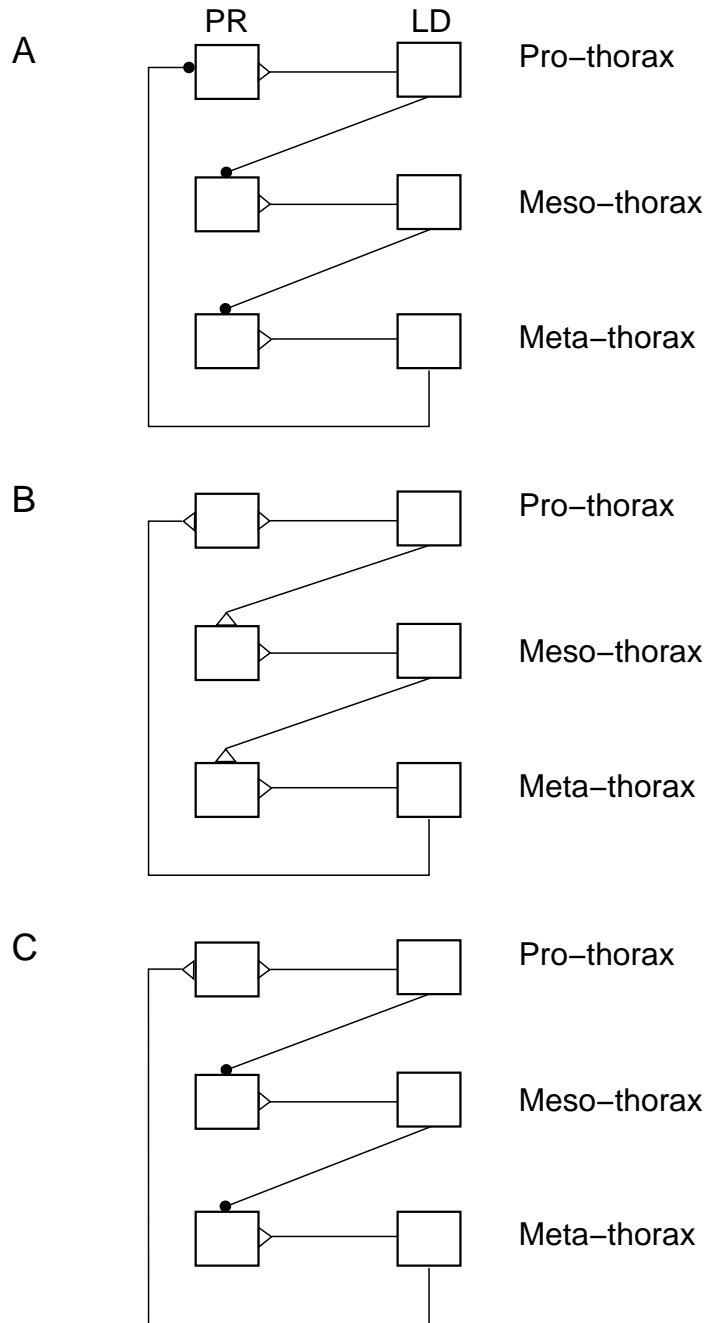


Figure 3.19: Simplified sketch of the network in figure 2.14 with different intersegmental coupling structures. Boxes: neuro-mechanical systems for the PR systems (left row) and the LD systems (right row); empty triangles: excitatory synapses; filled circles: inhibitory synapses. Upper boxes: front leg, middle boxes: middle leg, bottom boxes: hind leg. A: all intersegmental synapses are inhibitory; B: all intersegmental synapses are excitatory; C: intersegmental synapse from the hind to the front leg is excitatory, the others are inhibitory.

There are different possibilities for the intersegmental connections. Firstly, each connection can be excitatory and/or inhibitory. Secondly, the coupling strength can be strong or weak. Of course, the connections can reach from front to rear or from rear to front. From all those possibilities there are three ones examined. These are the simplest configurations that lead to the generation of the tripod and the tetrapod gait.

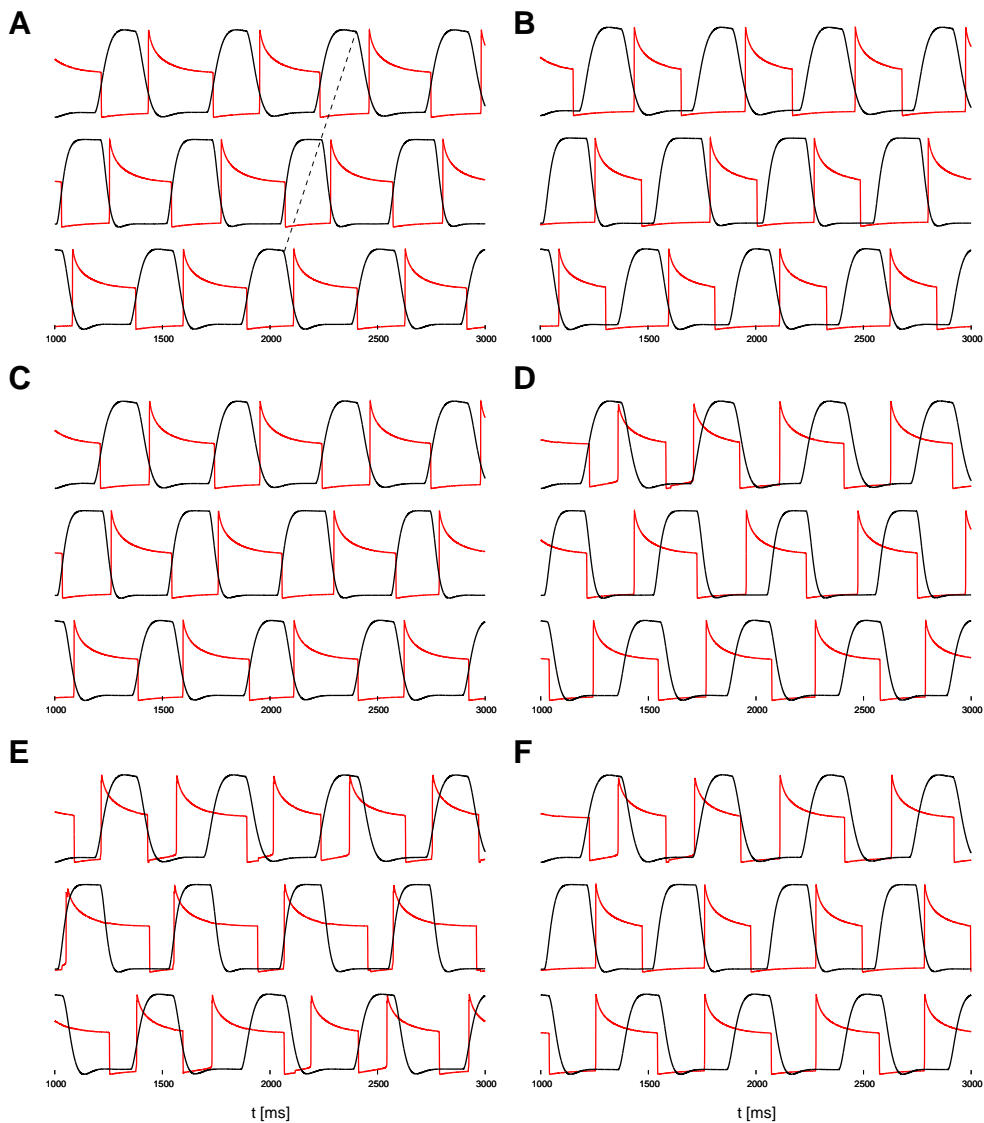


Figure 3.20: Subfigure A-F: Generation of the tetrapod for different intersegmental connections. Each subfigure: Time course of the angle  $\beta$  in the CTr-joint (black) and retractor CPG neuron (red) displayed for the pro-thorax (upper panel), the meso-thorax (middle panel) and the meta-thorax (bottom panel). A: all intersegmental synapses are weakly inhibitory, B: all intersegmental synapses are strongly inhibitory, C: all intersegmental synapses are weakly excitatory, D: all intersegmental synapses are strongly excitatory, E: weakly excitatory intersegmental connection emanating from front and hind leg, weakly inhibitory intersegmental connection emanating from middle leg, F: strongly excitatory intersegmental connection emanating from front and hind leg, strongly inhibitory intersegmental connection emanating from middle leg. The dashed line indicates the caudo-rostral metachronal wave. See also figures 3.19 A - C.



Figures 3.20 A-F exhibit the different setups of intersegmental connections. Figure 3.20 A comprises the applied weak inhibitory connection that is described above. In all parts the increase of the coupling strengths (figure 3.20 B) causes the protraction phases to begin during ground contact. Consequently, the retraction phases are shorter. This disturbs the propulsion of the body. The effect of these excitatory connections is that nearly the whole protraction takes place during ground contact. In this case, propulsion is not possible. The connections in figures 3.20 E and F show complex features. The most persuasive reason to reject these setups is that the protraction takes place during stance.

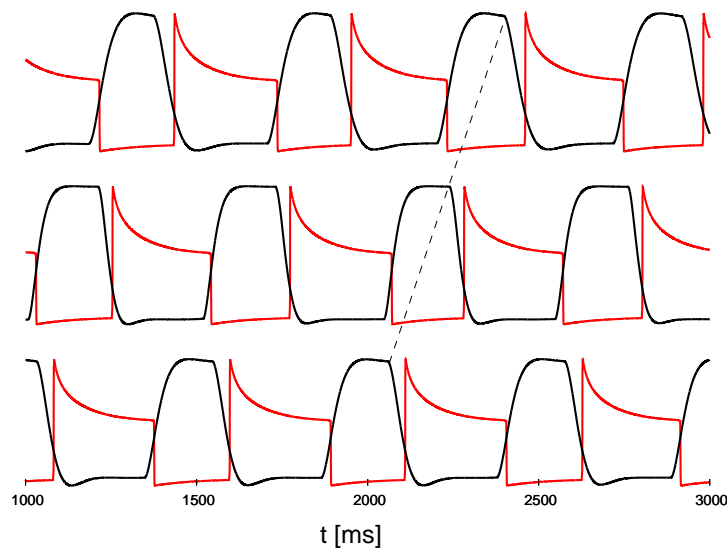


Figure 3.21: Time course of the angle  $\beta$  in the CTr-joint (black) and retractor CPG neuron (red) displayed for the pro-thorax (upper panel), the meso-thorax (middle panel) and the meta-thorax (bottom panel) during tetrapod. The dashed line indicates the caudo-rostral metachronal wave.

Figure 3.21 shows the time course of the activity of the retractor CPG neuron in the PR systems and the time course of the angle  $\beta$  in the respective

legs. This illustration allows one to compare the timing of the body propulsion with the ground contact. In the starting phase the hind leg begins (with a lift-off of the leg), the middle leg joins after a third of the cyclic period and after two thirds of the cyclic period the front leg starts as well. After one cycle period the hind leg is lifted off again. The retraction phases of all legs accompany the respective stance phases. Consequently, the protraction phases coincide with the lift-offs.

If now the starting times are chosen such that the front leg and the hind leg are simultaneous active (i.e. their stance and swing phases occur the same time) and the middle leg phases are shifted such that the stance and swing phases are contrary active, a tripod gait can be achieved. For reasons of symmetrically fitting the stance and swing phases of ipsilateral legs into each other, the central input to the CPGs of the LD systems has to be modified. This results in a 1:1 phase relation of depressor and levator activity, which has been observed in stick insects Graham (1972). Therefore, the conductances  $g_{app3}$  and  $g_{app4}$  are changed (from  $g_{app3} = 0.23$  nS and  $g_{app4} = 0.1843$  nS to  $g_{app3} = 0.26$  nS and  $g_{app4} = 0.17$  nS). Relating to the levator CPG neuron this is an increase and relating to the depressor CPG neuron this is a decrease. This leads to a shorter depressor activity and a longer levator activity. A further consequence is that the cyclic period shortens from  $T_{4pod} = 510$  ms for the tetrapod to  $T_{3pod} = 442$  ms.

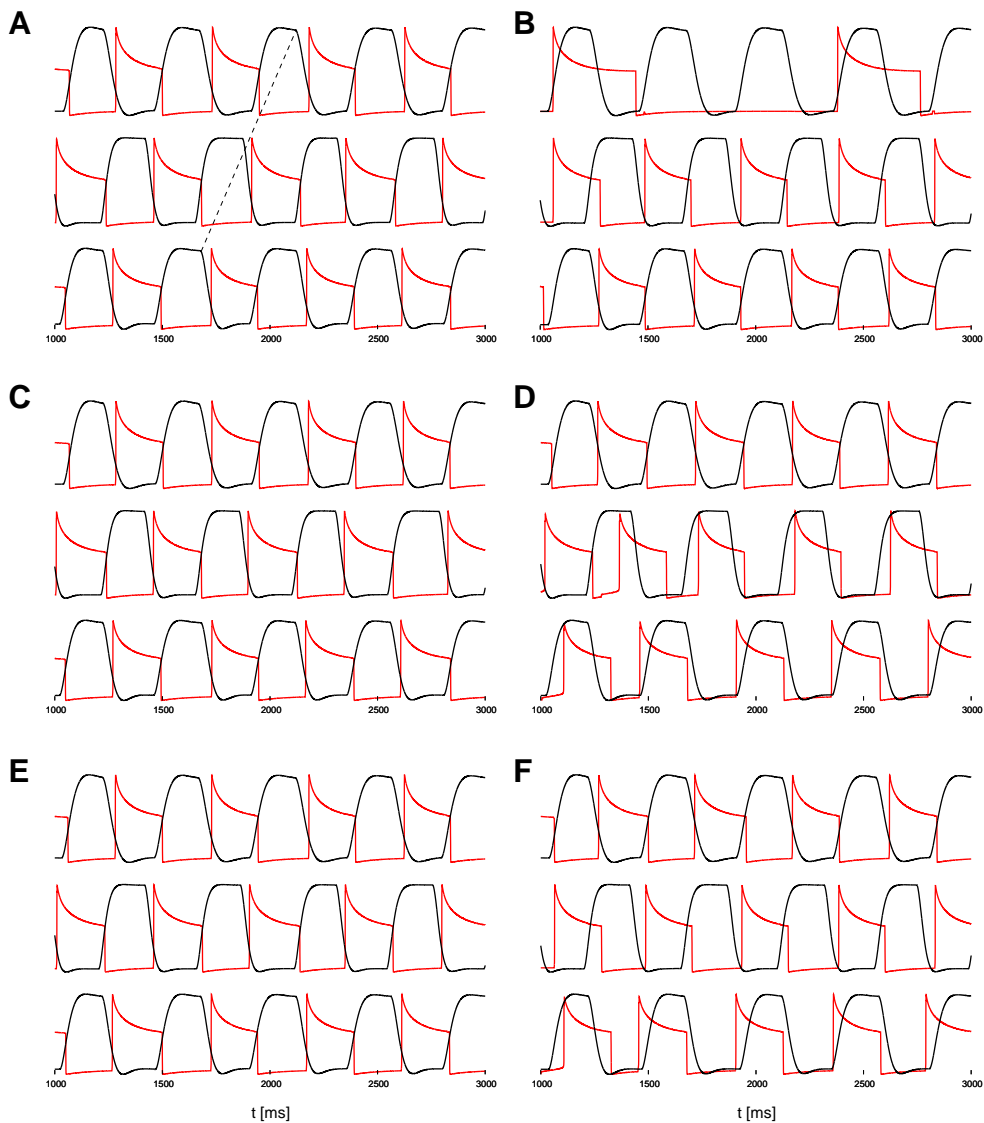


Figure 3.22: Subfigure A-F: Generation of the tripod for different intersegmental connections. Each subfigure: Time course of the angle  $\beta$  in the CTr-joint (black) and retractor CPG neuron (red) displayed for the pro-thorax (upper panel), the meso-thorax (middle panel) and the meta-thorax (bottom panel). A: all intersegmental synapses are weak inhibitory, B: all intersegmental synapses are strong inhibitory, C: all intersegmental synapses are weak excitatory, D: all intersegmental synapses are strong excitatory, E: weak excitatory intersegmental connection emanating from front and hind leg, weak inhibitory intersegmental connection emanating from middle leg, F: strong excitatory intersegmental connection emanating from front and hind leg, strong inhibitory intersegmental connection emanating from middle leg. The dashed line indicates the caudo-rostral metachronal wave. See also figures 3.19 A - C

Figures 3.22 A-F illustrate different setups of intersegmental connections with regards to their strengths and inhibitory or excitatory nature. Figures 3.22 A, C and E reveal an appropriate coordination of legs during the tripod gait. These setups have a weak intersegmental connection in common. The time courses in figures 3.22 B, D and F are unsuitable, since at least one of the legs shows a distorted stepping pattern.

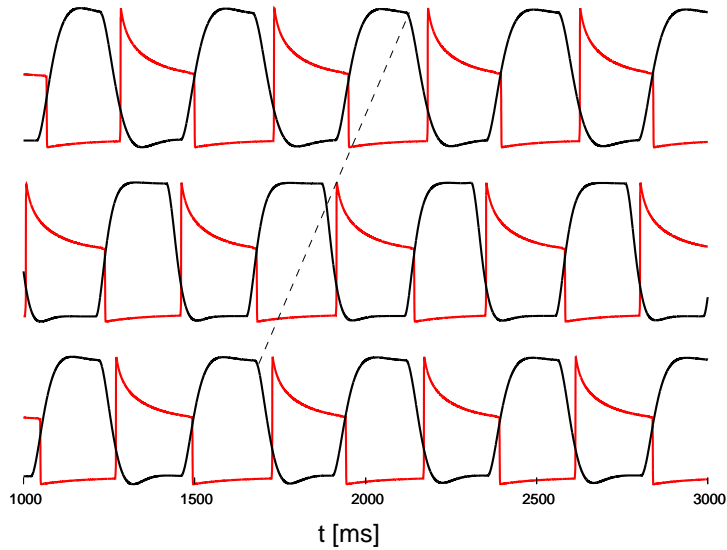


Figure 3.23: Time course of the angle  $\beta$  in the CTr-joint (black) and retractor CPG neuron (red) displayed for the pro-thorax (upper panel), the meso-thorax (middle panel) and the meta-thorax (bottom panel) during tripod. The dashed line indicates the caudo-rostral metachronal wave.

The simulations in figure 3.23 begin with the lift-off of the middle leg. It continues with simultaneous stepping of the front and the hind leg. Furthermore, the relation of levator and depressor phase is nearly 1:1. Visualizations of the tetrapod and the tripod gaits are shown in *Suppl11* and *Suppl12* (Gruhn Lab Webpage, 2012). In each gait simulation two identical data files are used for each side of the stick insect. In the case of the tetrapod these

files are started with a contralateral phase lag of 33% (see figure 2.17). In the case of the tripod these files are started with a contralateral phase lag of 50% (see figure 2.19).

In the following, two kinds of switches will be presented depending on the direction of switching between the gaits. The gait transition is successively executed when the legs have ground contact. In figure 3.24 the switch is first fulfilled immediately in the hind leg. The leg lifts off without delay and the retraction is terminated, i.e. the leg exerts the protraction phase. However, in the tripod this protraction phase is longer. The middle leg can just begin with its lift-off by the time the hind leg has ground contact. This provokes the middle leg to remain in the stance phase until it can be lifted off again. The same applies to the front leg. It stays in the stance leg until the middle leg has ground contact. Ongoing, the front leg is simultaneously lifted off with the hind leg. The foot fall pattern for the walking sequence is shown in figure 3.25. *Suppl13* (Gruhn Lab Webpage, 2012) shows a visualization of the switch from tetrapod to tripod.

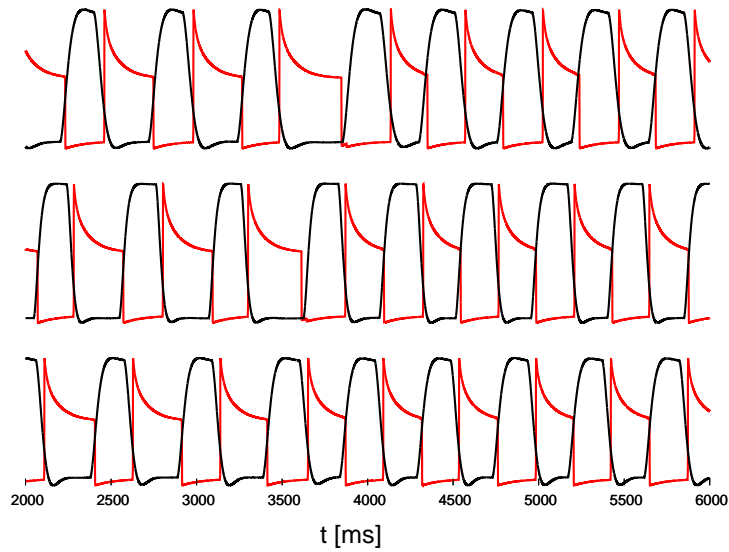


Figure 3.24: Time course of the angle  $\beta$  in the CTr-joint (black) and retractor CPG neuron (red) displayed for the pro-thorax (upper panel), the meso-thorax (middle panel) and the meta-thorax (bottom panel) during switching from tetrapod to tripod.

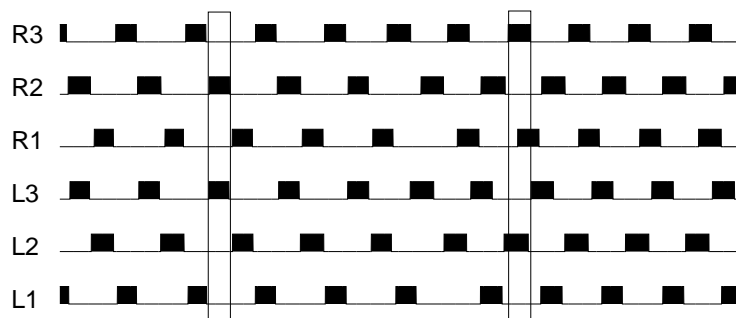


Figure 3.25: Foot fall pattern for the switching sequence between the tetrapod and tripod gait. Black boxes indicate the swing phase of a leg. The left box enframes two legs being simultaneously lifted off during the tetrapod gait. The right box enframes three legs simultaneously lifted off during the tripod gait.

If the tripod gait is switched to the tetrapod, the transition will happen in the front and hind leg at the same time. This is due to their simultaneous lift-off. The switch takes place by the time both, the hind and the front leg, enter the stance phase. The retraction phase and the cyclic period are adjusted and the hind leg lifts off when the retraction is performed. This is the beginning of a new cycle. The levator of the middle leg is suppressed until one third of the cyclic period is elapsed and the middle leg is lifted off. Analogously, after two thirds of the cyclic period the front leg is lifted off. The hind leg lifts off when the front leg touches ground and a new stepping cycle begins (c.f. figures 3.26 and 3.27 and *Suppl14* Gruhn Lab Webpage (2012)).

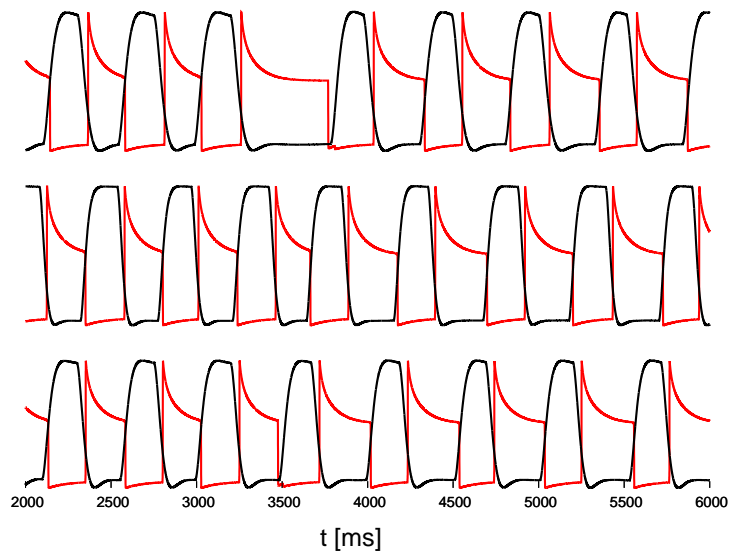


Figure 3.26: Time course of the angle  $\beta$  in the CTr-joint (black) and retractor CPG neuron (red) displayed for the pro-thorax (upper panel), the meso-thorax (middle panel) and the meta-thorax (bottom panel) during switching from tripod to tetrapod.

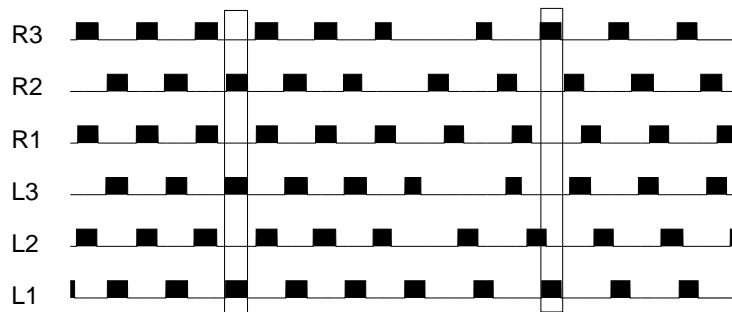


Figure 3.27: Foot fall pattern for the switching sequence between the tripod and tetrapod gait. Black boxes indicate the swing phase of a leg. The left box enframes three legs being simultaneously lifted off during the tripod gait. The right box enframes two legs simultaneously lifted off during the tetrapod gait.



# Chapter 4

## Discussion

### 4.1 Summary of the model structure and its properties

In this work, a mathematical model for insect locomotion has been developed. This model describes the motion of insect legs on the neuronal and mechanical basis. The cores of the neuronal system are central pattern generators (CPGs). Their activities are transferred via interneurons (INs) to motoneurons (MNs). For each one of the three main leg joints a mechanical model, with due regard to the geometry of the stick insects' anatomy, is developed. Leg joints are intrasegmentally and intersegmentally coupled per sensory pathway interneurons. Sensory signals that arise from the campaniform sensilla (CS) are lumped together into a single quantity represented by the joint angles from the LD systems of the three ipsilateral legs. A further intrajoint sensory signal in the FE system from the femoral chordotonal organ (fCO) is represented by the local joint angle and it guarantees the stabilization of the movement. This model is capable of mimicking experimental

findings. It comprises intrasegmental and intersegmental coupling via sensory feedback, forward stepping, backward stepping, sideward stepping and switching between them, applicability to front, middle and hind legs and the generation of walking gaits inclusive their transitions.

The model, which is presented here, uses existing blocks, such as the interneuron and the motoneuron model introduced in section 2 (Daun et al., 2009; Daun-Gruhn, 2011), the neuro-mechanical model for a two-joint system including a simple mechanism of switching in stepping direction (Toth et al., 2012) and intersegmental network models considering gait transitions (Daun-Gruhn and Toth, 2011; Daun-Gruhn et al., 2011). Following a summary of these existing models, the cooperative work on the third main joint of a middle leg including the coupling to the two-joint system, a switching mechanism for sideward stepping and including a model for curve walking (Knops et al., 2012) is presented. Subsequently, the model is novelly applied to the front and hind legs and with the assumed intersegmental connection of ipsilateral legs the model raises features in the generation of gaits and transition between them.

The muscle model used here is a simplification of the Hill model (c.f. section 2.3). There are more elaborate models, such as the one for the flexor-extensor muscle pair by Blümel (2012a,b,c). It concerns the determination of Hill-type muscle model parameters and their inter-individual variation. Furthermore, the model has to be applicable to all the muscle pairs in the stick insect legs. Due to its simplicity, the model does not require high computational power. So far, the model presented here takes only fast muscle fibers into account. Fast muscle fibers are responsible for the limb movement and the propulsion of the body. On the contrary, slow muscle fibers have impact on the posture of the body. These muscle fibers enable the treatment of environmental

constraints, such as the conquest of obstacles or the execution of search movements. Considering the recruitment of several slow and fast muscle fiber units, the number of fixed joint positions increases with the number of implemented fiber units.

The equations of mechanical motion are obtained separately. The three systems (PR, LD and FE) are, however, mechanically coupled. This passive mechanical coupling is very weak compared to the size of the elastic forces measured in the experiments. Indeed, Hooper et al. (2009) shows that the torques due to passive mechanical coupling can be neglected in small animals in general, and in the stick insect and cockroach locomotor system, in particular. This sufficiently justifies the separate treatment of the two mechanical systems (Toth et al., 2012; Knops et al., 2012).

In the model, gravitation is not considered, since muscle forces are large compared to gravitational forces (Hooper et al., 2009) and the latter can therefore be neglected.

Pools of neurons with equal functions are represented as single neurons. Despite of this simplification in the stick insect these pools are indeed quite small and consist of dozens of neurons (Toth et al., 2012). For example, the motoneurons innervating the same muscle must be simultaneously active. The situation is the same as it is with regard to the interneurons driving the motoneurons. Hence, the properties of a single neuron mirrors the properties of all the neurons in a pool.

## 4.2 Discussion of the results

This study begins with the modeling of the middle leg, because it is the best investigated leg in the stick insect. The model is extended to the front and the hind legs with minimal changes in parameters such as masses and lengths. The angular ranges in all joints of the animals show a high variety. In the first approach kinematical data from Schumm and Cruse (2006) are used for the simulation of  $\alpha$ ,  $\beta$  and  $\gamma$  in the middle leg. These data are obtained from a treadmill experiment and the angular motion in the FTi-joint is forced to a small range. While this range is widened in order to mimic the motion that is seen in video records, the motion in the ThC-joint and the CTr-joint seemed suitable.

Looking at the extension of the model to the front and the hind legs more closely, one can see that the minimal and maximal angles in the ThC-joint must match with regards to the AEP and PEP in each leg. As to that, data from M. Gruhn (not published yet) are taken. The angular range in the CTr-joint from Schumm and Cruse (2006) seems suitable for the simulation of the locomotion of all legs.

Considering a single leg, position, load and touch signals make contributions to the coupling of the individual CPGs in the stick insects' legs. In this model the sensory signals from the CS in each leg are lumped together into a single afferent signal represented by the angle in the respective LD system. This simplification can be justified because firstly, these afferent signals of different modality eventually converge on pre-motor and pre-CPG neurons acting in their entirety. Secondly, the partial impact of the individual sensory signals is not known in detail, hence, taking their integrated effect in form of a single signal to circumvent the weighting problem. Thirdly, walking on a plane surface is so simple that it does not require the differential effects of

the individual sensory signals. The threshold values of the angle  $\beta$  for the intraleg coupling are different in the FE and the PR system. This expresses the differential effects these sensory afferent signals exert on the two neuromuscular systems.

Experimental data show that single front leg stepping activates the ThC-joint CPG neurons of the ipsilateral middle leg and elicits alternating activity in the corresponding ThC-joint MNs (Ludwar et al., 2005; Borgmann et al., 2007). With pharmacological activation of the meta-thoracic segment the three ipsilateral ThC-joint MN pools are in phase active coupled to front leg stepping. This influence contributes to interleg coupling by keeping at least one caudal leg in phase with the front leg under the impact of sensory feedback (Borgmann et al., 2009). These conclusions lead to the following suggestions: There are excitatory connections from the ThC-joint CPG of the front leg to the ipsilateral middle and hind leg, and beyond these connections become magnified when sensory signals are present. Whereas the excitatory connection from the front to the hind leg is not enhanced by sensory feedback, because only increase in tonic activity has been measured in the meta-thorax MNs. There seems to be no interleg coupling between a stepping middle leg and the front or hind leg, since the corresponding ThC-joint MNs also show only an increase in tonic activity. Nevertheless, rhythmic activity of the hind leg is possible, in case of both the front and the hind leg being intact. This leads to the assumption that there is a weak excitatory connection by the presence of sensory signals. Furthermore, the activity of ThC-joint CPG neurons in the hind leg is independent from front leg stepping (Borgmann et al., 2009). This suggests inhibitory synaptic connections from i) the ThC-joint CPG of the front leg to that one of the middle leg and ii) the ThC-joint CPG of the middle leg to that one of the hind leg in

equal strength. A further inhibitory connection from the front leg to the hind leg is weaker than the aforementioned connections. Stepping of the hind leg enhances the inhibitory connection from the middle to the hind leg such that it becomes stronger than the connection from the front leg to the middle leg (Daun-Gruhn, 2011). In Daun-Gruhn and Toth (2011) a cyclic intersegmental connection that is theoretically necessary for the transition of gaits is suggested. At present M. Grabowska is working on the experimental evidence relating to this.

The generation of the tetrapod gait requires an inhibitory connection from front to rear (see section 3.3). The coupling strength can be varied about a wide range from weak influences to strong influences. For the generation of a rostral metachronal wave in the stepping pattern it is more appropriate setting the strength of the synaptic connection to a high value. This shortens the retraction phase of the next-caudal leg and supports the begin of its protraction during its swing phase. Otherwise, there is a little overlap of the retraction and levation phase in the intrasegmental coordination of a leg. This property is seen in the simulation with the middle-leg model and is a consequence of the discrepancy of the phase relations in the PR system (1:3) and the LD system (3:5).

During tripod gait the ipsilateral front and hind legs are simultaneously in the swing phase and the middle leg is in the stance phase. An excitatory connection between front and hind leg and an inhibitory connection between them and the middle leg is successfully tested and works well in a wide range of coupling strengths. However, a re-wiring of the intersegmental coupling due to a gait transition is less desirable. Hence, the tripod is performed with the configuration of the tetrapod and revealed reliability when the coupling strengths of all inhibitory intersegmental synapses are weak.

There is a discrepancy in the contralateral coupling of the legs during the gait transition into both directions. For example, if the transition from the tetrapod to the tripod is performed, the simulation will begin with a contralateral phase lag of  $1/3$ . The cyclic period is  $T_{4pod}$ , i.e.  $T_{4pod}/3$  in absolute time. Consequently, the transition takes place on both sides with a time shift of  $T_{4pod}/3$ . On one side the simulation ends earlier than it does on the other side by the amount  $T_{4pod}/3$ . For the ideal tripod the ideal contralateral phase lag is  $1/2$  and the cyclic period is  $T_{3pod}$ . In the ideal case this time shift equals  $T_{3pod}/2$ . In other words: When the ratio of cyclic periods  $T_{3pod}/T_{4pod}$  equals  $2/3$  the transition can take place without delay in certain legs. Deviations from this ratio lead to a conspicuousness in stepping pattern, such as occasionally extended stance phases, extended swing phases or multiple stepping. That has already been observed in experiments by Grabowska et al. (2012). The ratio  $T_{3pod}/T_{4pod}$  is a little higher than  $2/3$  because the cyclic period of the tripod could not be set to an arbitrary value. This is a limitation of the CPG model. The actual ratio of cyclic periods leads to a contralateral phase lag for the tripod that is smaller than  $1/2$  ( $\sim 5/12$ ). It has no strong effects, but the contralateral delay has to be compensated. The compensation could be achieved by the use of sensory organs. For example by holding the leg that is rushing ahead at its PEP until the proper phase lag is attained.

The switch from forward stepping to backward stepping or sideward stepping is carried out by redistributing the output of the CPG to the MNs instead of modifying the CPG activity in the PR system. This would have produced a transient time exceeding the stepping period ( $\approx 0.5$  s) that was not observed in experiments (Toth et al., 2012). Almost instantaneous changes and fast changes of motor patterns are achieved by changing solely one or two control variables in the same control network. This network structure (see figure

3.11) is chosen, because the mechanism should be mostly simple and it has to reproduce experimental observations at the same time.

### 4.3 Comparison to existing models

There are modeling studies based on experimental data by (Ludwar et al., 2005; Borgmann et al., 2007, 2009) where the intersegmental connection of legs are realized by weak inhibitory connections between protractor CPG neurons. These connections are enhanced by signals from the next-rostral levator motoneuron via sensory feedback (Daun-Gruhn, 2011). Therefore, they generate caudal walking patterns that help to coordinate leg movement. This model is extended by a motoneuron model with spike-frequency adaption properties, inhibitory CPG-to-MN linkage via additional interneurons and sensory stimulation inputs from the depressor peripheries modifying the cyclic intersegmental connections between retractor CPG neurons Daun-Gruhn and Toth (2011). The choice of a depressor-to-retractor activation is equivalent to a levator-to-protractor activation. Again, this model is extended now by the completion of the legs by the attachment of further leg joints and their coupling via a sensory pathway. The intersegmental coupling is done through the inhibition of one of the sensory pathway interneurons. In contrast to this, the excitatory and inhibitory synaptic connection via sensory interneurons can directly affect the retractor CPG neurons (Daun-Gruhn and Toth, 2011). A direct connection is not practicable in this model, since it is tested that the direct intersegmental connection to the CPG interferes with the intrasegmental sensory coupling of the leg. The intersegmental connection is carried out by a linkage to the sensory pathways of the PR system



and thereby to the retractor CPG neuron of the respective leg. Theoretically this synaptic connection can be inhibitory or excitatory, or both. The main intention in this instance is to implement a coupling scheme i) that is uniform for each of the three segments of the stick insect with respect to the coupling structure and coupling strength and ii) that is suitable to different gaits. In Toth and Gruhn (2011) the sensory pathway is introduced and finds its first application to the levator-depressor motor system in Daun-Gruhn et al. (2011). The modulation of the CPG neuron activities of the levator-depressor unit leads to MN activity patterns that resemble those found in extracellular recording in the stick insect. Moreover, the model yields information of biological properties of these measurements that depend on the applied stimuli to the animal.

Experiments on the kinematics of leg movement by Dürr et al. (2004) show that mechanical couplings play a dominant role in the coordination of contralateral legs in the stick insect. In contrast, the neuronal coupling between contralateral legs is weak (Borgmann et al., 2007, 2009; Westmark et al., 2009). Thus, it is sufficient to model the intersegmental coupling on the ipsilateral side of the stick insect and to attach the resulting stepping pattern to a time shifted copy of itself. The time shift equals the phase lag of the contralateral legs (see figures 2.17 and 2.19). Therewith, one can produce the two main gaits (tripod and tetrapod) in the stick insect. Particularly, one can distinguish between two kinds of tetrapod, depending on the timing of the lift-off of diagonal legs. There is no such differentiation made in this study, because these subgaits can be transferred into each other by mirroring. Regarding to this, there is no specification made here about the left side or the right side.

There are models that realize curve walking by the control retraction ampli-

tude, i.e. the change of stride length of the legs (Cruse et al., 1998; Dürr et al., 2004). The Walknet described and used in Cruse et al. (1998); Dürr et al. (2004), concerns the propulsion of the insects' body through the coordination of legs without the use of CPGs. Instead, displacement feedback from joint angles is transformed into active movement. Nevertheless, the implementation of a set of coordination rules leads to a decentralized generation of walking gaits. In particular, their model enables obstacle avoidance reflexes and cyclic searching movements.

Though these models seem to be suitable for small curvature, observations during curve walking with sharp curvatures raise a discrepancy to the models (Kindermann, 2002). The control mechanism allows a change of the stride length, but cannot make the exchange of retraction and protraction phases, i.e. for backward stepping. However, backward stepping is observed in stick insects during curve walking (Gruhn et al., 2009). A neuro-mechanical leg controller with sensor-motor pathways developed by (Ekeberg et al., 2004) enables the generation of coordinated forward walking in the stick insects middle leg. This model is built of artificial bistable control systems instead of CPGs and it exercises switching between forward, backward and sideward stepping. Another type of models generates locomotion by phase oscillators, such as models for salamanders (Ijspeert et al., 2007) and cockroaches (Holmes et al., 2006). They have successfully created neuro-muscular systems with predetermined activity patterns, but the relation between model parameters and biological quantities is still unknown. The phase oscillator model has been extended by Harischandra et al. (2010) in order to model curve walking in the salamander. The authors compare different turning strategies for terrestrial salamander locomotion: bending of the trunk, sideward stepping of the front legs or a combination of both. They conclude

that the walking gait of the animal plays an important role in efficiency of turning. That model does not consider backward stepping during turning although such events have been observed in the salamander (Cabelguen et al., 2010).

The hexaped controller presented in Twickel et al. (2011) is built of six identical single leg controllers. It is robust against perturbation and is capable of behavioral adaptation with the adjustment of parameters. The parameters are either hand-tuned or optimized by an evolutionary algorithm. Though various biological data are matched the model does not include intersegmental coupling between the six single leg controllers that build the hexaped controller.

Since it preserves a close correspondence between model parameters and physiological quantities, the approach in this work is different from that in those models mentioned above. The advantages of this approach are discussed in Daun-Gruhn and Büschges (2011).

## 4.4 Biological significance of the model and outlook

Owing to its detailed suggestions how this system can carry out coordinated movements in a number of natural conditions i.e. during forward walking, backward walking and turning, the model renders itself physiological relevant. Above, it shows how the changes between the walking modes might be brought about in its biological counterpart, the stick insect. The simplicity of the mechanisms by which these changes can be carried out is a particular merit of the model.

In addition to the capability of reproducing locomotion, the significance of the model lies in its ability to predictions in a neurophysiological context that can be tested in future experiments. In this respect, M. Grabowska is looking for the cyclic intersegmental connection, i.e. a connection from the hind leg to the front leg, in the stick insect. The inhibitory or excitatory nature, the strengths of those connections and the question, how central and sensory influences do interact during tetrapod and tripod, are of great interest. Furthermore, a reset of the CPG during the switch of the stepping direction can be disproved by simultaneous recordings of the E4 interneuron and the PR motoneurons.

Starting the intrinsic LD systems at proper times initiates the stable tripod or tetrapod gait. In a way, these walking gaits are artificial, because the LD systems are intrinsically active and not driven by sensory signals. The main approach is to implement a feedback from the PR system triggered by the AEP or PEP of the stick insects legs. This is done by giving a pulse to the peripheral input to the LD whenever the respective leg is in the vicinity of the PEP, so that the sense organs in the end elicit the depressor phase of the LD system. However, this signal causes both of the neurons of this CPG to be caught in their active phase. A subsequent reset of the CPG and a reconciliation with the actual parameters in the FE and the PR systems would also make gait generation in this model somehow artificial. This is a problem that has to be solved in the future. With an implementation of sensory feedback from the PR system to the LD system the response of the model to slight variations from stability could be tested.

Whereas this study focuses on middle legs during turning, it is also possible to pay attention to the front and hind legs. Especially the interplay of all legs with regard to their stepping directions might be of some interest. By

taking mechanical coupling into account one can get a clear idea of insect locomotion. The network including contralateral coupling could be realized by a load function that comprises weak neuronal and strong mechanical influences.

# Appendix A

## Summary of the model parameters

### A.1 Neuron models

Table A.1: Numerical values of the membrane capacitance and the time constant coefficient for all neurons.

CPG neurons	
time constant coefficient in PR	$\epsilon = 0.0019$
membrane capacitance in PR	$C_m = 1.1493 \text{ pF}$
time constant coefficient in LD	$\epsilon = 0.0012$
membrane capacitance in LD	$C_m = 1.8308 \text{ pF}$
time constant coefficient in FE	$\epsilon = 0.0023$
membrane capacitance in FE	$C_m = 0.9154 \text{ pF}$
Interneurons	
time constant coefficient	$\epsilon = 0.010$
membrane capacitance	$C_m = 0.210 \text{ pF}$
Motoneurons	
membrane capacitance in	$C_m = 1.0 \text{ pF}$

Table A.2: Numerical values of the parameters for the CPG neurons.

Parameters of persistent sodium current $I_{NaP}$	
All CPG neurons	$g_{NaP} = 10 \text{ nS}$
All CPG neurons	$E_{Na} = 50 \text{ mV}$
All CPG neurons	$V_{hm} = -37 \text{ mV}$
All CPG neurons	$\gamma_m = -1/6 \text{ mV}^{-1}$
All CPG neurons	$V_{hh} = -30 \text{ mV}$
All CPG neurons	$\gamma_h = -1/6 \text{ mV}^{-1}$
All CPG neurons	$V_{\tau h} = -30 \text{ mV}$
All CPG neurons	$\gamma_\tau = -1/12 \text{ mV}^{-1}$
Parameters of the leakage current $I_L$	
All CPG neurons	$g_L = 2.8 \text{ nS}$
All CPG neurons	$E_L = -65 \text{ mV}$
Parameters of driving current $I_{app}$	
Protractor CPG neurons	$g_{app} = 0.205 \text{ nS}$
Retractor CPG neurons	$g_{app} = 0.165 \text{ nS}$
Levator CPG neurons	$g_{app} = 0.230 \text{ nS}$
Depressor CPG neurons	$g_{app} = 0.184 \text{ nS}$
Extensor CPG neurons	$g_{app} = 0.209 \text{ nS}$
Flexor CPG neurons	$g_{app} = 0.100 \text{ nS}$
All CPG neurons	$E_{app} = 0 \text{ mV}$



Table A.3: Numerical values of the parameters for the interneurons.

Parameters of $I_{NaP}$	
Excitatory peripheral INs at PR and FE	$g_{NaP} = 5 \text{ nS}$
Excitatory peripheral INs at LD	$g_{NaP} = 7 \text{ nS}$
All other interneurons	$g_{NaP} = 10 \text{ nS}$
All interneurons	$E_{Na} = 50 \text{ mV}$
All interneurons	$V_{hm} = -37 \text{ mV}$
All interneurons	$\gamma_m = -1/6 \text{ mV}^{-1}$
All interneurons	$V_{hh} = -30 \text{ mV}$
All interneurons	$\gamma_h = -1/6 \text{ mV}^{-1}$
All interneurons	$V_{\tau h} = -30 \text{ mV}$
All interneurons	$\gamma_\tau = -1/12 \text{ mV}^{-1}$
Parameters of $I_L$	
INs to MNs	$g_L = 2.8 \text{ nS}$
Inhibitory peripheral INs	$g_L = 6.8 \text{ nS}$
Excitatory peripheral INs at PR and FE	$g_L = 10 \text{ nS}$
Excitatory peripheral INs at LD	$g_L = 9.85 \text{ nS}$
All interneurons	$E_L = -65 \text{ mV}$
Parameters of $I_{app}$	
All inhibitory INs to MNs	$g_{app} = 1.6 \text{ nS}$
All inhibitory INs to CPG	$g_{app} = 2.0 \text{ nS}$
Excitatory peripheral neurons	$g_{app} = 2.0 \text{ nS}$
Inhibitory peripheral neurons	$g_{app} = 0.0 \text{ nS}$
All inhibitory INs	$E_{app} = -80 \text{ mV}$
All excitatory INs	$E_{app} = 0 \text{ mV}$

Table A.4: Numerical values of the parameters for the synapses.

Parameters of $I_{syn}$ (CPG to CPG)	
All synapses	$V_{hs} = -43$ mV
All synapses	$\gamma_s = -10$ mV <sup>-1</sup>
All synapses	$g_{syn} = 1.0$ nS
All synapses	$E_{syn} = -80$ mV
Parameters of $I_{syn}$ (inhibitory IN to CPG)	
All synapses	$V_{hs} = -43$ mV
All synapses	$\gamma_s = -10$ mV <sup>-1</sup>
All synapses	$g_{syn} = 0.05$ nS
All synapses	$E_{syn} = -80$ mV
Parameters of $I_{syn}$ (excitatory IN to CPG)	
All synapses	$V_{hs} = -43$ mV
All synapses	$\gamma_s = -0.42$ mV <sup>-1</sup>
All synapses	$g_{syn} = 0.1$ nS
All synapses	$E_{syn} = 0$ mV
Parameters of $I_{syn}$ (inhibitory IN to MN)	
All synapses	$V_{hs} = -43$ mV
All synapses	$\gamma_s = -0.1$ mV <sup>-1</sup>
All synapses	$g_{syn} = 0.25$ nS
All synapses	$E_{syn} = -80$ mV
Parameters of $I_{syn}$ (excitatory CPG to IN)	
All synapses	$V_{hs} = -43$ mV
All synapses	$\gamma_s = -10$ mV <sup>-1</sup>
All synapses	$g_{syn} = 0.5$ nS
All synapses	$E_{syn} = 0$ mV

Table A.5: Numerical values of the parameters for the CPG motoneurons.

Parameters of persistent sodium current $I_{NaP}$	
All MNs	$g_{NaP} = 10$ nS
All MNs	$E_{Na} = 55$ mV
All MNs	$a_{m1} = 0.32$ mV
All MNs	$a_{m2} = -51.9$ mV <sup>-1</sup>
All MNs	$a_{m3} = 0.25$ mV
All MNs	$b_{m1} = -0.28$ mV
All MNs	$b_{m2} = -24.9$ mV <sup>-1</sup>
All MNs	$b_{m3} = -0.20$ mV
All MNs	$a_{h1} = 0.128$
All MNs	$a_{h2} = -48.0$ mV <sup>-1</sup>
All MNs	$a_{h3} = 0.056$ mV
All MNs	$b_{h1} = 4.0$
All MNs	$b_{h2} = -25.0$ mV <sup>-1</sup>
All MNs	$b_{h3} = 0.20$ mV

Table A.6: Numerical values of the parameters for the potassium current in the CPG motoneurons.

Parameters of the potassium current $I_K$	
All MNs	$g_K = 2 \text{ nS}$
All MNs	$E_K = -80 \text{ mV}$
All MNs	$a_{m1} = 0.016 \text{ mV}$
All MNs	$a_{m2} = -29.9 \text{ mV}^{-1}$
All MNs	$a_{m3} = 0.20 \text{ mV}$
All MNs	$b_{m1} = 0.25$
All MNs	$b_{m2} = -45.0 \text{ mV}^{-1}$
All MNs	$b_{m3} = 0.025 \text{ mV}$

Table A.7: Numerical values of the parameters for the adaptation current in the CPG motoneurons.

Parameters of the adaptation current $I_q$	
All MNs	$g_q = 12 \text{ nS}$
All MNs	$E_q = 12 \text{ mV}$
All MNs	$V_{hm} = -30 \text{ mV}$
All MNs	$\gamma_m = -0.6 \text{ mV}^{-1}$
All MNs	$r_q = 0.0005$

Table A.8: Numerical values of the parameters for the leakage current in the CPG motoneurons.

Parameters of the leakage current $I_L$	
All MNs	$g_L = 0.8 \text{ nS}$
All MNs	$E_L = -70.0 \text{ mV}$

Table A.9: Numerical values of the parameters for the applied current in the CPG motoneurons.

Parameters of the applied current $I_{app}$	
All MNs	$g_{app} = 0.19 \text{ nS}$
All MNs	$E_{app} = 0 \text{ mV}$

## A.2 Mechanical models

Table A.10: Geometrical parameters in the muscles used in the simulation measured by Guschlbauer et al. (2007) or estimated from their measurements. These parameters refer to the middle leg of the stick insect, but were also used for the simulation of the front leg and the hind leg.

	Extensor	Flexor
Minimal length of the fiber	$l_{E,min} = 1.05$ mm	$l_{F,min} = 1.50$ mm
Length of the fiber at $\gamma = 90^\circ$	$l_{E,0} = 1.41$ mm	$l_{F,0} = 2.11$ mm
Angle between tendon and muscle fiber at $\gamma = 90^\circ$	$\phi_{E0} = 13.5^\circ$	$\phi_{F0} = 12.6^\circ$
Distance between cuticle and tendon	$h_E = 0.34$ mm	$h_F = 0.42$ mm
Distance of tendon mounting and rotation point	$d = 0.28$ mm	$2d = 0.56$ mm

Table A.11: Geometrical parameters in the muscles used in the simulation estimated from Bässler (1983) (see Figure 2.3). These parameters refer to the middle leg of the stick insect, but are also used for the simulation of the front leg and the hind leg.

Minimal length of the levator fiber	$l_{L,min} = 1.05 \text{ mm}$
Minimal length of the depressor fiber	$l_{D,min} = 1.50 \text{ mm}$
Radius	$r = 1.0 \text{ mm}$
Distance $\overline{AB}$	$d = 3.5 \text{ mm}$

Table A.12: Geometrical parameters in the muscles used in the simulation estimated from Bässler (1983) (see Figure 2.3). These parameters refer to the middle leg of the stick insect, but are also used for the simulation of the front leg and the hind leg.

Minimal length of the levator fiber	$l_{P,min} = 1.0 \text{ mm}$
Minimal length of the depressor fiber	$l_{R,min} = 1.5 \text{ mm}$
Radius	$r = 2.5 \text{ mm}$
Distance	$d = 2.0 \text{ mm}$

Table A.13: Masses and lengths in all segments of the stick insect. Own measurements.

Pro-thorax	
Femur mass	0.0099 g
Femur length	16 mm
Tibia mass	0.0039 g
Tibia length	16 mm
Meso-thorax	
Femur mass	0.0073 g
Femur length	13 mm
Tibia mass	0.0021 g
Tibia length	12 mm
Meta-thorax	
Femur mass	0.0084 g
Femur length	15 mm
Tibia mass	0.0034 g
Tibia length	15 mm



Table A.14: Numerical values (estimated) of the extremal angles in the middle leg of the stick insect. Dynamical parameters in the muscles are obtained in simulations with an isolated FTi-joint.

Minimal angle	$\gamma_{min} = 45^\circ$
Maximal angle	$\gamma_{max} = 110^\circ$
Momentum of inertia of the tibia	0.1008 gmm <sup>2</sup>
Spring constants during extension	$k_E = 4050 \frac{\text{mN}}{\text{mm}^2}$ , $k_F = 55 \frac{\text{mN}}{\text{mm}^2}$
Spring constants during flexion	$k_E = 510 \frac{\text{mN}}{\text{mm}^2}$ , $k_F = 296 \frac{\text{mN}}{\text{mm}^2}$
Viscosity of the muscle	$b_{v,FE} = 12.5 \frac{\text{g}}{\text{s}}$

Table A.15: Numerical values of the extremal angles in the middle leg of the stick insect are estimated from Schumm and Cruse (2006). Dynamical parameters in the muscles are obtained in simulations with an isolated CTr-joint.

Minimal angle	$\beta_{min} = 30^\circ$
Maximal angle	$\beta_{max} = 60^\circ$
Effective momentum of inertia	0.9341 gmm <sup>2</sup>
Spring constants during levation	$k_L = 1868.1 \frac{\text{mN}}{\text{mm}^2}$ , $k_D = 160.0 \frac{\text{mN}}{\text{mm}^2}$
Spring constants during depression	$k_L = 879.21 \frac{\text{mN}}{\text{mm}^2}$ , $k_D = 800.0 \frac{\text{mN}}{\text{mm}^2}$
Viscosity of the muscle	$b_{v,LD} = 84.0 \frac{\text{g}}{\text{s}}$

Table A.16: Numerical values of the extremal angles in the stick insects middle leg taken from measurements from Gruhn (unpublished results). Dynamical parameters in the muscles are obtained in simulations with an isolated ThC-joint.

Minimal angle	$\alpha_{min} = 70^\circ$
Maximal angle	$\alpha_{max} = 120^\circ$
Effective momentum of inertia	0.9341 gmm <sup>2</sup>
Spring constants during protraction	$k_P = 300 \frac{\text{mN}}{\text{mm}^2}$ , $k_R = 228.42 \frac{\text{mN}}{\text{mm}^2}$
Spring constants during retraction	$k_P = 30 \frac{\text{mN}}{\text{mm}^2}$ , $k_R = 236.75 \frac{\text{mN}}{\text{mm}^2}$
Viscosity of the muscle	$b_{v,PR} = 25.5 \frac{\text{g}}{\text{s}}$

Table A.17: Alternative set of numerical values of the extremal angles estimated from Schumm and Cruse (2006). Dynamical parameters in the muscles are obtained in simulations with an isolated ThC-joint.

Minimal angle	$\alpha_{min} = 28^\circ$
Maximal angle	$\alpha_{max} = 128^\circ$
Effective momentum of inertia	0.288 gmm <sup>2</sup>
Spring constants during protraction	$k_P = 1000 \frac{\text{mN}}{\text{mm}^2}$ , $k_R = 16 \frac{\text{mN}}{\text{mm}^2}$
Spring constants during retraction	$k_P = 25 \frac{\text{mN}}{\text{mm}^2}$ , $k_R = 429 \frac{\text{mN}}{\text{mm}^2}$
Viscosity of the muscle	$b_{v,PR} = 25.5 \frac{\text{g}}{\text{s}}$

Table A.18: Dynamical parameters of the muscles in the front leg (obtained in simulations with an isolated FTi-joint). Numerical values of the extremal angles are borrowed from the estimations in the middle leg A.14.

Minimal angle	$\gamma_{min} = 45^\circ$
Maximal angle	$\gamma_{max} = 110^\circ$
Momentum of inertia of the tibia	$0.3328 \text{ gmm}^2$
Spring constants during extension	$k_E = 5967 \frac{\text{mN}}{\text{mm}^2}$ , $k_F = 81.39 \frac{\text{mN}}{\text{mm}^2}$
Spring constants during flexion	$k_E = 867 \frac{\text{mN}}{\text{mm}^2}$ , $k_F = 503.54 \frac{\text{mN}}{\text{mm}^2}$
Viscosity of the muscle	$b_{v,FE} = 30.6 \frac{\text{g}}{\text{s}}$

Table A.19: Dynamical parameters in the muscles of the front leg (obtained in simulations with an isolated CTr-joint). Numerical values of the extremal angles are borrowed from the estimations in the middle leg A.15.

Minimal angle	$\beta_{min} = 30^\circ$
Maximal angle	$\beta_{max} = 60^\circ$
Effective momentum of inertia	$2.38 \text{ gmm}^2$
Spring constants during levation	$k_L = 2428.5 \frac{\text{mN}}{\text{mm}^2}$ , $k_D = 208.0 \frac{\text{mN}}{\text{mm}^2}$
Spring constants during depression	$k_L = 967.13 \frac{\text{mN}}{\text{mm}^2}$ , $k_D = 880.0 \frac{\text{mN}}{\text{mm}^2}$
Viscosity of the muscle	$b_{v,LD} = 134.4 \frac{\text{g}}{\text{s}}$

Table A.20: Dynamical parameters of the muscles in the front leg (obtained in simulations with an isolated ThC-joint). Numerical values of the extremal angles taken from measurements from Gruhn (unpublished results).

Minimal angle	$\alpha_{min} = 45^\circ$
Maximal angle	$\alpha_{max} = 100^\circ$
Effective momentum of inertia	2.38 gmm <sup>2</sup>
Spring constants during protraction	$k_P = 440 \frac{\text{mN}}{\text{mm}^2}$ , $k_R = 88.5 \frac{\text{mN}}{\text{mm}^2}$
Spring constants during retraction	$k_P = 82.5 \frac{\text{mN}}{\text{mm}^2}$ , $k_R = 209.39 \frac{\text{mN}}{\text{mm}^2}$
Viscosity of the muscle	$b_{v,PR} = 32.5 \frac{\text{g}}{\text{s}}$

Table A.21: Dynamical parameters of the muscles in the hind leg (obtained in simulations with an isolated FTi-joint). Numerical values of the extremal angles are estimated.

Minimal angle	$\gamma_{min} = 25^\circ$
Maximal angle	$\gamma_{max} = 60^\circ$
Momentum of inertia of the tibia	0.255 gmm <sup>2</sup>
Spring constants during extension	$k_E = 13000 \frac{\text{mN}}{\text{mm}^2}$ , $k_F = 53.642 \frac{\text{mN}}{\text{mm}^2}$
Spring constants during flexion	$k_E = 6300 \frac{\text{mN}}{\text{mm}^2}$ , $k_F = 197.02 \frac{\text{mN}}{\text{mm}^2}$
Viscosity of the muscle	$b_{v,FE} = 19.0 \frac{\text{g}}{\text{s}}$

Table A.22: Dynamical parameters in the muscles of the hind leg (obtained in simulations with an isolated CTr-joint). Numerical values of the extremal angles are borrowed from the estimations in the middle leg A.15.

Minimal angle	$\beta_{min} = 30^\circ$
Maximal angle	$\beta_{max} = 60^\circ$
Effective momentum of inertia	1.81 gmm <sup>2</sup>
Spring constants during levation	$k_L = 2428.5 \frac{\text{mN}}{\text{mm}^2}$ , $k_D = 208.0 \frac{\text{mN}}{\text{mm}^2}$
Spring constants during depression	$k_L = 1143.0 \frac{\text{mN}}{\text{mm}^2}$ , $k_D = 1440.0 \frac{\text{mN}}{\text{mm}^2}$
Viscosity of the muscle	$b_{v,LD} = 126.0 \frac{\text{g}}{\text{s}}$

Table A.23: Dynamical parameters of the muscles in the hind leg (obtained in simulations with an isolated ThC-joint). Numerical values of the extremal angles taken from measurements from Gruhn (unpublished results).

Minimal angle	$\alpha_{min} = 90^\circ$
Maximal angle	$\alpha_{max} = 145^\circ$
Effective momentum of inertia	2.38 gmm <sup>2</sup>
Spring constants during protraction	$k_P = 698.48 \frac{\text{mN}}{\text{mm}^2}$ , $k_R = 765.39 \frac{\text{mN}}{\text{mm}^2}$
Spring constants during retraction	$k_P = 34.419 \frac{\text{mN}}{\text{mm}^2}$ , $k_R = 1108.5 \frac{\text{mN}}{\text{mm}^2}$
Viscosity of the muscle	$b_{v,PR} = 107.1 \frac{\text{g}}{\text{s}}$

# Appendix B

## Simulation with the coupled femur and tibia

For the simulation of the coupled system of femur and tibia the same parameters are used as listed in tables A.15 and A.14. Quantities such as  $A$ ,  $B$ ,  $C$ , etc. introduced in section 2.4 are derived from those. Figure B.1

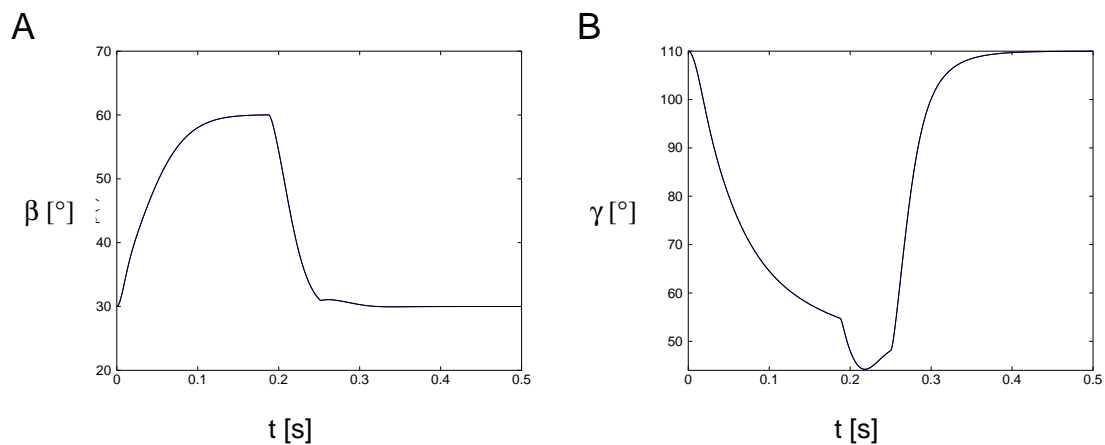


Figure B.1: Time courses of the angles in the CTr-joint (A) and the FTi-joint (B) for the mechanically coupled system.

shows the time course of the angle  $\beta$  in the CTr-joint and the angle  $\gamma$  in

## *APPENDIX B. SIMULATION WITH THE COUPLED FEMUR AND TIBIA*<sup>126</sup>

the FTi-joint ensuing from the coupled mechanical system. The simulation in the CTr-joint begins with the levation and then switches to depression. Shortly before the angle  $\beta$  reaches its minimum there is a little disturbance visible. This is caused by the switch from extension to flexion in the FTi-joint. The same issue can be seen in the time course of the angle  $\gamma$  in the FTi-joint having a greater impact. During extension the motion is affected by the switch in the CTr-joint from levation to depression. All in all, the changes in the angular motion with a mechanically coupled system are not dramatic in comparison to the isolated joints. The implementation of the coupled system would implicate longer computation times and is therefore omitted.

# List of Figures

2.1	Schematic illustration of the leg joints and the basic movement directions . . . . .	12
2.2	Hill's muscle model and simplified muscle model used in this model . . . . .	13
2.3	Front view and plan view of the stick insect's middle leg . . .	14
2.4	Top view on the thorax of the stick insect . . . . .	16
2.5	Front view on the thorax of the stick insect . . . . .	17
2.6	Geometric arrangement of the flexor and extensor muscles . .	21
2.7	Distance between tendon and cuticle . . . . .	22
2.8	Geometry of the levator and depressor muscle pair . . . . .	24
2.9	Top view of the simplified geometrical arrangement in the ThC-joint . . . . .	25
2.10	Sketch of the two limb system for the integration of kinetic energy . . . . .	33
2.11	Sketch of a double pendulum . . . . .	34
2.12	Neuro-mechanical network of a single joint . . . . .	41
2.13	Neuro-mechanical network of a three-joint system . . . . .	43
2.14	Neuro-mechanical network of a three-leg system . . . . .	45
2.15	Simplified sketch of a three-leg network . . . . .	46
2.16	Foot fall pattern during a tetrapod gait . . . . .	48



2.17	Phase lags in the tetrapod gait . . . . .	49
2.18	Foot fall pattern during a tripod gait . . . . .	50
2.19	Phase lags in the tripod gait . . . . .	51
3.1	Motion of the joint angle $\gamma$ in the FTi-joint under the variation of the spring constant . . . . .	57
3.2	Simulation results obtained with the model of a single, isolated FTi-joint . . . . .	59
3.3	Mechanical movement in the neuro-mechanical system . . . . .	60
3.4	Comparison between experimental and simulated results . . . . .	62
3.5	Timing of the movement of the tibia under variation of the critical angle $\beta_{thr}$ . . . . .	64
3.6	Timing of the movement of the tibia under variation of the critical angle $\gamma_{thr}$ . . . . .	65
3.7	Timing of the movement of the tibia under variation of the coupling intrajoint strength . . . . .	66
3.8	Time courses of the three joint angles in the middle leg . . . . .	67
3.9	Known sensory influences on the timing of motor activity . . . . .	68
3.10	Time courses of the three joint angles in the middle leg includ- ing switching between forward and backward stepping . . . . .	70
3.11	Proposed neuronal switching mechanism between stepping di- rections . . . . .	71
3.12	Mechanical movement and neuronal activity in the PR system before and after fixing the retraction position of the femur . . . . .	73
3.13	Curve walking of the simulated stick insect in two different modes . . . . .	77
3.14	Trajectory of the simulated stick insect walking in the plane . . . . .	78
3.15	Time courses of the three joint angles in the front leg . . . . .	80

3.16	Time courses of the three joint angles in the middle leg . . . . .	81
3.17	Modified FE network in the hind leg . . . . .	82
3.18	Time courses of the three joint angles in the hind leg . . . . .	83
3.19	Sketch of a three-leg network with different couplings . . . . .	85
3.20	Generation of the tetrapod for different intersegmental connections . . . . .	87
3.21	Time course of the angle $\beta$ and the retractor CPG neuron for the front, middle and hind leg during tetrapod . . . . .	88
3.22	Generation of the tripod for different intersegmental connections	90
3.23	Time course of the angle $\beta$ and the PR CPG for the front, middle and hind leg during tripod . . . . .	91
3.24	Time course of the angle $\beta$ and the PR CPG for the front, middle and hind leg during switching from tetrapod to tripod	93
3.25	Foot fall pattern for the switching sequence between the tetrapod and tripod gait . . . . .	93
3.26	Time course of the angle $\beta$ and the PR CPG for the front, middle and hind leg during switching from tripod to tetrapod	94
3.27	Foot fall pattern for the switching sequence between the tripod and tetrapod gait . . . . .	95
B.1	Time courses of the angles in the CTr-joint (A) and the FTi-joint (B) for the mechanically coupled system . . . . .	125

# List of Tables

A.1	Numerical values of the membrane capacitance and the time constant coefficient for all neurons . . . . .	110
A.2	Numerical values of the parameters for the CPG neurons . . .	111
A.3	Numerical values of the parameters for the interneurons . . . .	112
A.4	Numerical values of the parameters for the synapses . . . . .	113
A.5	Numerical values of the parameters for the CPG motoneurons	114
A.6	Numerical values of the parameters for the potassium current in the CPG motoneurons . . . . .	115
A.7	Numerical values of the parameters for the adaptation current in the CPG motoneurons . . . . .	115
A.8	Numerical values of the parameters for the leakage current in the CPG motoneurons . . . . .	116
A.9	Numerical values of the parameters for the applied current in the CPG motoneurons . . . . .	116
A.10	Geometrical parameters in the muscles used in the simulation I	117
A.11	Geometrical parameters in the muscles used in the simulation II	118
A.12	Geometrical parameters in the muscles used in the simulation III . . . . .	118
A.13	Masses and lengths in all segments of the stick insect . . . . .	119

A.14 Numerical values of the extremal angles in EF system of the middle leg . . . . .	120
A.15 Numerical values of the extremal angles in LD system of the middle leg . . . . .	120
A.16 Numerical values of the extremal angles in PR system of the middle leg . . . . .	121
A.17 Alternative numerical values of the extremal angles in PR system of the middle leg . . . . .	121
A.18 Dynamical parameters of the muscles in the FE system of the front leg . . . . .	122
A.19 Dynamical parameters of the muscles in the LD system of the front leg . . . . .	122
A.20 Dynamical parameters of the muscles in the PR system of the front leg . . . . .	123
A.21 Dynamical parameters of the muscles in the FE system of the hind leg . . . . .	123
A.22 Dynamical parameters of the muscles in the LD system of the hind leg . . . . .	124
A.23 Dynamical parameters of the muscles in the PR system of the hind leg . . . . .	124

# Bibliography

Akay T, Haehn S, Schmitz J, Büschges A. Signals from load sensors underlie interjoint coordination during stepping movements of the stick insect leg. *J Neurophysiol* 92: 42-51, 2004.

Bässler U. *Neural Basis of Elementary Behavior in Stick Insects*. Springer-Verlag: Berlin-Heidelberg-New York, 1983.

Bässler D, Büschges A, Meditz S, Bässler U. Correlation between muscle structure and filter characteristics of the muscle-joint system in three orthopteran insect species. *J Exp Biol* 199: 2169-2183, 1996.

Bässler U, Büschges A. Pattern generation for stick insect walking movements multisensory control of a locomotor program. *Brain Res Rev* 27: 65-88, 1998.

Blümel M. Locomotor system simulations and muscle modeling of the stick insect (*Carausius morosus*). Ph.D. Thesis, University of Cologne, Germany, 2011.

Blümel M, Guschlbauer C, Gruhn S, Hooper SL, Büschges A. Hill-type muscle model parameters determined from experiments on single muscle show large animal-to-animal variation. *Biol Cybern* 106:559571, 2012.

- Blümel M, Guschlbauer C, Hooper SL, Büschges A. Using individual-muscle specific instead of across-muscle mean data halves muscle simulation error. *Biol Cybern* 106:573585, 2012.
- Blümel M, Hooper SL, White WE, Guschlbauer C, Büschges A. Determining all parameters necessary to build Hill-type muscle models from experiments on single muscles. *Biol Cybern* 106:543558, 2012.
- Borgmann A, Scharstein H, Büschges A. Intersegmental coordination: influence of a single walking leg on the neighboring segments in the stick insect walking system. *J Neurophysiol* 98: 1685-1696, 2007.
- Borgmann A, Hooper SL, Büschges A. Sensory feedback induced by front-leg stepping entrains the activity of central pattern generators in caudal segments of the stick insect walking system. *J Neurosci.* 29(9): 2972-83, 2009.
- Borgmann A, Toth TI, Gruhn M, Daun-Gruhn S, Büschges A. Dominance of local sensory signals over inter-segmental effects in a motor system: experiments. *Biol Cybern* 105: 399-411, 2011.
- von Buddenbrock W, Der Rhythmus der Schreitbewegungen der Stabheuschrecke *Dyxippus*. *Zoolog Zentralblatt* 41: 41-48, 1921.
- Büschges A. Role of local nonspiking interneurons in the generation of rhythmic motor activity in the stick insect. *J Neurobiol* 27: 488-512, 1995.
- Büschges A. Inhibitory synaptic drive patterns motoneuronal activity in rhythmic preparations of isolated thoracic ganglia in the stick insect. *Brain Res* 783: 262-271, 1998.

- Büschges A, Ludwar BCh, Bucher D, Schmidt J, DiCaprio RA. Synaptic drive contributing to rhythmic activation of motoneurons in the deafferented stick insect system. *Eur J Neurosci* 19: 1856-1862, 2004.
- Büschges A. Sensory control and organization of neural networks mediating coordination of multisegmental organs for locomotion. *J Neurophysiol* 93: 1127-1135, 2005.
- Büschges A, Akay T, Gabriel JP, Schmidt J. Organizing network action for locomotion: Insights from studying insect walking. *Brain Res Rev* 57: 162-171, 2008.
- Büschges A, Scholz H, El Manira A. New moves in motor control. *Curr Biol* 21(13): R513-24, 2011.
- Büschges A, Gruhn M. Mechanosensory feedback in walking: from joint control to locomotor patterns. *Adv Insect Physiol* 34: 193-230, 2008.
- Cabelguen J-M, Ijspeert A, Lamarque S, Ryczko D. Axial dynamics during locomotion in vertebrates: lesson from the salamander. *Prog Brain Res* 187: 149-162, 2010.
- Calabrese, R. L. (1995). Half-center oscillators underlying rhythmic movements. In M. Arbib (Ed.), *The handbook of brain theory and neural networks* (pp. 444). Cambridge, MA: MIT press.
- Cohen SD, Hindmarsh AC. CVODE, a stiff/nonstiff ODE solver in C. *Computers in Physics* 10: 138-143, 1996.
- Cruse H. What mechanisms coordinate leg movement in walking arthropods? *Trends in Neurosci.* 13: 15-21, 1990.

- Cruse H, Kindermann T, Schumm M, Dean J, Schmitz J. Walknet – a biologically inspired network to control six-legged walking. *Neural Netw* 11: 1435-1447, 1998.
- Cruse H, Ehmanns I, Stübner S, Schmitz J. Tight turns in stick insects. *J Comp Physiol A* 195: 299-309, 2009.
- Daun S, Rybak IA, Rubin J. The response of a half-center oscillator to external drive depends on the intrinsic dynamics of its components: a mechanistic analysis. *J comput Neurosci* 27: 3-36, 2009.
- Daun-Gruhn S. A mathematical modeling study of inter-segmental coordination during stick insect walking. *J comput Neurosci* 30: 255-278, 2011.
- Daun-Gruhn S, Büschges A. From neuron to behavior: dynamic equation-based prediction of biological processes in motor control. *Biol Cybern* 105: 71-88, 2011.
- Daun-Gruhn S, Toth TI. An inter-segmental network model and its use in elucidating gait-switches in the stick insect. *J comput Neurosci* 31: 43-60, 2011.
- Daun-Gruhn S, Toth TI, Borgmann A. Dominance of local sensory signals over inter-segmental effects in a motor system: modeling studies. *Biol Cybern* 105: 413-426, 2011.
- Delcomyn, F. (1971). The locomotion of the cockroach *Periplaneta Americana*. *Journal of Experimental Biology* 54: 443-452, 1971.
- Delcomyn, F. (1989). Walking of the American cockroach: The timing of motor activity in the legs during straight walking. *Biological Cybernetics* 60: 373-384, 1989.



- Van Drongelen, W., Koch, H., Elsen, F. P., Lee, H. C., Mrejeru, A., Doren, E., et al.. The role of persistent sodium current in bursting activity of mouse neocortical networks in vitro. *Journal of Neurophysiology* 96: 2564-2577, 2006.
- Dürr V, Ebeling W. The behavioural transition from straight to curve walking: kinetics of leg movement parameters and the initiation of turning. *J Exp Biol* 208: 2237-2252, 2005.
- Dürr V, Schmitz J, Cruse H. Behaviour-based modelling of hexapod locomotion: linking biology and technical application. *Arthropod Structure & Development* 33: 237-250, 2004.
- Eaton, John W. and others. GNU Octave, version 3.0.5. <http://www.octave.org>, 2008.
- Ekeberg Ö, Blümel M, Büschges A. Dynamic simulation of insect walking. *Arthropod Structure & Development* 33: 287-300, 2004.
- Ekeberg Ö, Pearson K. Computer simulation of stepping in the hind legs of the cat: an examination of *J Neurophysiol* 94: 4256-4268, 2005.
- Gabriel JP. Activity of leg motoneurons during single leg walking of the stick insect: From synaptic inputs to motor performance. Ph.D. Thesis, University of Cologne, Germany, 2005.
- Grabowska M, Godlewska E, Schmidt J, Daun-Gruhn S. Quadropedal gaits in hexapod animals - stepping patterns in free walking adult stick insects. *J exper Biol* 215: 4255-66, 2012.
- Graham D. A behavioural analysis of the temporal organisation of walking

- movements in the 1st instar and adult stick insect (*Carausius morosus*). J comp Physiol 81: 23-52, 1972.
- Graham, D. Pattern and control of walking in insects. Advances in Insect Physiology 18: 31-140, 1985.
- Grillner S, Markram H, De Schutter E, Silberberg G, LeBeau FE. Micro-circuits in action—from CPGs to neocortex. Trends Neurosci. 28:525-33, 2005.
- Gruhn M, Hoffmann O, Dübbert M, Scharstein H, Büschges A. Tethered stick insect walking: A modified slippery surface setup with optomotor stimulation and electrical monitoring of tarsal contact. J Neurosci Meth 158: 195-206, 2006.
- Gruhn M, Zehl L, Büschges A. Straight walking and turning on a slippery surface. J Exp Biol 212: 194-209, 2009.
- Gruhn Lab Webpage <http://www.neuro.uni-koeln.de/11798.html>, accessed on November 16 2012.
- Guschlbauer Ch. Characterisation of the biomechanical, passive, and active properties of femur-tibia joint leg muscles in the stick insect *Carausius morosus*. Ph.D. Thesis, University of Cologne, Germany, 2009.
- Guschlbauer Ch, Scharstein H, Büschges A. The extensor tibiae muscle of the stick insect: biomechanical properties of an insect walking leg muscle. J Exp Biol 210: 1092-1108, 2007.
- Harischandra N, Cabelguen J-M, Ekeberg Ö. A 3D musculo-mechanical model of the salamander for the study of different gaits and modes of locomotion. Frontiers in Neurorobotics 4: 112-122, 2010.

- Hill AV. The mechanics of active muscle. Proc Roy Soc Lond (Biol), 141: 104-117, 1953.
- Hodgkin AL, Huxley AF. A quantitative description of membrane current and its application to conduction and excitation in nerve. J Physiol 117: 500-544, 1952.
- Holmes P, Full RJ, Koditschek D, Guckenheimer J. The dynamics of legged locomotion: models, analyses, and challenges. SIAM Rev 48: 207-304, 2006.
- Hooper SL, Guschlbauer Ch, Blümel M, Rosenbaum P, Gruhn M, Akay T, Büschges A. Neural control of unloaded leg posture and leg swing in stick insect, cockroach, and mouse differs from that in larger animals. J Neurosci 29: 4109-4119, 2009.
- Ijspeert AJ, Crespi A, Ryczko D, Cabelguen JM. From swimming to walking with a salamander robot driven by a spinal cord model. Science, 315: 1416-1420, 2007.
- Izhikevich, E. M. (2007). Dynamical systems in neuroscience: The geometry of excitability and bursting. Cambridge: MIT press, Massachusetts Institute of Technology.
- Jander JP. Untersuchungen zum Mechanismus und zur zentralnervösen Steuerung des Kurvenlaufs bei Stabheuschrecken (*Carausius morosus*). PhD thesis, University of Cologne, Germany, 1982.
- Jander JP. Mechanical stability in stick insects when walking straight and around curves. In: *Insect Locomotion*, edited by Gewecke M, Wendler G. Berlin, Hamburg: Paul Parey, 1985, p. 33-42.

- Katz, P. S., Hooper, S. L. Invertebrate central pattern generators. In G. North and R. J. Greenspan (Eds.), *Invertebrate neurobiology* (pp. 251-280). Cold Spring Harbor: Cold Spring Harbor Laboratory Press.
- Kindermann T. Behavior and adaptability of a six-legged walking system with highly distributed control. *Adapt Behav* 9: 16-41, 2002.
- Knops SA, Toth TI, Guschlbauer C, Gruhn M, Daun-Gruhn S. A neuro-mechanical model for curve walking in the stick insect. *J Neurophysiol* 109: 679-691, 2013. doi:10.1152/jn.00648.2012
- Lagrange JL (Author), Boissonnade A (Translator), Vagliente VN (Translator) *Analytical Mechanics* (Boston Studies in the Philosophy of Science). Springer, 1997.
- Ludwar, B. C., Westmark, S., Büschges, A., Schmidt, J. Modulation of membrane potential in mesothoracic moto- and interneurons during stick insect front leg walking. *Journal of Neurophysiology* 93: 1255-1265, 2005.
- Nolting W. *Grundkurs Theoretische Physik 2: Analytische Mechanik*. Springer Berlin Heidelberg, 8. Auflage, 2010.
- Orlovsky GN, Deliagina TG, Grillner S. *Neuronal Control of Locomotion*. Oxford: Oxford University Press, 1999.
- Pearson K, Ekeberg Ö, Büschges A. Assessing sensory function in locomotor systems using neuro-mechanical simulations. *Trends Neurosci.* 29, 625-631, 2006.
- Ritzmann R, Büschges A. Adaptive motor behavior in insects. *Curr Opin Neurobiol* 17: 629-636, 2007.

- Rosano H, Webb B. A dynamic model of thoracic differentiation for the control of turning in the stick insect. *Biol Cybern* 97: 229-246, 2007.
- Rosenbaum P, Wosnitza A, Büschges A, Gruhn M. Activity patterns and timing of muscle activity in the forward walking and backward walking stick insect *Carausius morosus*. *J Neurophysiol* 104: 1681-1695, 2010.
- Satterlie, R. A. (1985). Reciprocal inhibition and postinhibitory rebound produce reverberation in a locomotor pattern generator. *Science*, 229, 402404, 1985.
- Schmidt J, Grund, M. Rhythmic activity in a motor axon induced by axotomy. *Neuroreport* 14: 1267-1271, 2003.
- Schumm M, Cruse H. Control of swing movement: influences of differently shaped substrate. *J Comp Physiol A* 192: 1147-1164, 2006.
- Selverston, A. I. and Moulins, M. (1985). Oscillatory neural networks. *Annual Review Physiology*, 47, 2948, 1985.
- Open Dynamics Engine 2006 Smith R. <http://www.ode.org>, accessed on November 16 2012.
- Toth TI, Gruhn S. A putative neuronal network controlling the activity of the leg motoneurons of the stick insect *NeuroReport* 2011, 22:943-946, 2011.
- Toth TI, Knops S, Gruhn S. A neuro-mechanical model explaining forward and backward stepping in the stick insect. *J Neurophysiol* 107: 3267-3280, 2012.
- Traub RD, Wong RK, Miles R, Michelson H. A model of a CA3 hippocampal pyramidal neuron incorporating voltage-clamp data on intrinsic conductances. *J Neurophysiol* 1991 66:(2) 635-650, 1991.

- Von Twickel A, Büschges A, Pasemann F. Deriving neural network controllers from neuro-biological data: implementation of a single-leg stick insect controller. *Biological Cybernetics* 2011 104: 95-119, 2011.
- Weidler DJ and Diecke FPJ. The role of cations in conduction in the central nervous system of the herbivorous insect *Carausius morosus*. *J comp physiol A* 64: 372-399, 1969.
- Wendler G. The Co-Ordination of Walking Movements in Arthropods. *Symp Soc Exp Biol* 20: 229-249, 1965.
- Wendler G. Lokomotion: das Ergebnis zentral-peripherer Interaktion (Locomotion: the result of central-peripheral interaction). *Verhandlungen der Deutschen Zoologischen Gesellschaft* 80-96, 1978.
- Westmark S, Oliveira EE, Schmidt J. Pharmacological Analysis of Tonic Activity in Motoneurons During Stick Insect Walking. *J Neurophysiol* 102: 1049-1061, 2009.
- Zhong, G., Masino, M. A., Harris-Warrick, R. M. Persistent sodium currents participate in fictive locomotion generation in neonatal mouse spinal cord. *Journal of Neuroscience* 27: 4507-4518, 2007.
- Zill S, Schmitz J, Büschges A. Load sensing and control of posture and locomotion. *Arthropod Structure & Development* 33: 273-286, 2004.
- Zill SN, Keller BR, Duke ER. Sensory signals of unloading in one leg follow stance onset in another leg: transfer of load and emergent coordination in cockroach walking. *J Neurophysiol* 101: 2297-2304, 2009.
- Zill SN, Büschges A, Schmitz J. Encoding of force increases and decreases by

tibial campaniform sensilla in the stick insect, *Carausius morosus*. *J Comp Physiol A*: 197: 851-867, 2011.

# Danksagung

Diese Arbeit wäre nicht zu Stande gekommen ohne das Mitwirken verschiedener Personen. Daher möchte ich allen Mitgliedern der AG Büschges, AG Wellmann and AG Gruhn für die angenehme Arbeitsatmosphäre und hilfreiche Diskussionen meinen Dank aussprechen. Ganz besonders möchte ich Dr. Silvia Gruhn für die intensive Betreuung meiner Doktorarbeit, für motivierende Ratschläge und die Bereitschaft, sämtliche Angelegenheiten schnellstmöglich zu klären, danken. Überdies danke ich Prof. Dr. Ansgar Büschges für die Einnahme der Position als Zweitgutachter meiner Dissertation. Ebenfalls danke ich Prof. Dr. Martin Hülskamp für die Übernahme des Vorsitzes meiner Disputation, Dr. Christoph Guschlbauer für die Zusage der Protokollführung während meiner Disputation. Dr. Tibor Toth für hilfreiche Diskussionen und Verbesserungsvorschläge bezüglich meiner Dissertation und Unterstützung innerhalb der gesamten Zeit. PD Dr. Joachim Schmidt danke ich herzlich für hilfreiche Diskussionen und Verbesserungsvorschläge zu meiner Dissertation. Tobias Schulze danke ich für technische Hilfe und für die Erstellung einer Webseite, die das ergänzende Material zu dieser Arbeit enthält. Nicht zuletzt möchte ich Melanie Kaesler M.A. für den Beistand während der gesamten Zeit und das Interesse an meiner Doktorarbeit und Korrekturvorschläge zu meiner Dissertation danken.



# Erklärung

Ich versichere, dass ich die von mir vorgelegte Dissertation selbständig angefertigt, die benutzten Quellen und Hilfsmittel vollständig angegeben und die Stellen der Arbeit — einschließlich Tabellen, Karten und Abbildungen —, die anderen Werken im Wortlaut oder dem Sinn nach entnommen sind, in jedem Einzelfall als Entlehnung kenntlich gemacht habe; dass diese Dissertation noch keiner anderen Fakultät oder Universität zur Prüfung vorgelegen hat; dass sie — abgesehen von den nachfolgend angegebenen Teilpublikationen — noch nicht veröffentlicht worden ist sowie, dass ich eine solche Veröffentlichung vor Abschluss des Promotionsverfahrens nicht vornehmen werde. Die Bestimmungen der Promotionsordnung sind mir bekannt. Die von mir vorgelegte Dissertation ist von Dr. Silvia Gruhn betreut worden.

# Teilpublikationen

## Articles

- Knops SA, Toth TI, Guschlbauer C, Gruhn M, Daun-Gruhn S.  
A neuro-mechanical model for curve walking in the stick insect.  
J Neurophysiol 109: 679-691, 2013.
- Toth TI, Knops S, Gruhn S.  
A neuro-mechanical model explaining forward and backward stepping  
in the stick insect.  
J Neurophysiol 107: 3267-3280, 2012.

## Abstracts

- Knops SA, Toth TI, Guschlbauer C, Gruhn M, Daun-Gruhn S.  
Neuro-mechanical control of forwards, backwards and sideways walking  
NeuroVisionen 8, Aachen Oct 26 2012.
- S. Knops and S. Gruhn  
Modeling Neuro-Mechanical Intra-Leg Coordination of Insects During Locomotion  
ik 2011, Günne Mar 25 - Apr 1 2011.
- S. Knops and S. Gruhn  
Modeling Neuro-Mechanical Intra-Leg Coordination of Insects During Locomotion  
Crossroads in Biology, Köln Feb 4 - 5 2010.

# Curriculum Vitae

Sascha Alexander Knops

Südstr. 214

52134 Herzogenrath

sknops0@uni-koeln.de

\* 05.Juni 1978 in Stolberg (Rhld.)

## **Education**

- 2009 - present: Institute of Zoology, University of Cologne, PhD program,  
Advisor: Dr. Silvia Gruhn
- 2003 - 2009: Studies of Physics at the RWTH Aachen
- 2000 - 2003: Abitur at the Abendgymnasium Aachen

## **Professional experience**

- 2009 - present: Research fellow, Emmy Noether Group, Institute of Zoology,  
University of Cologne
- 2006 - 2009: Supervision of practical and theoretical courses in Physics for  
students
- 2001 - 2002: Receptionist at the Technology Center Aachen
- 1995 - 1999: Vocational training (mechanist)